



universität
wien

MASTERARBEIT

Titel der Masterarbeit

„Ab initio molecular dynamics study of the relaxation of
purine after UV excitation considering singlet-triplet
interactions“

verfasst von

Clemens Rauer, BSc

angestrebter akademischer Grad

Master of Science (MSc)

Wien, 2013

Studienkennzahl lt. Studienblatt:

A 066 862

Studienrichtung lt. Studienblatt:

Masterstudium Chemie

Betreut von:

Univ.-Prof. Dr. Leticia González Herrero

ABSTRACT

In this work, the relaxation dynamics of purine after UV light irradiation is investigated. By using non-adiabatic ab initio molecular dynamics in the basis of spin-orbit coupled states, the role of triplet states during relaxation is evaluated. Our calculations show, that after an ultrafast conversion from S_2 to S_1 , 50% of the population relax to the ground state and 10% perform intersystem crossing to T_2 , followed by internal conversion to T_1 . These processes can be summarized as $S_2 \rightarrow S_1 \rightarrow S_0$ for the relaxation to the ground state, and $S_1 \rightarrow T_2 \rightarrow T_1$ for the intersystem crossing process. As a prerequisite to the dynamics, the quantum chemistry of purine is also investigated using high-level ab initio methods. By testing different methods, a suitable level of theory for the dynamics is identified. By analyzing the crossing points in the dynamics, the relevant geometries, both for the IC and the ISC processes, are found and optimized. Our results are used to explain the experimental observations of Prof. Crespo (CWRU, Cleveland, Ohio) and are complementary to the quantum chemical calculations of Dr. Corral (UAM, Madrid). Comparing the molecular dynamics results with the ones obtained by our collaborators gives us a novel understanding of the relaxation process of purine, and of the role of intersystem crossings in the dynamics.

ABSTRACT

In dieser Arbeit wird die Dynamik der Relaxation von Purin nach Anregung mit UV-Strahlen untersucht. Mittels nicht-adiabatischer ab initio Molekulardynamik in der Basis von Spin-Bahn-gekoppelten Zuständen wird die Rolle von Triplett-Zuständen für die Dynamik bestimmt. Unsere Berechnungen zeigen einen ultraschnellen Übergang vom S_2 in den S_1 Zustand. Danach relaxieren 50 % der Trajektorien in den Grundzustand, und 10 % der Trajektorien führen Interkombination zum T_2 Zustand, gefolgt von einer internen Umwandlung zu T_1 , durch. Diese Prozesse können folgendermaßen zusammengefasst werden: Die Relaxation zum Grundzustand folgt dem $S_2 \rightarrow S_1 \rightarrow S_0$ Prozess, und die Interkombination folgt dem $S_1 \rightarrow T_2 \rightarrow T_1$ Prozess. Als Vorbedingung für die Dynamik-Simulationen wird die Quantenchemie von Purin mit verschiedenen ab initio Methoden untersucht. Dadurch ermitteln wir eine geeignete quantenchemische Methode für die Dynamik. Die relevanten konischen Durchschneidungen und Kreuzungspunkte der Zustände können gefunden und ihre Geometrien optimiert werden. Unsere Ergebnisse ergänzen sich mit den quantenchemischen Berechnungen von Dr. Corral (UAM, Madrid), und das Gesamtergebnis wird benutzt um die experimentellen Beobachtungen von Prof. Crespo (CWRU, Cleveland, Ohio) zu erklären. Durch den Vergleich unserer Daten mit denen unserer Kooperationspartner können wir zum ersten Mal die Relaxationsdynamik von Purin und die Rolle von Interkombination untersuchen.

CONTENTS

ABSTRACT	i
FREQUENTLY USED ACRONYMS	v
LIST OF SYMBOLS	vi
1 INTRODUCTION	1
2 THEORY	3
2.1 The Schrödinger Equation	3
2.2 The Born-Oppenheimer Approximation	4
2.3 Ab Initio Molecular Dynamics	5
2.3.1 Newton's Equation of Motion	6
2.3.2 Surface Hopping	7
2.4 The Hartree-Fock Approximation	9
2.4.1 The Hartree-Fock Equations	10
2.5 Single-Reference Correlation Methods	10
2.5.1 Configuration Interaction	11
2.5.2 Perturbation Theory	13
2.5.3 The Coupled-Cluster Method	16
2.6 Multi-reference correlation methods	19
2.6.1 The Multi-Configurational Self Consistent Field Method	20
2.6.2 Active Space based MCSCF	21
2.6.3 Complete Active Space Perturbation Theory	22
2.6.4 Multi-Reference Configuration Interaction	24
2.7 Calculation of important properties	24
2.7.1 General Property Calculations	25
2.7.2 Gradient Calculations	26
2.7.3 Non-Adiabatic Couplings	26
2.7.4 Dipole Moments	27
2.8 Spin-Orbit Coupling	28
2.8.1 The Spin-Orbit Operator	28
3 ABOUT PURINE	31
3.1 Prototropic Tautomerism	31
3.2 Previous Research	31
4 RESULTS FROM ELECTRONIC STRUCTURE	33
4.1 Purine Geometries in the electronic ground state	33
4.2 Excited state calculations	34
4.2.1 Nomenclature of the employed methods	34
4.2.2 Choice of the Active Space	35
4.2.3 Performance of the quantum chemical methods on the vertical excitation energies	36
4.2.4 Comparison to previous theoretical work	41
4.2.5 Method used in Dynamics	42
5 MOLECULAR DYNAMICS RESULTS	45

5.1	Absorption Spectra	45
5.1.1	Experimental Absorption Spectra	45
5.1.2	Theoretical Absorption Spectra	46
5.2	Ab Initio Molecular Dynamics	48
5.3	Conical Intersection Geometries	51
5.4	Comparison with quantum chemical and experimental results	53
6	SUMMARY	57
7	OUTLOOK	59
A	APPENDIX	61
A.1	Triplet states	61
A.2	Conical Intersection Geometries	62
	BIBLIOGRAPHY	65
	ACKNOWLEDGEMENTS	75

FREQUENTLY USED ACRONYMS

A	Adenine
G	Guanine
C	Cytosine
T	Thymine
U	Uracil
UV	ultraviolet
ISC	intersystem crossing
SOC	spin-orbit coupling
IC	internal conversion
PES	potential energy surface
NAC	non-adiabatic coupling
SHARC	surface hopping including arbitrary couplings
BOA	Born–Oppenheimer approximation
MD	molecular dynamics
TDSE	time-dependent Schrödinger equation
TISE	time-independent Schrödinger equation
AIMD	ab initio molecular dynamics
MCH	molecular Coulomb Hamiltonian
HF	Hartree–Fock
RHF	Restricted Hartree–Fock
UHF	Unrestricted Hartree–Fock
MO	molecular orbital
CI	configuration interaction
PT	Perturbation theory
CC	Coupled cluster
CSF	Configuration state function
CID	CI using doubles
CISD	CI using singles and doubles
CISDTQ	CI using up to quadruples
MP ₁	Møller–Plesset first-order
MP ₂	Møller–Plesset second-order
MP ₃	Møller–Plesset third-order
MP ₄	Møller–Plesset fourth-order
EOM-CC	Equation of motion - coupled cluster
EOM-CCSD	EOM-CC using singles and doubles
MCSCF	Multi-configurational self consistent field
CASSCF	Complete active space self consistent field
SA-CASSCF	State averaged CASSCF
CASPT ₂	Complete active space perturbation theory second order
MS-CASPT ₂	Multi-state CASPT ₂
FOS	first-order interaction space
MRCI	Multi-reference CI
MRCISD	MRCI using singles and doubles
AMFI	atomic mean field integrals

LIST OF SYMBOLS

\hbar	Planck's reduced constant
\mathbf{r}	Electronic coordinate vector
\mathbf{R}	Nuclear coordinate vector
ϵ_0	Permittivity of free space
∇	Nabla operator
t	time
N	Number of nuclei
n	Number of electrons
m_e	Electron mass
e	Elementary charge
M_a	Mass of nucleus A
$Z_A e$	Charge of nucleus A
r	Interelectronic distance
R	Internuclear distance
$\bar{\mathbf{R}}$	Parametric dependence on the nuclear coordinates
\mathbf{v}	Nuclear velocity vector
\mathbf{a}	Nuclear acceleration vector
\hat{H}	Hamiltonian
\hat{H}_e	electronic Hamiltonian
\hat{T}_n	Nuclear kinetic energy operator
\hat{T}_e	Electronic kinetic energy operator
\hat{V}_{nn}	Internuclear potential energy operator
\hat{V}_{ee}	Interelectronic potential energy operator
\hat{V}_{ne}	Nuclear-electrons potential energy operator
\hat{f}	One-electron fock operator
\hat{h}	One-electron operator
\hat{J}	Coulomb operator
\hat{K}	Exchange operator
\hat{S}^2	Total squared spin momentum operator
\hat{a}	Annihilation operator
\hat{a}^\dagger	Creation operator
$\hat{\mathcal{T}}$	Cluster operator
$\hat{\mathcal{T}}_1$	One-particle excitation operator
$\hat{\mathcal{T}}_2$	Two-particle excitation operator
\hat{E}_{ij}	Single excitation operator
$\hat{E}_{ij,kl}$	Double excitation operator
\hat{C}	Configuration operator
\hat{F}	CASSCF Fock operator

\hat{H}'	Perturbation operator
\hat{h}_D	Dirac operator
\hat{G}	Breit operator
\hat{H}^{SO}	General spin-orbit operator
$\hat{H}_{\text{BP}}^{\text{SO}}$	Breit–Pauli spin-orbit operator
\hat{H}^{MCH}	Molecular Coulomb Hamiltonian
\hat{H}^{coup}	Hamiltonian containing all relevant couplings
\hat{H}^{total}	Total MCH and coupling Hamiltonian
\hat{H}^{diag}	Diagonalized Hamiltonian
$\hat{\mathbf{r}}$	One-electron displacement operator
$\hat{\mathbf{p}}$	One-electron momentum operator
$\hat{\mathbf{s}}$	One-electron spin operator
$\hat{L}_x/y/z$	Components of the angular momentum operator
δ_{ij}	Dirac delta function
ω	Spin coordinate
$\langle i \hat{h} j\rangle$	One electron integral
$\langle ij kl\rangle$	Two-electron integral
$\langle ij kl\rangle$	Anit-symmetrised two-electron integral
$h_{ij}, (i \hat{h} j)$	One-electron integral (spatial orbitals)
$g_{ijkl}, (ij kl)$	Two-electron integral (spatial orbitals)
$C_{i\mu}$	MO expansion coefficients
\mathbf{C}	MO expansion coefficient matrix
$S_{\mu\nu}$	Overlap matrix elements
\mathbf{S}	Overlap matrix
$F_{\mu\nu}$	Fock matrix elements
\mathbf{F}	Fock matrix
c_a^r	CI-expansion coefficient for a singly-excited determinant
c_{ab}^{rs}	CI-expansion coefficient for a doubly-excited determinant
c_{abc}^{rst}	CI-expansion coefficient for a triply-excited determinant
c_{abcd}^{rstu}	CI-expansion coefficient for a quadruply-excited determinant
λ	Perturbation parameter
t_i^r	One-particle excitation operator amplitude
t_{ij}^{rs}	Two-particle excitation operator amplitude
D_{ij}^{mn}	One-electron coupling coefficient
P_{ijkl}^{mn}	Two-electron coupling coefficient
D_{ij}	First order reduced density matrix
P_{ijkl}	Second order reduced density matrix
ω_i	MCSCF weight of state i
N_{CAS}	Number of CSFs in MCSCF
n_{CAS}	Number of electrons in the CAS

m_{CAS}	Number of orbitals in the CAS
$n_{\text{CAS}1/2/3}$	Number of electrons in the RAS ₁ , RAS ₂ , RAS ₃
$m_{\text{CAS}1/2+3}$	Number of orbitals in the RAS ₁ , RAS ₂ , RAS ₃
$\boldsymbol{\mu}$	Dipole moment
$\boldsymbol{\mu}_0$	Permanent dipole moment
$\boldsymbol{\mu}^{\beta\alpha}$	Transition dipole moment
S	Total spin
M_S	Spin projection
ϵ	Orbital energy
ϵ	Orbital energy matrix
ϵ	Orbital energy matrix
\mathbf{H}	Hamiltonian matrix
H_{ij}	Hamiltonian matrix element
$H_{ij}^{(0)}$	Unperturbed Hamiltonian matrix element
$H_{ij}^{(0)}$	Perturbed Hamiltonian matrix element
\mathbf{c}	MO and CI expansion coefficient vector
$\boldsymbol{\kappa}$	Lagrangian multiplier vector
\mathbf{E}	External field strength
E_{total}	Total energy
E_e	Electronic energy
E_{trial}	Energy of a trial wavefunction
E_{exact}	Exact non-relativistic wavefunction
E_{corr}	Correlation energy
E_{corr}	Dynamic part of the correlation energy
E_{stat}	Static part of the correlation energy
E_Q	Davidson correction energy
E_{HF}	HF energy
E_{CISD}	CISD energy
$E_{(0)}$	zeroth-order perturbation energy
$E_{(1)}$	first-order perturbation energy
$E_{(2)}$	second-order perturbation energy
E_{CC}	CC energy
E_{MCSCF}	MCSCF energy
$E_{\text{MCSCF}}^{\text{av}}$	Averaged MCSCF energy
$ \psi\rangle$	Wavefunction
$ \psi_e\rangle$	Electronic wavefunction
$ \psi_n\rangle$	Nuclear wavefunction
$ \psi_{\text{trial}}\rangle$	Trial wavefunction
$ \Psi\rangle$	Slater determinant
$ \Psi_{\text{HF}}\rangle$	Hartree–Fock wavefunction
$ \chi\rangle$	Spin orbital
$ \phi\rangle$	Spatial orbital
$ \alpha\rangle, \beta\rangle$	One-electron spin eigenfunctions

$ \xi\rangle$	Atomic basis function
$ \Psi_a^r\rangle, S$	Singly-excited configuration
$ \Psi_{ab}^{rs}\rangle, D$	Doubly-excited configuration
$ \Psi_{abc}^{rst}\rangle, T$	Triply-excited configuration
$ \Psi_{abcd}^{rstu}\rangle, Q$	Quadruply-excited configuration
$ \Phi_{CI}\rangle$	Full CI wavefunction
$ \phi^{(0)}\rangle$	Zeroth-order perturbed wavefunction
$ \phi^{(1)}\rangle$	First-order perturbed wavefunction
$ \phi^{(2)}\rangle$	Second-order perturbed wavefunction
$ \Phi\rangle$	Linear combination of Slater determinants (CI type wavefunction)
$ \Phi_{CI}\rangle$	CI wavefunction
$ \Phi_{CC}\rangle$	CC wavefunction
$ \Phi_{MCSCF}\rangle$	MCSCF wavefunction
$ \Phi_R\rangle$	MRCI reference wavefunction
$ \Psi_I\rangle$	Internal function (n -electron)
$ \Psi_S\rangle$	$n-1$ electron function
$ \Psi_S^r\rangle$	Single external function
$ \Psi_P\rangle$	$n-2$ electron function
$ \Psi_P^{rs}\rangle$	Double external function
$ \Phi_{MRCISD}\rangle$	MRCISD wavefunction
R	MRCI reference space
I	MRCI internal space
S	Space of $n - 1$ electron functions
P	Space of $n - 2$ electron functions
Γ	Irreducible representation
\mathcal{L}	Lagrangian
T_1, T_2	Non-adiabatic coupling terms
$T_{\beta\alpha}^1$	Scalar non-adiabatic coupling
$T_{\beta\alpha}^{1,CI}$	CI term of the scalar non-adiabatic coupling
$T_{\beta\alpha}^{1,CSF}$	CSF term of the scalar non-adiabatic coupling
$c_{\alpha/\beta}$	Coefficient of state α, β
N_α	Number of trajectories in state α
N_T	Total number of trajectories
$P_{\beta\rightarrow\dots}$	Surface hopping probability in and out of state β
$P_{\beta\rightarrow\alpha}$	Surface hopping probability between states α and β
$K_{\beta\alpha}$	NAC between states α and β
$\hat{\mathbf{K}}^{\text{diag}}$	NAC matrix in the diagonal basis
\mathbf{U}	Unitary transformation matrix
\mathbf{A}	Total propagator used in SHARC

INTRODUCTION

DNA is an important macromolecule inherent in all lifeforms on earth. It is formed by the four nucleobases adenine (A), guanine (G), cytosine (C), and thymine (T), with latter being replaced by uracil (U) in RNA. These either purine based (A,G) or pyrimidine based (C,T,U) nucleobases are connected via a backbone of sugars and phosphate to build up a closely packed double helical structure. The functionality of DNA is based on the intra- and intermolecular interactions of these nucleobases. There are various possibilities that these interactions can be inhibited causing mutations or other damages, including ultraviolet (UV) radiation¹. The specific chromophores active under UV irradiation are the previously mentioned nucleobases². The relaxation processes of these nucleobases have been a topic of extensive research in the previous decades, see e.g.³⁻⁵. With the advent of ultrafast time-resolved spectroscopy⁶⁻¹² and modern ab initio methods¹³⁻¹⁵, the investigation of these ultrafast processes has been enabled, both experimentally and theoretically. The results of these studies are necessary in order to fully understand the relaxation mechanisms giving DNA and RNA the remarkable resistance against damage induced by UV irradiation.

In this thesis, the relaxation dynamics of purine (Figure 1.1) is examined, as it is the skeletal structure for A and G. Although there has been extensive research on the relaxation process for the nucleobases^{3,4}, there has been no investigation on the deactivation of the purine molecule itself. By comparing the results to experimental findings, we can create a homology series, in order to get a better understanding into the relaxation process.

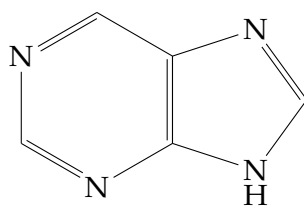


Figure 1.1: Geometry of purine

One major point of controversy regarding relaxation processes is the influence of triplet states. It is possible for singlet states to interact with triplet states, giving rise to intersystem crossings (ISC). These processes have often been dismissed arguing that they are too slow to actually contribute significantly¹⁶. Traditionally, spin-change is forbidden in a non-relativistic treatment. Only in a relativistic description of the electrons, the spin-orbit couplings (SOCs) – the coupling of an electron's spin with the electron's motion – arise. Due to its dependence on the nuclear charge, the SOC for molecules consisting solely of light atoms have been usually neglected¹⁷.

However, there are several rules of thumb existing for SOCs, which predict different results. According to the El-Sayed rule^{18,19}, the SOC between singlet and triplet states of different orbital symmetry is relatively large, compared to states of the same symmetry. Also, the energy gap law²⁰ argues that the ISC transition probability depends exponentially on the adiabatic energy difference between the corresponding states. In addition to these rules, theoretical²¹⁻²³ and spectroscopic²⁴⁻²⁹ studies suggested ISC on a femtosecond timescale for numerous systems. These ISC pathways would actually compete with the internal conversion (IC) singlet deactivation pathway.

In order to interpret and understand experimental data, the use of quantum chemical and dynamical methods has been increased significantly in the last decades. Using quantum dynamics, based on the precalculation of potential energy surfaces (PESs), a very accurate picture of the underlying processes can be obtained. Unfortunately, full quantum dynamics is not feasible for all but very small systems with limited degrees of freedom. Another problem that occurs in most quantum dynamics simulations involving coupled states is diabatisation, and is due to the Born-Oppenheimer approximation.

A convenient alternative to full quantum dynamics is non-adiabatic semi-classical *ab initio* dynamics³⁰. Here, while the nuclei are treated classically, the electrons are described by *ab initio* quantum mechanics methods. Treatment of non-adiabatic couplings (NACs) is governed by a surface hopping algorithm in which the system can jump from one electronic state onto another. By running an ensemble of trajectories, one can approximate the full quantum dynamics result. This semi-classical treatment allows for the investigation of larger systems, as the number of electronic structure calculations no longer depends on the number of degrees of nuclear freedom.

However, *ab initio* molecular dynamics considering the interaction of states of different multiplicity, i.e. ISC, has not been established until recently. In 2011, Richter et al.¹⁵ developed the SHARC (Surface Hopping including ARbitrary Couplings) method which uses a variant of Tully's fewest switches algorithm³¹. By including SOC terms in the potential energy matrix, and subsequent diagonalization, the trajectories can be run on spin-orbit coupled electronic states. In this basis IC and ISC are not fundamentally different anymore, and they can be described in a convenient way.

It is the goal of this thesis to investigate the relaxation behaviour of purine using SHARC, thereby describing the role of ISC, both qualitatively and quantitatively. This project is a cooperation with an experimental, and another theoretical group. In the experimental group of Prof. C. Crespo Hernández (CWRU, Cleveland, Ohio) the relaxation of purine has been investigated using time-resolved femtosecond spectroscopy. The theoretical group of Dr. I. Corral (UAM, Madrid) is exploring the potential energy surface of purine using minimum energy pathways (MEPS) and single point calculations at a higher level of theory. Together with the results of Dr. I. Corral, our dynamics is expected to contribute to explain the experimental results obtained by Prof. C. Crespo Hernández.

THEORY

The following chapter provides an overview of the theoretical aspects underlying this work. After introducing the Schrödinger equation (section 2.1) and the Born-Oppenheimer approximation (BOA) (2.2) we look at ab initio molecular dynamics (MD) (2.3) to express the motion of our nuclei in a semi-classical way. We will also review some methods for approximating the electronic Schrödinger equation (2.4,2.5,2.6), as well as calculating several properties which are needed for the molecular dynamics simulations.

2.1 THE SCHRÖDINGER EQUATION

The behavior of a system in time relative to its surroundings is governed by the time-dependent Schrödinger equation (TDSE), which has been proposed by Erwin Schrödinger in 1926³²:

$$\hat{H}(\mathbf{R}, \mathbf{r}, t) |\psi(\mathbf{R}, \mathbf{r}, t)\rangle = i\hbar \frac{\partial}{\partial t} |\psi(\mathbf{R}, \mathbf{r}, t)\rangle, \quad (2.1.1)$$

where $\hat{H}(\mathbf{R}, \mathbf{r}, t)$ is the time-dependent Hamiltonian of the system, containing all internal and external interactions. It is therefore dependent on the coordinates of the nuclei \mathbf{R} and of the electrons \mathbf{r} . $|\psi(\mathbf{R}, \mathbf{r}, t)\rangle$ is the wavefunction which contains all possible information about the described system and is also dependent on the coordinates.

This equation can be separated into a spatial (i.e. time-independent) and a temporal part, if the system is in an eigenstate of a time independent-Hamiltonian. In this case, we get two separate equations, one for each part. The temporal part can be solved analytically and results in a complex phase for the wavefunction. The spatial part is better known as the time-independent Schrödinger equation (TISE):

$$\hat{H}(\mathbf{R}, \mathbf{r}) |\Psi(\mathbf{R}, \mathbf{r})\rangle = E_{\text{total}} |\Psi(\mathbf{R}, \mathbf{r})\rangle. \quad (2.1.2)$$

$\hat{H}(\mathbf{R}, \mathbf{r})$ is now the time-independent Hamiltonian and E is the total energy of the system.

As stated above, the Hamiltonian contains all interactions in our system. For N nuclei with mass M_A , charge $Z_A e$, position R_m , and n electrons with mass m_e , charge e , and position r_e , it has the following terms:

$$\hat{H}(\mathbf{R}, \mathbf{r}) = \hat{T}_{nu}(\mathbf{R}) + \hat{T}_e(\mathbf{r}) + \hat{V}_{nu,nu}(\mathbf{R}) + \hat{V}_{nu,e}(\mathbf{R}, \mathbf{r}) + \hat{V}_{ee}(\mathbf{r}). \quad (2.1.3)$$

$\hat{T}_{nu}(\mathbf{R})$ and $\hat{T}_e(\mathbf{r})$ are the sum of the kinetic energies of the N nuclei and n electrons, respectively. The potential energy is separated into the Coulomb interactions of the nuclei $\hat{V}_{nu,nu}(\mathbf{R})$, the electrons $\hat{V}_{ee}(\mathbf{r})$, and into the interaction between the two of them $\hat{V}_{nu,e}(\mathbf{R}, \mathbf{r})$.

Using atomic units, i.e. setting m_e , \hbar , $\frac{1}{4\pi\epsilon_0}$, and e to 1, and expressing the mass of the nuclei M_A in units of m_e the kinetic energy terms $\hat{T}_{nu}(\mathbf{R})$ and $\hat{T}_e(\mathbf{r})$ can be expressed as:

$$\hat{T}_{nu}(\mathbf{R}) = - \sum_{A=1}^N \frac{1}{2M_A} \nabla_A^2 \quad \hat{T}_e(\mathbf{r}) = - \sum_{i=1}^n \frac{1}{2} \nabla_i^2 \quad (2.1.4)$$

where A runs over all nuclei with their respective mass M_A , and i runs over all electrons. The potential energy terms can be expressed as:

$$\hat{V}_{nu,nu} = \sum_{A=1}^N \sum_{B>A}^N \frac{Z_A Z_B}{r_{AB}}, \quad (2.1.5)$$

$$\hat{V}_{ee} = \sum_{i=1}^n \sum_{j>i}^n \frac{1}{r_{ij}}, \quad (2.1.6)$$

$$\hat{V}_{nu,e} = - \sum_{i=1}^n \sum_{A=1}^N \frac{Z_A}{r_{Ai}}, \quad (2.1.7)$$

where $r_{AB} = |\mathbf{R}_A - \mathbf{R}_B|$ is the distance between the two nuclei A and B . Similarly, $r_{ij} = |\mathbf{r}_i - \mathbf{r}_j|$ is the distance between the electrons i and j , and $r_{Ai} = |\mathbf{R}_A - \mathbf{r}_i|$ the distance between the nucleus A and the electron i .

2.2 THE BORN-OPPENHEIMER APPROXIMATION

The full TISE with the above mentioned Hamiltonian (2.1.3) leads to a $(N + n)$ -body problem which cannot be solved analytically for systems where $(N + n) > 2$. In 1927, Born and Oppenheimer³³ proposed an approximation that allows us to treat the nuclei and the electrons separately. Thus, we can split the wavefunction into a nuclear part $|\psi_n(\mathbf{R})\rangle$ and an electronic part $|\psi_e(\mathbf{r}; \bar{\mathbf{R}})\rangle$:

$$|\psi(\mathbf{R}, \mathbf{r})\rangle = |\psi_n(\mathbf{R})\rangle |\psi_e(\mathbf{r}; \bar{\mathbf{R}})\rangle \quad (2.2.1)$$

It could be shown^{34,35}, that this separation on its own is no approximation and can be done for any wavefunction in general. However, if we choose the electronic Hamiltonian \hat{H}_e as described below, and if $|\psi_e\rangle$ is an eigenfunction of this Hamiltonian, then this splitting is in fact an approximation.

The nuclear wavefunction $|\psi_n\rangle$ depends on the nuclear coordinates \mathbf{R} , and the electronic wavefunction $|\psi_e\rangle$ depends on the electronic coordinates \mathbf{r} and only parametrically on the nuclear coordinates, as indicated by $\bar{\mathbf{R}}$. This parametric dependence is based on the fact that the nuclei are about 10^3 times heavier than the electrons. Therefore, we can assume that the electrons move in a field of fixed nuclei and can instantly respond to any change in the nuclear coordinates. The nuclei, however, move in an averaged field of the electrons. Thereby it is possible to calculate the electronic TISE separately:

$$\hat{H}_e(\mathbf{r}; \bar{\mathbf{R}}) |\psi_e(\mathbf{r}; \bar{\mathbf{R}})\rangle = E_e(\bar{\mathbf{R}}) |\psi_e(\mathbf{r}; \bar{\mathbf{R}})\rangle. \quad (2.2.2)$$

Here, \hat{H}_e contains only the electron-specific terms, namely \hat{T}_e , \hat{V}_{ee} , and $\hat{V}_{nu,e}$. The effective potential energy of the nuclei moving in an average

field generated by the electrons is given by the sum of the electronic energy and the nuclear repulsion energy ⁱ:

$$E_{\text{PES}} = E_e + V_{nu,nu} = E_e + \sum_{A=1}^N \sum_{B>A}^N \frac{Z_A Z_B}{r_{AB}}. \quad (2.2.3)$$

Equation 2.2.3 still presents a n -body problem that cannot be solved analytically, but there are several methods that allow us to achieve approximate solutions. We will deal with these solutions later on, beginning in section 2.4. The resulting energies at different nuclear geometries form a PES on which the nuclei move along according to the nuclear Schrödinger equation. To obtain the nuclear Schrödinger equation we substitute Eqns 2.2.1 and 2.2.2 into our TISE (2.1.3), and using the relation given in Eqn 2.2.3, yields

$$[\hat{T}_{nu} + E] |\psi_e\rangle |\psi_{nu}\rangle = E_{\text{total}} |\psi_e\rangle |\psi_{nu}\rangle. \quad (2.2.4)$$

In this equation, T_{nu} still acts on the whole wavefunction Ψ :

$$\begin{aligned} \hat{T}_{nu} |\psi_e\rangle |\psi_n\rangle &= \sum_{A=1}^N \frac{1}{2M_A} \nabla^2 |\psi_e\rangle |\psi_{nu}\rangle \\ &= \sum_{A=1}^N \frac{1}{2M_A} \left(|\psi_e\rangle \nabla_A^2 |\psi_{nu}\rangle + 2\nabla_{\mathbf{A}} |\psi_e\rangle \nabla_{\mathbf{A}} |\psi_{nu}\rangle + |\psi_{nu}\rangle \nabla_A^2 |\psi_e\rangle \right) \\ &= \sum_{A=1}^N \frac{1}{2M_A} \left(|\psi_e\rangle \nabla_A^2 |\psi_{nu}\rangle + 2T_1 \nabla_{\mathbf{A}} |\psi_{nu}\rangle + |\psi_{nu}\rangle T_2 \right). \end{aligned} \quad (2.2.5)$$

T_1 and T_2 are the first and second derivatives of ψ_e with respect to the nuclear coordinates. They are known as the NACs. Within the BOA, these terms are set to zero and the motion of the nuclei is only dependent on the average field of the electrons, as explained above. Therefore the BOA is called an adiabatic approximation, and the resulting PES are also called adiabatic. This is in analogy to the adiabatic theorem postulated by Born in 1928³⁶ which states that for an adiabatic change the system will stay in the current state.

There are occasions where the condition that the electronic motion is much faster than the nuclear one does not apply anymore. This is the case when two PESs get close in energy. Then, the BOA breaks down as T_1 and T_2 can no longer be expected to vanish. Examples for this behavior are avoided crossings and conical intersections. In these cases the approximation to set T_1 and T_2 to zero is no longer valid and coupling between the different states has to be considered.

2.3 AB INITIO MOLECULAR DYNAMICS

Knowing the PES of a system one can explore the nuclear motion on it by solving the nuclear Schrödinger equation. While this may be a reasonable strategy for small systems, it is not practicable for larger ones. As the dimensionality increases linearly with the size of the system, the number of grid points to use for the PES grows exponentially. It is therefore not feasible to calculate the whole PES – or the part one is interested in – in advance. An popular alternative

ⁱ From now on we will omit the variables. Just bear in mind that ψ_e is only parametrically dependent on the nuclear coordinates \mathbf{R} .

is to use on-the-fly methods like semi-classical ab initio MD (AIMD) methods.

The essential point of AIMD is the fact that while the electrons are treated quantum mechanically, i.e. by solving the electronic Schrödinger equation (2.1.2), the nuclei are treated classically. By doing so one does not need to solve the nuclear Schrödinger equation (2.2.4), as only the nuclear coordinates are needed to solve the TISE on-the-fly. If one calculates both the electronic energy and the energy gradients – the first derivatives of the electronic energy with respect to the nuclear coordinates – one can represent the forces acting on the nuclei. Using these forces one can then solve Newton’s equations of motion, yielding a trajectory. Because of the semiclassical ansatz, this trajectory itself is only a crude approximation to a quantum dynamical calculation. In order to get an improved picture, one has to run a series of trajectories and then analyze them statistically.

2.3.1 Newton’s Equation of Motion

Sir Isaac Newton postulated the classical laws of motion more than 300 years ago³⁷. He established three laws that govern the motion of any macroscopic body. These laws are the principle of inertia, the action principle, and the reaction principle. Using the action principle, which states that the force acting upon the body is parallel to its acceleration times mass one gets Newton’s equation of motion:

$$M_A \frac{d^2}{dt^2} \mathbf{R}_A = -\nabla_A E_{\text{PES}}(\bar{\mathbf{R}}) \quad (2.3.1)$$

$\nabla_A E_{\text{PES}}(\bar{\mathbf{R}})$ is a vector containing all spatial derivatives of the potential energy with respect to the coordinates of atom A^{ii} .

Integrating Eqn. 2.3.1, one can calculate the complete trajectory of a molecule for any set of initial coordinates $\mathbf{R}(t=0)$ and velocities $\mathbf{v}(t=0)$. As analytical integration is not possible, one has to use numerical methods. In these methods, one discretizes time to an interval of δt , and calculates $\mathbf{R}(t+\delta t)$ and $\mathbf{v}(t+\delta t)$ from $\mathbf{v}(t)$, $\mathbf{R}(t)$, and the potential energy. As δt approaches 0, the accuracy of the methods increases and one gets closer to the analytical result.

There are several numerical methods to solve Eqn. 2.3.1 but the most prominent one is the Velocity-Verlet algorithm proposed by Verlet in 1967³⁸, based on the following equations:

$$\mathbf{R}(t+\Delta t) = \mathbf{R}(t) + \mathbf{v}(t)\Delta t + \mathbf{a}(t)\frac{\Delta t^2}{2}, \quad (2.3.2)$$

$$\mathbf{v}(t+\Delta t) = \mathbf{v}(t) + \frac{\Delta t}{2} \left(\mathbf{a}(t) + \mathbf{a}(t+\Delta t) \right), \quad (2.3.3)$$

$$\mathbf{a}(t+\Delta t) = -\frac{1}{m} \nabla E(\mathbf{R})|_{\mathbf{R}=\mathbf{R}(t+\Delta t)}. \quad (2.3.4)$$

The benefit of this method is that, compared to simpler mechanism like the Euler algorithm³⁹, the new velocity $\mathbf{v}(t+\Delta t)$ can be calculated simultaneously to the new coordinates $\mathbf{R}(t+\Delta t)$.

ii From now on, until section 2.4 we will be dealing with nuclear coordinates only, so the index A will be dropped

2.3.2 Surface Hopping

As adiabatic dynamics cannot account for processes described with a superposition of states, enhanced methods need to be employed. When using full quantum dynamics, a wavepacket can spread onto several PESs at the same time. As full quantum dynamics is not feasible for all but very small systems with limited degrees of freedom, the state hopping method was developed⁴⁰, in order to describe semi-classical MD involving several PESs. There, the trajectory is propagated on a single surface at any time step, but is allowed to change to another surface in a probabilistic manner. These surface changes are based on the NACs. When running multiple trajectories, a subsequent statistical analysis can reproduce the spread of the wavepacket, and therefore a comparison with full quantum dynamics. is possible

There are several surface hopping methods available (see the comprehensive review by Barbatti³⁰) and they are all based on the calculation of state hopping probabilities computed according to a set of state coefficients c_α . The probability of finding the trajectory in the electronic state α is given by $c_\alpha c_\alpha^* = |c_\alpha|^2$. The time evaluation of these coefficients can be calculated by numerical integration of the TDSE, as will be described below. For completeness, these coefficients have to be normalized according to

$$\sum_{\alpha} |c_{\alpha}|^2 = 1. \quad (2.3.5)$$

One popular hopping algorithm is Tully's Fewest Switches Criterion³¹, which he proposed in 1990. Tully's algorithm assures that within the ensemble the actual population of the states is consistent with the state coefficients. Simpler methods, like Ehrenfest dynamics, cannot assure this for non-vanishing coefficients⁴¹.

Tully's algorithm only allows hops into states with increasing and out of states with decreasing coefficients. Let us assume an ensemble of N_T trajectories, with $N_\beta(t_n)$ of them in state β at time t_n . As the coefficients determine the population of a state, we have

$$\frac{N_\beta(t_n)}{N_T} = |c_\beta(t_n)|^2. \quad (2.3.6)$$

In the time interval $[t_n; t_{n+1}]$ the population of state β is now decreased by $\Delta N = N_\beta(t_n) - N_\beta(t_{n+1})$. If we consider ΔN hops out of β into any other state and no hops into β from any other state the probability to jump out of β is

$$P_{\beta \rightarrow \dots} = \frac{\Delta N}{N_\beta(t_n)} = \frac{N_\beta(t_n) - N_\beta(t_{n+1})}{N_\beta(t_n)} = \frac{|c_\beta(t_n)|^2 - |c_\beta(t_{n+1})|^2}{|c_\beta(t_n)|^2}. \quad (2.3.7)$$

Considering a sufficiently small timestep $\Delta t = t_{n+1} - t_n$, we can rewrite the numerator on the right-hand-side of Equation (2.3.7) as

$$|c_\beta(t_n)|^2 - |c_\beta(t_{n+1})|^2 = \frac{\delta}{\delta t} |c_\beta|^2 \Delta t, \quad (2.3.8)$$

in which the time derivative can be expressed as

$$\frac{\delta}{\delta t} |c_\beta|^2 = \frac{\delta}{\delta t} (c_\beta c_\beta^*) = \left(\frac{\delta}{\delta t} c_\beta^* \right) c_\beta + c_\beta^* \left(\frac{\delta}{\delta t} c_\beta \right) \quad (2.3.9)$$

$$= \left(c_\beta^* \frac{\delta}{\delta t} c_\beta \right)^* + c_\beta^* \frac{\delta}{\delta t} c_\beta = 2\Re \left(c_\beta^* \frac{\delta}{\delta t} c_\beta \right). \quad (2.3.10)$$

Inserting the right-hand-side of Eqn (2.3.10) into equation (2.3.7) yields

$$P_{\beta \rightarrow \dots} = -\frac{2\Delta t}{c_\beta^* c_\beta} \Re \left(c_\beta^* \frac{\delta}{\delta t} c_\beta \right). \quad (2.3.11)$$

In order to be able to calculate time derivatives, we define an electronic wavefunction $|\psi\rangle$ as a linear combination of the electronic state wavefunctions, i.e. the electronic states under consideration:

$$|\psi\rangle = \sum_\alpha c_\alpha |\psi_\alpha\rangle. \quad (2.3.12)$$

Inserting equation 2.3.12 into the TDSE, and projecting on $\langle\psi_\beta|$, yields an equation for the time-evolution of the state coefficients:

$$\frac{\partial}{\partial t} c_\beta = -\sum_\alpha c_\alpha [iH_{\beta\alpha} + K_{\beta\alpha}], \quad (2.3.13)$$

where $H_{\beta\alpha}$ is a matrix element of \hat{H}_e and $K_{\beta\alpha}$ is the NAC term $\langle\psi_\beta|\partial/\partial t|\psi_\alpha\rangle$.

The surface hopping propbability from state β to state α can then be written as

$$P_{\beta \rightarrow \alpha} = \frac{2\Delta T}{c_\beta^* c_\beta} \Re \left(c_\beta^* c_\alpha [iH_{\beta\alpha} + K_{\beta\alpha}] \right). \quad (2.3.14)$$

Surface Hopping including Arbitrary Couplings

Tully's surface hopping is carried out in the basis of the eigenfunctions of the molecular Coulomb Hamiltonian (MCH). This MCH consists, within the BO, of the following terms:

$$\hat{\mathbf{H}}^{\text{MCH}} = \hat{T}_e + \hat{V}_{ee} + \hat{V}_{nu,e} + \hat{V}_{nu,nu} \quad (2.3.15)$$

Additional coupling terms not included in the MCH have to be considered separately, yielding the total Hamiltonian $\hat{\mathbf{H}}^{\text{total}}$:

$$\hat{\mathbf{H}}^{\text{total}} = \hat{\mathbf{H}}^{\text{MCH}} + \hat{\mathbf{H}}^{\text{coup}}. \quad (2.3.16)$$

As $\hat{\mathbf{H}}^{\text{total}}$ contains off-diagonal elements, the calculation can lead to difficulties, as the total Hamiltonian is not adiabatic anymore. To re-adiabatize, a second Hamiltonian in a diagonal basis, $\hat{\mathbf{H}}^{\text{diag}}$, is introduced via unitary transformation:

$$\hat{\mathbf{H}}^{\text{diag}} = \mathbf{U}^\dagger \hat{\mathbf{H}}^{\text{BO}} \mathbf{U} \quad (2.3.17)$$

Equations (2.3.12) and (2.3.13) can now be rewritten in this diagonal basis as

$$|\psi\rangle^{\text{diag}} = \sum_{\alpha} c_{\alpha}^{\text{diag}} |\psi_{\alpha}\rangle^{\text{diag}}, \quad (2.3.18)$$

$$\frac{\delta}{\delta t} \mathbf{c}^{\text{diag}} = -\mathbf{c}^{\text{diag}} \left[i\mathbf{H}^{\text{diag}} + \mathbf{K}^{\text{diag}} \right], \quad (2.3.19)$$

and using the transformation introduced in equation (2.3.17), the propagation of the coefficients can be expressed as

$$\frac{\delta}{\delta t} \mathbf{c}^{\text{diag}} = -\mathbf{c}^{\text{diag}} \mathbf{U}^{\dagger} \left[i\hat{\mathbf{H}}^{\text{BO}} + \hat{\mathbf{K}}^{\text{BO}} \right] \mathbf{U} \quad (2.3.20)$$

In SHARC, equation (2.3.20) is integrated numerically for a small time step Δt , i.e.

$$\mathbf{c}^{\text{diag}}(t) = \mathbf{U}^{\dagger}(t) e^{-[i\hat{\mathbf{H}}^{\text{MCH}}(t) + \hat{\mathbf{K}}^{\text{MCH}}(t)]\Delta t} \mathbf{U}(t_0) \mathbf{c}^{\text{diag}}(t_0) = \mathbf{A}(t, t_0) \cdot \mathbf{c}^{\text{diag}}(t_0), \quad (2.3.21)$$

with $\mathbf{A}(t, t_0)$ being the total propagator from $t_0 \rightarrow t$. Using this ansatz, the occurrence of highly-peaked non-adiabatic couplings occurring from small couplings in $\hat{\mathbf{H}}^{\text{coup}}$ is avoided. The actual surface-hopping is still done using the diagonal basis, which is the optimal basis for this step, see Granucci et al.⁴². Now the probabilities for surface hopping including arbitrary couplings can be expressed as

$$P_{\beta \rightarrow \alpha} = \left(1 - \frac{|c_{\beta}^{\text{diag}}(t)|^2}{|c_{\beta}^{\text{diag}}(t_0)|^2} \right) \times \frac{\Re \left[c_{\alpha}^{\text{diag}} A_{\alpha\beta}^* (c_{\beta}^{\text{diag}})^*(t_0) \right]}{|c_{\alpha}^{\text{diag}}(t_0)|^2 - \Re \left[c_{\beta}^{\text{diag}} A_{\beta\beta}^* (c_{\beta}^{\text{diag}})^*(t_0) \right]}. \quad (2.3.22)$$

Equation (2.3.22) is based on the equation of Granucci et al.⁴³, which is used in Local Diabatization⁴⁴.

2.4 THE HARTREE–FOCK APPROXIMATION

In the previous sections, we first split our TISE into a nuclear and an electronic part using the BOA, and then dealt with the nuclear part in a classical way.

The rest of the chapter will deal with how to obtain the potential on which we run our MD. the accuracy of the electronic wavefunction, and the calculation of its properties, which are used in the dynamics. Different methods to solve the electronic TISE, and their accuracy will be presented. We will start with the Hartree–Fock (HF) method, as it is the most basic ab initio method. Almost all quantum chemistry programs use the solutions or the concepts of the HF approximation.

One very important feature of the HF method is the variational principle. It states that the energy obtained from any trial wavefunction $|\psi_{\text{trial}}\rangle$ is equal or higher than the exact energy E_{exact} , i.e.

$$\langle \psi_{\text{trial}} | \hat{H} | \psi_{\text{trial}} \rangle = E_{\text{trial}} \geq E_{\text{exact}}. \quad (2.4.1)$$

Therefore, the best wavefunction is always the one yielding the lowest energy.

2.4.1 The Hartree–Fock Equations

As the electronic Schrödinger equation still presents a n -body problem which cannot be solved analytically one needs to approach this task in an approximate way. One prominent method of doing so is the Hartree–Fock method which reduces the n -body problem to n one-body problems. Since electrons are fermions and the Pauli principle states that a wavefunction for any fermionic many-body system must be antisymmetric with respect to an interchange of two particles, the used many-electron wavefunction must obey this principle, and one way of imposing this constraint mathematically is writing the Hartree–Fock wavefunction ($|\Psi_{\text{HF}}\rangle$) as a Slater determinant:

$$|\Psi_{\text{HF}}\rangle = \frac{1}{\sqrt{n!}} \begin{vmatrix} \chi_1(1) & \chi_1(2) & \dots & \chi_1(n) \\ \chi_2(1) & \chi_2(2) & \dots & \chi_2(n) \\ \vdots & & \ddots & \vdots \\ \chi_n(1) & \chi_n(2) & \dots & \chi_n(n) \end{vmatrix}. \quad (2.4.2)$$

We thereby manage to approach the n -body problem – which, as stated above, cannot be treated analytically – into n one-body problems, i.e. n one-body functions. Each of these functions consists of n one-electron spin orbitals $|\chi_i(\mathbf{x}_j)\rangle$, which themselves consist of a spatial orbital $|\phi_i\rangle$ and a spin part.

In the HF approximation, the Fock operator \hat{f} is introduced as^{45(p. 114)}

$$\hat{f}(1) = -\frac{1}{2}\Delta_1^2 - \sum_{A=1}^N \frac{Z_A}{r_{1A}} + \hat{v}_{\text{HF}}(1). \quad (2.4.3)$$

$\hat{v}_{\text{HF}}(1)$ is the average potential acting on electron 1, caused by all other electrons.

The HF equations are now defined as

$$\hat{f}(1) |\chi_i(1)\rangle = \epsilon_i |\chi_i(1)\rangle, \quad (2.4.4)$$

with ϵ_i being the orbital energy of orbital i .

To simplify the HF equations one can restrict the method to closed-shell configurations, which is known as restricted HF (RHF). One can also describe the mathematically more demanding open-shell systems using unrestricted HF (UHF)⁴⁶.

The HF equations are solved using the the Roothaan–Hall formalism⁴⁷. In it, the n coupled differential equations are transformed to n linear equations by expressing the space orbitals ϕ as linear combination of basis functions $|\zeta\rangle$, with C being the molecular orbital (MO) expansion coefficients.

$$|\phi_i\rangle = \sum_{\mu=1}^G C_{i\mu} |\zeta_\mu\rangle. \quad (2.4.5)$$

2.5 SINGLE-REFERENCE CORRELATION METHODS

The HF method may be quite successful in some cases, but it has many limitations, and often fails to give quantitatively or even qualitatively correct results. The error comes from the mean-field approximation,

In the limit of the number of spatial orbitals $K \rightarrow \infty$, equation 2.5.5 represents a full CI wavefunction, considering all excitations up to the maximum level.

Looking at the expectation value of the total energy of the system $E_{\text{CI}} = \langle \Phi_{\text{CI}} | \hat{H} | \Phi_{\text{CI}} \rangle$, and applying the variational principle yields the full CI matrix:

$$\begin{pmatrix} \langle \Psi_{\text{HF}} | \hat{H} | \Psi_{\text{HF}} \rangle & 0 & \langle \Psi_{\text{HF}} | \hat{H} | D \rangle & 0 & 0 & \dots \\ & \langle S | \hat{H} | S \rangle & \langle S | \hat{H} | D \rangle & \langle S | \hat{H} | T \rangle & 0 & \dots \\ & & \langle D | \hat{H} | D \rangle & \langle D | \hat{H} | T \rangle & \langle D | \hat{H} | Q \rangle & \dots \\ & & & \langle T | \hat{H} | T \rangle & \langle T | \hat{H} | Q \rangle & \dots \\ & & & & \langle Q | \hat{H} | Q \rangle & \dots \\ \vdots & \vdots & \vdots & \vdots & \vdots & \ddots \end{pmatrix} \quad (2.5.7)$$

S , D , T , and Q represent single, double, triple, and quadruple excitations, respectively. The full CI matrix is hermitian, therefore only the upper triangle is shown. According to Brillouin's theorem^{45(p. 158)} the matrix elements between the HF determinant and single excited determinants are zero. The other zero-valued matrix elements occur as a result of the Slater–Condon rules^{45(p. 70)}, which state that elements whose determinants differ by more than two spin orbitals are zero. Applying both Brillouin's theorem and the Slater–Condon rules leads to a sparse and approximately block-diagonal $\binom{2K}{n} \times \binom{2K}{n}$ matrix. Since it is not feasible to calculate this matrix for all but very small systems, one has to obtain a smaller, more manageable matrix by reducing the size of the n -electron basis. One method to do so is truncating the CI expansion. One example of this approximation is to allow only double excitations to interact directly with the HF determinant. When looking at the calculation of E_{corr} for the full CI wavefunction

$$E_{\text{corr}} = \sum_{a < b} \sum_{r < s} c_{ab}^{rs} \langle \Psi_{\text{HF}} | \hat{H} | \Psi_{ab}^{rs} \rangle, \quad (2.5.8)$$

one can see that using only double excitations yields a good approximation for the ground state correlation energy⁵⁰. Nevertheless, it is not exact, as one has to consider that the coefficients c_{ab}^{rs} are dependent on the inclusion of other excitation levels. This scheme is called CI doubles (CID). Even if the single excited Slater determinants do not contribute directly in equation 2.5.8, they do affect the doubles coefficients and therefore the correlation energy. Although this effect is rather small it is important for many molecular properties, like dipole moments. As there are only $n(2K - n)$ singles, compared to $n(2K - n)(n - 1)(2K - n - 1)$ doubles they are also normally included in the CI calculation, resulting in the so-called CI singles and doubles (CISD) method. Including higher levels of excitation results in very small contributions, at least for small molecules. When also introducing triples and quadruples (CISDTQ) one can get quite close to the full CI result for small systems,⁵⁰ but unfortunately this method scales with K^{10} , compared to K^6 for CISD. This scaling makes it effectively as impractical as full CI for most systems.

A major drawback of truncated CI is its size inconsistency. As the CI expansion is cut at a certain level of excitation the error in energy does

not scale linearly with the system size, i.e. the number of particles. Therefore, when using the same truncated CI method, the error in energy for a non-interacting ensemble of molecules is not the same as the sum of the errors for the individual isolated molecules. There are several correction methods available with the most widely known being the Davidson correction⁵¹. By applying

$$\Delta E_Q = (1 - c_{\text{HF}})^2 (E_{\text{CISD}} - E_{\text{HF}}) \quad (2.5.9)$$

a posteriori to the total energy one can estimate the contribution of quadruples to the CISD, thereby improving the size-consistency. CISD using this Davidson correction is usually denoted as CISD+Q.

Another useful approximation to reduce the CI problem is the frozen core approximation. In it, all excitations from low-lying occupied orbitals are neglected. The reason this can be done is that these orbitals lie energetically much lower than the valence shell orbitals and there is no relevant excitation occurring between them. So the error introduced by using the frozen core approximation is constant with respect to the electronic state, and when calculating energy differences, the error cancels out.

2.5.2 Perturbation Theory

PT is an approach that works as an alternative to the variational but size inconsistent CI method. The general idea is that the unknown problem we want to solve is very close to an already solved problem. Thereby our solutions, like energies or wavefunctions, are very close to the solutions of the known system and the aim of PT is to find these small, although significant change as a function of the already known equation.

General Perturbation Theory

The crucial part of the PT is splitting up the Hamiltonian into a reference (zeroth-order) part $\hat{H}^{(0)}$, and the above mentioned “small” perturbation part \hat{H}' using

$$\hat{H} = \hat{H}^{(0)} + \lambda \hat{H}', \quad (2.5.10)$$

with $0 \leq \lambda \leq 1$. Assuming we know the solutions of the unperturbed Schrödinger equation, i.e. of the eigenvalue equation of $\hat{H}^{(0)}$ formulating the $\{|\phi_{\mathcal{K}}^{(0)}\rangle\}$ as a complete set, we get

$$\hat{H}^{(0)} |\phi_{\mathcal{K}}^{(0)}\rangle = E_{\mathcal{K}}^{(0)} |\phi_{\mathcal{K}}^{(0)}\rangle. \quad (2.5.11)$$

Looking at the perturbed Schrödinger equation

$$\hat{H} |\phi_{\mathcal{K}}\rangle = E_{\mathcal{K}} |\phi_{\mathcal{K}}\rangle, \quad (2.5.12)$$

one can set $\lambda = 0$ to obtain equation 2.5.11. By gradually increasing the perturbation, i.e. by increasing λ , the changes in $E_{\mathcal{K}}$ and $|\phi_{\mathcal{K}}\rangle$ can be expressed as a power series expansion with respect to λ :

$$E_{\mathcal{K}}(\lambda) = E_{\mathcal{K}}^{(0)} + \lambda E_{\mathcal{K}}^{(1)} + \lambda^2 E_{\mathcal{K}}^{(2)} + \dots \quad (2.5.13)$$

$$|\phi_{\mathcal{K}}\rangle(\lambda) = |\phi_{\mathcal{K}}^{(0)}\rangle + \lambda |\phi_{\mathcal{K}}^{(1)}\rangle + \lambda^2 |\phi_{\mathcal{K}}^{(2)}\rangle + \dots \quad (2.5.14)$$

Inserting these two series and equation 2.5.10 into equation 2.5.12 yields

$$\begin{aligned} & \left(\hat{H}^{(0)} + \lambda \hat{H}^{(1)} \right) \left(\left| \phi_{\mathcal{K}}^{(0)} \right\rangle + \lambda \left| \phi_{\mathcal{K}}^{(1)} \right\rangle + \lambda^2 \left| \phi_{\mathcal{K}}^{(2)} \right\rangle + \dots \right) = \\ & \left(E_{\mathcal{K}}^{(0)} + \lambda E_{\mathcal{K}}^{(1)} + \lambda^2 E_{\mathcal{K}}^{(2)} + \dots \right) \left(\left| \phi_{\mathcal{K}}^{(0)} \right\rangle + \lambda \left| \phi_{\mathcal{K}}^{(1)} \right\rangle + \lambda^2 \left| \phi_{\mathcal{K}}^{(2)} \right\rangle + \dots \right). \end{aligned} \quad (2.5.15)$$

Collecting the terms in which the coefficients of the same powers of λ are equal on both sides produces a series of equations, one for each power of λ :

$$\begin{aligned} \lambda^0 : \hat{H}^{(0)} \left| \phi_{\mathcal{K}}^{(0)} \right\rangle &= E_{\mathcal{K}}^{(0)} \left| \phi_{\mathcal{K}}^{(0)} \right\rangle \\ \lambda^1 : \hat{H}^{(0)} \left| \phi_{\mathcal{K}}^{(1)} \right\rangle + \hat{H}^{(1)} \left| \phi_{\mathcal{K}}^{(0)} \right\rangle &= E_{\mathcal{K}}^{(0)} \left| \phi_{\mathcal{K}}^{(1)} \right\rangle + E_{\mathcal{K}}^{(1)} \left| \phi_{\mathcal{K}}^{(0)} \right\rangle \\ \lambda^2 : \hat{H}^{(0)} \left| \phi_{\mathcal{K}}^{(2)} \right\rangle + \hat{H}^{(1)} \left| \phi_{\mathcal{K}}^{(1)} \right\rangle &= E_{\mathcal{K}}^{(0)} \left| \phi_{\mathcal{K}}^{(2)} \right\rangle + E_{\mathcal{K}}^{(1)} \left| \phi_{\mathcal{K}}^{(1)} \right\rangle + E_{\mathcal{K}}^{(2)} \left| \phi_{\mathcal{K}}^{(0)} \right\rangle \\ &\vdots \\ \lambda^v : \hat{H}^{(0)} \left| \phi_{\mathcal{K}}^{(v)} \right\rangle + \hat{H}^{(1)} \left| \phi_{\mathcal{K}}^{(v-1)} \right\rangle &= \sum_{i=0}^v E_{\mathcal{K}}^{(i)} \left| \phi_{\mathcal{K}}^{(v-i)} \right\rangle \end{aligned} \quad (2.5.16)$$

By normalizing the resulting wavefunction

$$\left\langle \phi_{\mathcal{K}} \left| \phi_{\mathcal{K}}^{(0)} \right\rangle = 1, \quad (2.5.17)$$

one ensures that all correction terms are orthogonal to the unperturbed wavefunction, i.e. that

$$\left(\left\langle \phi_{\mathcal{K}}^{(0)} \left| + \lambda \left\langle \phi_{\mathcal{K}}^{(1)} \left| + \lambda^2 \left\langle \phi_{\mathcal{K}}^{(2)} \left| + \dots \right\rangle \right| \phi_{\mathcal{K}}^{(0)} \right\rangle = 1, \quad (2.5.18)$$

$$\left\langle \phi_{\mathcal{K}}^{(v)} \left| \phi_{\mathcal{K}}^{(0)} \right\rangle = \delta_{0v}. \quad (2.5.19)$$

Now it is possible to project the last equation in 2.5.16 on $\left\langle \phi_{\mathcal{K}}^{(0)} \left| \right.$ to obtain an expression for the correction term

$$E_{\mathcal{K}}^{(1)} = \left\langle \phi_{\mathcal{K}}^{(0)} \left| \hat{H}^{(1)} \left| \phi_{\mathcal{K}}^{(i-1)} \right\rangle, \quad (2.5.20)$$

which is useful only if we calculate $\phi_{\mathcal{K}}^{(i-1)}$. If we express $\left| \phi_{\mathcal{K}}^{(1)} \right\rangle$ as a linear combination of the $\left\{ \left| \phi_{\mathcal{K}}^{(0)} \right\rangle \right\}$ we get

$$\left| \phi_{\mathcal{K}}^{(1)} \right\rangle = \sum_{v \neq \mathcal{K}} c_v \left| \phi_v^{(0)} \right\rangle, \quad (2.5.21)$$

which can be done as we defined earlier that $\left\{ \left| \phi_{\mathcal{K}}^{(0)} \right\rangle \right\}$ forms a complete set. Putting above equation into the λ^1 part of equation 2.5.16 yields

$$\sum_{v \neq \mathcal{K}} = \left(\hat{H}^{(0)} - E_{\mathcal{K}}^{(0)} \right) c_v \left| \phi_v^{(0)} \right\rangle + \hat{H}^{(1)} \left| \phi_{\mathcal{K}}^{(0)} \right\rangle = E_{\mathcal{K}}^{(1)} \left| \phi_{\mathcal{K}}^{(0)} \right\rangle. \quad (2.5.22)$$

Now, using equation 2.5.11, projecting on $\left\langle \phi_l^{(0)} \left| \right.$, and considering equation 2.5.19 we get

$$c_l = \frac{\left\langle \phi_l^{(0)} \left| \hat{H}^{(1)} \left| \phi_{\mathcal{K}}^{(0)} \right\rangle \right\rangle}{E_{\mathcal{K}}^{(0)} - E_l^{(0)}} \quad (2.5.23)$$

for all $l \in v$. To obtain the second order energy correction we combine equations 2.5.20 and 2.5.23

$$E_{\mathcal{K}}^{(2)} = \sum_{v \neq \mathcal{K}} \frac{\langle \phi_v^{(0)} | \hat{H}^{(1)} | \phi_{\mathcal{K}}^{(0)} \rangle \langle \phi_{\mathcal{K}}^{(0)} | \hat{H}^{(1)} | \phi_v^{(0)} \rangle}{E_{\mathcal{K}}^{(0)} - E_v^{(0)}}, \quad (2.5.24)$$

which can be done analogously for higher powers of λ , resulting in higher-order corrections.

Møller–Plesset Perturbation Theory

To perform PT calculations, one needs a suitable definition of $\hat{H}^{(0)}$, $|\phi_{\mathcal{K}}^{(0)}\rangle$, and $\hat{H}^{(1)}$. One very prominent way of doing so is the Møller–Plesset (MP) perturbation theory⁵² in which the unperturbed wavefunctions $|\phi^{(0)}\rangle$ ⁱⁱⁱ are the solutions of the HF equations, and $\hat{H}^{(0)}$ is the sum of the fock operators, i.e.

$$\hat{H}^{(0)} = \sum_i \sum_j \hat{f}(i) = \sum_i \left(\hat{h}(i) + \sum_j \left[\hat{f}_j^{\text{HF}}(i) - \hat{K}_j^{\text{HF}}(i) \right] \right). \quad (2.5.25)$$

The corresponding zeroth-order energy is

$$E^{(0)} = \langle \phi^{(0)} | \hat{H}^{(0)} | \phi^{(0)} \rangle = \sum_{i=1}^n \epsilon_i, \quad (2.5.26)$$

which is just the sum of the energies of the occupied HF orbitals ϵ_i . As this is less accurate than the HF energy, one has to include higher order terms to improve the energies.

According to equation 2.5.10 the first-order perturbed Hamiltonian is

$$\hat{H}^{(1)} = \hat{H} - \hat{H}^{(0)} = \sum_i \sum_{j>i}^n \frac{1}{r_{ij}} - \sum_i \sum_b \left(\hat{f}_b^{\text{HF}}(i) - \hat{K}_b^{\text{HF}}(i) \right) \quad (2.5.27)$$

Therefore, the perturbation is equal to the real electron-electron repulsion minus the averaged HF potential. The first order perturbation energy is

$$E^{(1)} = \langle \phi^{(0)} | \hat{H}^{(1)} | \phi^{(0)} \rangle, \quad (2.5.28)$$

which we can combine with equation 2.5.26 to get

$$\begin{aligned} E^{(0)} + E^{(1)} &= \langle \phi^{(0)} | \hat{H}^{(0)} | \phi^{(0)} \rangle + \langle \phi^{(0)} | \hat{H}^{(1)} | \phi^{(0)} \rangle \\ &= \langle \phi^{(0)} | \hat{H}^{(0)} + \hat{H}^{(1)} | \phi^{(0)} \rangle = \langle \phi^{(0)} | \hat{H} | \phi^{(0)} \rangle. \end{aligned} \quad (2.5.29)$$

Going from zeroth to first-order is equivalent to the HF result. If we want to go beyond the HF level, and include electron correlation effects, we need to use at least Møller–Plesset second-order (MP2) corrections.

To get the MP2 correction energy $E^{(2)}$, we need the matrix elements $\langle \phi^{(0)} | \hat{H}^{(1)} | \phi_{\mathcal{K}}^{(0)} \rangle$, as introduced in equation 2.5.24. Here, $\langle \phi^{(0)} |$ is the ground state wavefunction $\langle \Psi_{\text{HF}} |$, and $|\phi_{\mathcal{K}}^{(0)}\rangle$ are the excited Slater

ⁱⁱⁱ We will drop the index k unless it is explicitly necessary, as we will only deal with the ground state wavefunction in this section

determinants, with $\mathcal{K} \neq 0$. As mentioned above, the Slater–Condon rules dictate that for two-electron operators, considering the ground state, only terms up to double excitations are not zero. The single excitation term, defining $S = \sum_{ar} |\phi_a^r\rangle$, is

$$\begin{aligned} \langle \Psi_{\text{HF}} | \hat{H}^{(1)} | S \rangle &= \langle \Psi_{\text{HF}} | \hat{H} - \hat{H}^{(0)} | S \rangle = \\ \langle \Psi_{\text{HF}} | \hat{H} - \sum_{i=1}^n \hat{f}(i) | S \rangle &= \langle \Psi_{\text{HF}} | \hat{H} | S \rangle - \sum_{i=1}^n \epsilon_i \langle \Psi_{\text{HF}} | S \rangle. \end{aligned} \quad (2.5.30)$$

The first term of the result in the above equation is zero due to the Brillouin’s theorem, as mentioned before, and the second term vanishes due to the orthonormality of the Slater determinants. Therefore, we do not have to consider the single excitation term in our calculation of equation 2.5.24, and it becomes a sum over doubly-excited Slater determinants $|\phi_{ab}^{rs}\rangle$ only. Expressing the denominator according to equation 2.5.26 and applying the Slater–Condon rules yields (in Dirac notation):

$$E^{(2)} = \sum_{a < b} \sum_{r < s} \frac{(\langle ab | rs \rangle - \langle ab | sr \rangle)^2}{\epsilon_a + \epsilon_b - \epsilon_r - \epsilon_s} \quad (2.5.31)$$

This equation is an expression for the MP2 correlation energy which, as stated above is an improvement to the MP1 energy, where the latter is equal to the HF result.

The MP approach is size-consistent but it is non-variational. Adding higher terms of correlation will cause the energies to oscillate around the exact value and diverge at higher MP orders. However, since we are usually dealing with relative energies this is not such a crucial problem. When going to higher orders of correlation computer time increases. MP2 is a widely used method and scales with K^5 . MP3 is usually not used as it yields poor results due to the oscillations around the exact value, and MP4 scales with K^7 .

2.5.3 The Coupled-Cluster Method

Another method to describe electron correlation by an infinite series expansion is the coupled cluster (CC) method. The general idea is to add correlation terms to non-interacting electrons. These terms describe the contribution by independent electron pairs (this correlates to the doubles contribution in CI or MP), independent electron pair groups (two or more independent electron pairs), and so on. The resulting CC wavefunction can now be expressed as

$$|\Psi_{\text{CC}}\rangle = e^{\hat{T}} |\Psi_{\text{HF}}\rangle. \quad (2.5.32)$$

The exponential term can be expressed as a Taylor expansion,

$$e^{\hat{T}} = 1 + \hat{T} + \frac{1}{2}\hat{T}^2 + \frac{1}{6}\hat{T}^3 + \dots, \quad (2.5.33)$$

with the cluster operator \hat{T} defined as

$$\hat{T} = \sum_{i=1}^n \hat{T}_i. \quad (2.5.34)$$

The different \hat{T}_i operators create all the respective i -tuple excited configurations from the ground state $|\Psi_{\text{HF}}\rangle$. In the second quantisation formalism, they are expressed as

$$\hat{T}_1 = \sum_a \sum_r t_a^r \hat{a}_r^\dagger \hat{a}_a, \quad (2.5.35)$$

$$\hat{T}_2 = \sum_{a<b} \sum_{r<s} t_{ab}^{rs} \hat{a}_s^\dagger \hat{a}_b^\dagger \hat{a}_r \hat{a}_a, \quad (2.5.36)$$

with $t_a^r, t_{ab}^{rs}, \dots$ being the amplitudes, or expansion coefficients. By expanding the exponential in equation 2.5.33 by 2.5.34 and inserting into 2.5.32 one gets

$$e^{\hat{T}} |\Psi_{\text{HF}}\rangle = \sum_{i=0}^N \hat{C}_i |\Psi_{\text{HF}}\rangle, \quad (2.5.37)$$

with N being the number of electrons, and \hat{C} being the configuration operators

$$\begin{aligned} \hat{C}_0 &= 1 \\ \hat{C}_1 &= \hat{T}_1 \\ \hat{C}_2 &= \hat{T}_2 + \frac{1}{2} \hat{T}_1^2 \\ \hat{C}_3 &= \hat{T}_3 + \hat{T}_1 \hat{T}_2 + \frac{1}{6} \hat{T}_1^3 \\ \hat{C}_4 &= \hat{T}_4 + \hat{T}_1 \hat{T}_3 + \frac{1}{2} \hat{T}_2^2 + \frac{1}{2} \hat{T}_1^2 \hat{T}_2 + \frac{1}{24} \hat{T}_1^4 \\ &\vdots \qquad \qquad \qquad \vdots \end{aligned} \quad (2.5.38)$$

Here, we see which terms apply at which excitation level. \hat{C}_0 leaves the HF wavefunction intact, and \hat{C}_1 adds singly excited states. When looking at \hat{C}_2 , there are two terms that contribute to the description of doubly excited states, which are the description of an interacting \hat{T}_2 , or a non-interacting \hat{T}_1 electron pair. The higher terms in equation 2.5.38 have more processes contributing, like e.g. interaction of an electron triple, denoted as \hat{T}_3 .

Carrying out the expansion to infinity, one obtains the CI wavefunction. As this is, like in the CI case, not feasible for most systems the CC wavefunction has to be truncated. However, compared to CI, the truncation does not happen at a certain level of excitation, but rather at a certain level of \hat{T}_n in the exponential. As a result, when cutting at the \hat{T}_2 level, the terms $\hat{T}_1 + \hat{T}_2, \frac{1}{2} \hat{T}_1^2, \hat{T}_1 \hat{T}_2, \frac{1}{2} \hat{T}_2^2, \dots$ are still present. It can be shown that this method of truncation leaves the wavefunction size-consistent.^{53(p. 547)}

The most common CC method is the coupled-cluster singles and doubles (CCSD) model. It uses the Taylor expansion until the \hat{T}_2 term. This includes not only the $\hat{T}_1 + \hat{T}_2$ term, but also the terms $\frac{1}{2} \hat{T}_1^2, \hat{T}_1 \hat{T}_2, \frac{1}{2} \hat{T}_2^2, \dots$ resulting in a better description of the systems than with CISD.

THE COUPLED CLUSTER EQUATIONS Having defined our wavefunction, we have to solve the TISE:

$$\hat{H} e^{\hat{T}} |\Psi_{\text{HF}}\rangle = E e^{\hat{T}} |\Psi_{\text{HF}}\rangle. \quad (2.5.39)$$

Multiplying both sides with $e^{-\hat{T}}$ yields the equation

$$e^{-\hat{T}} \hat{H} e^{\hat{T}} |\Psi_{\text{HF}}\rangle = E |\Psi_{\text{HF}}\rangle, \quad (2.5.40)$$

whose left hand side can be expressed as a commutator expansion:^{53(P. 544)}

$$\begin{aligned} e^{-\hat{T}} \hat{H} e^{\hat{T}} &= \hat{H} + [\hat{H}, \hat{T}] + \frac{1}{2!} [[\hat{H}, \hat{T}], \hat{T}] \\ &\quad + \frac{1}{3!} [[[\hat{H}, \hat{T}], \hat{T}], \hat{T}] + \frac{1}{4!} [[[[\hat{H}, \hat{T}], \hat{T}], \hat{T}], \hat{T}]. \end{aligned} \quad (2.5.41)$$

$[\hat{H}, \hat{T}] = \hat{H}\hat{T} - \hat{T}\hat{H}$ is the commutator of the corresponding operators. It can be shown that this expansion is finite by using the second quantization formalism, and the anticommutator relations⁵⁴.

In order to find the CC wavefunction, one needs to find all the amplitudes $t_{a'}^r, t_{ab'}^{rs}, \dots$ which have not been set equal to 0 by the truncation of \hat{T} . By projecting $\langle \Psi_{ab\dots}^{rs\dots} |$ onto the TISE (2.5.40), yielding a set of non-linear equations, which we can set equal 0 due to the orthogonality of the Slater determinants:

$$\begin{aligned} \langle \Psi_{ab\dots}^{rs\dots} | \hat{H} + [\hat{H}, \hat{T}] + \frac{1}{2!} [[\hat{H}, \hat{T}], \hat{T}] + \frac{1}{3!} [[[[\hat{H}, \hat{T}], \hat{T}], \hat{T}] \\ + \frac{1}{4!} [[[[[[\hat{H}, \hat{T}], \hat{T}], \hat{T}], \hat{T}] | \Psi_{\text{HF}}\rangle = 0. \end{aligned} \quad (2.5.42)$$

This set of equations can now be solved iteratively until all the amplitudes have converged. Then, equation 2.5.40 can be projected on $\langle \Psi_{\text{HF}} |$ yielding

$$E = \langle \Psi_{\text{HF}} | e^{-\hat{T}} \hat{H} e^{\hat{T}} | \Psi_{\text{HF}} \rangle. \quad (2.5.43)$$

One has to keep in mind that this formulation is non-variational, as the above formulation for the energy differs from the variational expression

$$E^{\text{var}} = \langle \Psi_{\text{HF}} | \hat{H} | \Psi_{\text{HF}} \rangle, \quad (2.5.44)$$

as $e^{-\hat{T}} \neq e^{\hat{T}}$.

EQUATION OF MOTION COUPLED CLUSTER The equation of motion coupled cluster (EOM-CC) method allows the calculation of excited state energies. We introduce an operator \hat{U}_k which, acting on $|\Psi_{\text{CC}}\rangle$, creates the k th excited wavefunction

$$|\phi_k\rangle = \hat{U}_k |\Psi_{\text{CC}}\rangle. \quad (2.5.45)$$

The \hat{U}_k operators are defined as

$$\hat{U}_k = \sum_{i=0}^n \hat{U}_{k,i}, \quad (2.5.46)$$

which for double excitations, i.e. EOM-CCSD, means a cutoff at $i = 2$ resulting in

$$\begin{aligned}\hat{U}_{k,0} &= \tau_0(k), \\ \hat{U}_{k,1} &= \sum_a \sum_r \tau_a^r(k) \hat{a}_r^\dagger \hat{a}_a, \\ \hat{U}_{k,2} &= \sum_{a<b} \sum_{r<s} \tau_{ab}^{rs}(k) \hat{a}_s^\dagger \hat{a}_b \hat{a}_r^\dagger \hat{a}_a.\end{aligned}\quad (2.5.47)$$

Inserting equation 2.5.47 into 2.5.45 yields

$$\begin{aligned}|\phi_k\rangle &= \tau_0(k) |\Psi_{\text{HF}}\rangle + \sum_a \sum_r \tau_a^r(k) t_a^r \hat{a}_r^\dagger \hat{a}_a |\Psi_{\text{HF}}\rangle \\ &\quad + \sum_{a<b} \sum_{r<s} \tau_{ab}^{rs}(k) t_{ab}^{rs} \hat{a}_s^\dagger \hat{a}_b \hat{a}_r^\dagger \hat{a}_a |\Psi_{\text{HF}}\rangle\end{aligned}\quad (2.5.48)$$

as a formula for the construction of the excited wavefunctions. Inserting equation 2.5.48 into the TISE one obtains

$$\hat{H} |\phi_k\rangle = E_k |\phi_k\rangle, \quad (2.5.49)$$

which can be expanded by equations 2.5.39 and 2.5.45 into

$$\hat{H} \hat{U}_k e^{\hat{T}} |\Psi_{\text{HF}}\rangle = E_k \hat{U}_k |\Psi_{\text{HF}}\rangle. \quad (2.5.50)$$

Using the fact that \hat{U}_k and $e^{-\tau}$ commute^{53(p. 158)} we can premultiply the above equation with $e^{-\tau}$, yielding

$$e^{-\tau} \hat{H} e^{\tau} \hat{U}_k |\Psi_{\text{HF}}\rangle = E_k \hat{U}_k |\Psi_{\text{HF}}\rangle. \quad (2.5.51)$$

If we do not take the CC ground state equation equation 2.5.40, premultiply with \hat{U}_k , and subtract equation 2.5.51, we get

$$\left[e^{-\hat{T}} \hat{H} e^{\hat{T}}, \hat{U}_k \right] |\Psi_{\text{HF}}\rangle = (E_k - E_0) \hat{U}_k |\Psi_{\text{HF}}\rangle. \quad (2.5.52)$$

In order to obtain the amplitudes $\tau_{ij\dots}^{rs\dots}$, we project the equation above on $\langle \Psi_{ab\dots}^{rs\dots} |$ to get the EOM-CCSD equations

$$\left\langle \Psi_{ab\dots}^{rs\dots} \left| \left[e^{-\hat{T}} \hat{H} e^{\hat{T}}, \hat{U}_k \right] \right| \Psi_{\text{HF}} \right\rangle = (E_k - E_0) \langle \Psi_{ab\dots}^{rs\dots} | \hat{U}_k | \Psi_{\text{HF}} \rangle. \quad (2.5.53)$$

The number of equations needed for each excited state is equal to the number of Slater determinants of all excited states plus the ground state. The excitation energies are defined as the $E_k - E_0$.

2.6 MULTI-REFERENCE CORRELATION METHODS

Single-reference correlation methods, as presented in section 2.5, are based on a single HF Slater determinant reference wavefunction. As said before, this ansatz is a poor approximation for systems with a large amount of static correlation. In these cases, a single Slater determinant as reference wavefunction cannot yield accurate results. One way to improve these results is to use linear combinations of multiple Slater determinants as reference functions

$$|\Phi_{\text{MCSCF}}\rangle = \sum_{\mathcal{M}} c_{\mathcal{M}} |\Psi_{\mathcal{M}}\rangle, \quad (2.6.1)$$

yielding a multiconfigurational wavefunction. This equation is similar to the CI expansion (2.5.5) shown before, but, unlike CI, not only the expansion coefficients $c_{\mathcal{M}}$, but also the configuration (the orbital coefficients from 2.4.5) themselves are optimized at once. The problem of which configurations contribute more to the energy depends heavily on the applied method. In the following, when introducing the multiconfigurational self consistent field (MCSCF) method, we will stick to the general form of the wavefunction, before discussing the choice of reference configurations.

2.6.1 The Multi-Configurational Self Consistent Field Method

In the MCSCF method, one can express the electronic Hamiltonian as⁵⁵

$$\hat{H} = \sum_{ij} \langle \chi_i | \hat{h} | \chi_j \rangle \hat{a}_i^\dagger \hat{a}_j + \frac{1}{2} \sum_{ijkl} \langle \chi_i \chi_j | \chi_k \chi_l \rangle \hat{a}_i^\dagger \hat{a}_j \hat{a}_k^\dagger \hat{a}_l, \quad (2.6.2)$$

by expressing the one- and two-electron integrals in the Dirac notation (see section 2.4), and letting the addends go over all spin orbitals. Considering the fact, that the Hamiltonian is not spin-dependent one can reformulate using spatial orbitals:

$$\begin{aligned} \hat{H} &= \sum_{ij} (\phi_i | \hat{h} | \phi_j) \hat{E}_{ij} + \frac{1}{2} \sum_{ijkl} (\phi_i \phi_j | \phi_k \phi_l) \hat{E}_{ij,kl} \\ &= \sum_{ij} h_{ij} \hat{E}_{ij} + \frac{1}{2} \sum_{ijkl} g_{ijkl} \hat{E}_{ijkl}. \end{aligned} \quad (2.6.3)$$

h_{ij} and g_{ijkl} are the one-electron and two-electron orbitals introduced in section 2.4, and \hat{E}_{ij} and \hat{E}_{ijkl} are the spin-summed excitation operators

$$\hat{E}_{ij} = \hat{a}_{i\alpha}^\dagger \hat{a}_{j\alpha} + \hat{a}_{i\beta}^\dagger \hat{a}_{j\beta}, \quad (2.6.4)$$

$$\hat{E}_{ijkl} = \hat{E}_{ij} \hat{E}_{kl} - \delta_{jk} \hat{E}_{il}. \quad (2.6.5)$$

The expectation value of this Hamiltonian is

$$\begin{aligned} E_{\text{MCSCF}} &= \langle \Phi_{\text{MCSCF}} | \hat{H} | \Phi_{\text{MCSCF}} \rangle = \sum_{ij} h_{ij} \sum_{mn} c_m^* c_n \langle \Psi_m | \hat{E}_{ij} | \Psi_n \rangle \\ &+ \frac{1}{2} \sum_{ijkl} g_{ijkl} \sum_{mn} c_m^* c_n \langle \Psi_m | \hat{E}_{ijkl} | \Psi_n \rangle. \end{aligned} \quad (2.6.6)$$

To simplify this equation one can define the matrix elements

$$D_{ij}^{mn} = \langle \Psi_m | \hat{E}_{ij} | \Psi_n \rangle, \quad (2.6.7)$$

$$P_{ijkl}^{mn} = \frac{1}{2} \langle \Psi_m | \hat{E}_{ijkl} | \Psi_n \rangle, \quad (2.6.8)$$

as the one- and two-electron coupling coefficients, respectively, which themselves form

$$D_{ij} = \sum_{mn} c_m^* c_n D_{ij}^{mn}, \quad (2.6.9)$$

$$P_{ijkl} = \sum_{mn} c_m^* c_n D_{ijkl}^{mn}, \quad (2.6.10)$$

as the first- and second-order reduced density matrices. Using these relations, equation 2.6.6 can be simplified to

$$E_{\text{MCSCF}} = \sum_{ij} h_{ij} D_{ij} + \sum_{ijkl} g_{ijkl} P_{ijkl}. \quad (2.6.11)$$

Here, \mathbf{D} and \mathbf{P} depend on the expansion coefficients $c_{\mathcal{M}}$ from equation 2.6.1 and the integrals h_{ij} and g_{ijkl} contain all information about the molecular coefficients $C_{i\mu}$ (see equation 2.4.5). Both kinds of coefficients serve as variational parameters of the wavefunction. In a SCF approach the parameters are mostly optimized by combining a CI calculation and a variational determination of the MO coefficients.

STATE-AVERAGING As MCSCF is a multi-configurational method, it can be used to calculate excited states. Each excited state could be calculated separately with its own set of orbitals and CI coefficients. Although this is a valid approach, the downside is that the states are not necessarily orthogonal. This drastically complicates transition property calculations between those states. Therefore, and for the fact that it simplifies non-global minimum optimisations, another ansatz is also often used, which optimises the averaged energy of k states:

$$E_{\text{MCSCF}}^{\text{av}} = \sum_{\rho}^u \omega_{\rho} E_{\text{MCSCF},\rho} = \sum_{\rho}^u \omega_{\rho} \langle \Phi_{\text{MCSCF},\rho} | \hat{H} | \Phi_{\text{MCSCF},\rho} \rangle, \quad (2.6.12)$$

with ω_i as the normalized weights, i.e.

$$\sum_{\rho}^u \omega_{\rho} = 1. \quad (2.6.13)$$

State-averaging creates a set of orthogonal, non-interacting electronic states based on a set of common averaged orbitals. Although these orbitals are not the ideal ones for each state (compared to the respective single-state calculations), they allow the calculation of transition properties, as well as the calculation of states very close in energy, e.g. at a crossing point.

2.6.2 Active Space based MCSCF

When performing a MCSCF calculation, the choice of configurations to enter the wavefunction (2.6.1) is a crucial step in the correct description of the system. The right choice depends on the chemical problem that needs to be calculated. For ground state problems, all configurations that contribute to the ground state should be taken into account. Similarly for a bond-breaking simulation, all configurations with electrons in the involved bonding and antibonding orbitals should be considered. A very popular selection method is the complete active space self consistent field (CASSCF) approach which uses hand-selected configurations.

THE CASSCF METHOD In the CASSCF method, a certain amount of orbitals are chosen to be important and are therefore considered active. They are usually selected based on their qualitative shape from a previous RHF or UHF calculation. The configuration space is

generated by performing a full CI in the predefined active space. The remaining occupied and unoccupied orbitals are considered inactive and no excitations in and out of them are allowed. The general formalism for CASSCF calculations is $\text{CASSCF}(n_{\text{CAS}}, m_{\text{CAS}})$ with n_{CAS} active electrons in m_{CAS} active orbitals. Unfortunately, the size of the active space is limited due to the computational cost of the method. For $\text{CASSCF}(n_{\text{CAS}}, m_{\text{CAS}})$, the number of configurations of a wavefunction with a total spin S can be evaluated using the Weyl formula⁵⁶

$$N_{\text{CAS}} = \frac{2S + 1}{m_{\text{CAS}} + 1} \binom{m_{\text{CAS}} + 1}{n_{\text{CAS}}/2 - S} \binom{m_{\text{CAS}} + 1}{n_{\text{CAS}}/2 + S + 1}. \quad (2.6.14)$$

2.6.3 Complete Active Space Perturbation Theory

In the CASSCF expansion, all excitations, and therefore all correlations, in the active space are considered. Unfortunately, no correlation outside of the active space is recovered. One way to include the correlation is by using the perturbation theory on the CASSCF wavefunctions. This method is called the Complete Active Space Perturbation Theory second order (CASPT2) method⁵⁷. Similar to the Møller-Plesset theory (section 2.5.2), the Hamiltonian is partitioned with the zero-order Hamiltonian employing the CASSCF Fock operator:

$$\hat{F} = \sum_{ij} f_{ij} \hat{E}_{ij}, \quad (2.6.15)$$

with^{iv}

$$f_{ij} = h_{ij} + \sum_{ij} D_{ij} \left(g_{ijkl} - \frac{1}{2} g_{ijkl} \right). \quad (2.6.16)$$

Additionally, the first-order interaction space (FOS) is defined as

$$\hat{E}_{ij} \hat{E}_{rs} |\Phi_{\text{MCSCF}}\rangle. \quad (2.6.17)$$

The FOS includes all states generated by double excitations out of the CASSCF reference wavefunction $|\Phi_{\text{MCSCF}}\rangle$ into inactive orbitals. This is similar to MP2 where double excitations interact with the HF reference wavefunction $|\Phi_{\text{HF}}\rangle$ (section 2.5.2).

After setting up the zero-order Hamiltonian the perturbation has to be set up (see Eqn 2.5.27) before the perturbation equations (Eqn 2.5.16) can be solved. In this way, the second-order perturbed Hamiltonian can be obtained. One big problem of this approach is the presence of intruder states. Intruder states are states in the FOS with the corresponding eigenvalue to $(\hat{H}^{(0)})$ close to the eigenvalue of $|\Phi_{\text{CASSCF}}\rangle$. These intruder states cause the second-order energy to grow too large. The best way to deal with intruder states is to increase the active space to include the orbitals which cause the intruder state to interfere. This is not always possible, as one cannot increase the active space indefinitely (as explained in section 2.6.1). Therefore, a level-shift technique can be used, in which an arbitrary level-shift parameter is added to the zeroth-order Hamiltonian⁵⁸. In order to compensate the errors introduced by the level-shift, a level-shift correction is applied, which

iv the notation is the same as in section 2.4

removes the effect on the second-order energy. Therefore, if intruder states occur, the level-shift will remove them without affecting the rest of the second-order energy. If there are no intruder states however, it will have a negligible effect.

Multi-State CASPT2

For CASPT2, the CI coefficients in the multiconfigurational expansion (Eqn 2.6.1) cannot vary, as $|\Phi_{\text{MCSCF}}\rangle$ is fixed. For state averaged calculations, these wavefunctions cannot be used as a reference, and the multi-state CASPT2 (MS-CASPT2)⁵⁹ ansatz has to be used. In this ansatz, a k -dimensional reference space spanned by k state-averaged CASSCF (SA-CASSCF) wavefunctions is spanned. The reference state for any state n can be expressed as a linear combination of all the SA-CASSCF wavefunctions.

The resulting first-order wavefunction of the k CASPT2 calculations is

$$|\Psi_n\rangle = |\Phi_{\text{MCSCF},n}\rangle + |\Phi_n^{(1)}\rangle. \quad (2.6.18)$$

The k equations form the basis for the solutions for

$$(\mathbf{H} - E\mathbf{S})\mathbf{C}^{\text{MS}} = 0, \quad (2.6.19)$$

with the mixing coefficients C_{ij}^{MS} .

The matrix elements S_{ij} are defined as

$$S_{ij} = \langle \Psi_i | \Psi_j \rangle = \delta_{ij} + \langle \Psi_i^{(1)} | \Psi_j^{(1)} \rangle = \delta_{ij} + s_{ij}. \quad (2.6.20)$$

The H_{ij} matrix elements are obtained by applying a state-dependent MP partitioning of \hat{H}

$$\hat{H} = \hat{H}_i^{(0)} + \hat{H}_i^{(1)}, \quad (2.6.21)$$

and using MCSCF energies E_i and the matrix elements ϵ_{ij}

$$\langle \Phi_i | \hat{H}_i^{(0)} | \Phi_i \rangle = E_i^{(0)}, \quad (2.6.22)$$

$$\langle \Phi_i | \hat{H} | \Psi_j^{(1)} \rangle = \epsilon_{ij}. \quad (2.6.23)$$

The matrix elements H_{ij} can now be expressed as⁶⁰

$$H_{ij} = \langle \Psi_i | \hat{H} | \Psi_j \rangle = \delta_{ij}E_i + \frac{1}{2} \left(s_{ij} (E_i^{(0)} + E_j^{(0)}) + \epsilon_{ij} + \epsilon_{ji} \right). \quad (2.6.24)$$

We obtain k solutions of equation 2.6.19, which can be used in order to construct new MS-CASPT2 wavefunctions using the mixing coefficients C_{ij}^{MS}

$$|\Psi_j^{\text{MS}}\rangle = \sum_{i=1}^n C_{ij}^{\text{MS}} |\Psi_n\rangle. \quad (2.6.25)$$

2.6.4 Multi-Reference Configuration Interaction

Another method to obtain dynamic correlation outside of the CASSCF active space is the multi-reference configuration interaction (MRCI) method. The most frequently used MRCI method is MRCI using singles and doubles (MRCISD). Similarly to CI, one can use higher methods including e.g. triples, up to full MRCI.

In MRCI, the orbital space is divided into subspaces. The low lying core orbitals, whose correlation energy is independent of the environment, are denoted as frozen orbitals. All other orbitals which are occupied in any of the reference wavefunctions are called internal orbitals. Finally, all other orbitals, which are empty in any reference configurations, are external orbitals. They are used in order to correlate the internal orbitals. There is also a reference space R defined, which consists of all configurations present in the MCSCF wavefunction

$$|\Psi_R\rangle = \left(c_{\text{HF}} |\Psi_{\text{HF}}\rangle + \sum_a \sum_r c_a^r |\Psi_a^r\rangle + \sum_{ab} \sum_{rs} c_{ab}^{rs} |\Psi_{ab}^{rs}\rangle + \dots \right) \in |\Phi_{\text{MCSCF}}\rangle. \quad (2.6.26)$$

Acting all double annihilation operators $\hat{a}_a \hat{a}_b$ on each reference space function yields the $(n-2)$ -electron states $|\Psi_P\rangle$ forming the P -space. Furthermore, the S -space, containing the $(n-1)$ -electron states $|\Psi_S\rangle$ can be obtained by applying all possible creation operators \hat{a}_c^\dagger on the P space. Applying another creation operator on the S -space yields the internal space I . Therefore, the internal space is a superset of the reference space R . The MRCISD wavefunction can now be expressed as

$$|\Phi_{\text{MRCISD}}\rangle = \sum_I c_I |\Psi_I\rangle + \sum_S \sum_r c_S^r |\Psi_S^r\rangle + \sum_P \sum_{rs} c_P^{rs} |\Psi_P^{rs}\rangle, \quad (2.6.27)$$

where the single-external configurations $|\Psi_S^r\rangle$ are generated by applying \hat{a}_r^\dagger to a function of space S , and the doubly-external configurations $|\Psi_P^{rs}\rangle$ are generated by applying $\hat{a}_r^\dagger \hat{a}_s^\dagger$ to a function of space P .

2.7 CALCULATION OF IMPORTANT PROPERTIES

The previous section was dealing with the solution to the electronic TISE. For semi-classical dynamics we need a number of molecular properties which can be calculated using some of the methods explained above. The most important properties are the total energy and the gradient (i.e. the the first spatial derivative of the energy). Knowing the gradients one can evaluate the nuclear forces acting on the molecule without preliminary knowledge of the whole PES, making on-the-fly calculations possible. The important couplings for non-adiabatic dynamics are the NACs, which indicate state hopping probabilities, and the transition dipole moment, which is necessary in order to calculate the interactions with electromagnetic fields or determine initial conditions. To include surface hopping between states of different multiplicity, e.g. singlet and triplet, SOCs are also needed in the dynamics.

2.7.1 General Property Calculations

Many molecular properties can be expressed as the response of a wavefunction, operator, or an energy to a perturbation⁶¹. These perturbations can be external electric fields, geometry changes, or any other operators not included in the Hamiltonian. Similar to section 2.5.2, a parameter λ is introduced, which defines the perturbation strength. Expanding in a Taylor series, the perturbed energy is expressed as

$$E(\lambda) = E_0 + \frac{\partial E}{\partial \lambda} \lambda + \frac{1}{2} \frac{\partial^2 E}{\partial \lambda^2} \lambda^2 + \dots \quad (2.7.1)$$

This perturbed energy $E(\lambda)$ is the expectation value of the unperturbed Hamiltonian $\hat{H}^{(0)}$ with a perturbation \hat{H}' :

$$E(\lambda) = \langle \phi(\lambda) | \hat{H}^{(0)} + \lambda \hat{H}' | \phi(\lambda) \rangle. \quad (2.7.2)$$

As the wavefunction ϕ is also dependent on λ , the first derivative of the energy at $\lambda = 0$ is

$$\begin{aligned} \frac{\partial E}{\partial \lambda} \Big|_{\lambda=0} &= \left\langle \phi(0) \left| \frac{\partial}{\partial \lambda} \hat{H}^{(0)} + \lambda \hat{H}' \right| \phi(0) \right\rangle \\ &+ \left\langle \frac{\partial \phi(0)}{\partial \lambda} \left| \hat{H}^{(0)} \right| \phi(0) \right\rangle + \left\langle \phi(0) \left| \hat{H}^{(0)} \right| \frac{\partial \phi(0)}{\partial \lambda} \right\rangle. \end{aligned} \quad (2.7.3)$$

The first term is the expectation value of the perturbation over the unperturbed wavefunction, i.e.

$$\left\langle \phi(0) \left| \frac{\partial}{\partial \lambda} \hat{H}^{(0)} + \lambda \hat{H}' \right| \phi(0) \right\rangle = \langle \phi(0) | \hat{H}' | \phi(0) \rangle, \quad (2.7.4)$$

which equates the result from Rayleigh-Schrödinger perturbation theory. The two additional terms in equation 2.7.3, which are identical for a real wavefunction, are describing the response of the unperturbed wavefunction to the perturbation. Although there exists some doubt whether one can disregard these terms and still get valid property estimates⁶², there are some cases where these wavefunction responses do vanish. These wavefunctions are said to obey the Hellmann-Feynman theorem.⁶³

The wavefunctions for which this holds can be derived by looking at the response terms (equation 2.7.3):⁶¹

$$\frac{\partial \psi}{\partial \lambda} = \frac{\partial \psi}{\partial \mathfrak{C}} \frac{\partial \mathfrak{C}}{\partial \lambda} + \frac{\partial \psi}{\partial \phi} \frac{\partial \phi}{\partial \lambda}, \quad (2.7.5)$$

with \mathfrak{C} being the wavefunction parameters including both orbital and state coefficients, and ϕ being the basis function. As HF and MCSCF wavefunctions are variational, the condition that $\frac{\partial \psi}{\partial \mathfrak{C}} = 0$ must hold. If the basis functions are also independent of the perturbation (i.e. $\frac{\partial \phi}{\partial \lambda} = 0$) the Hellmann-Feynman theorem holds. For non-variational wavefunctions, as applied in state-averaged MCSCF, CI, PT, or CC the wavefunction response does not vanish and needs to be considered in all calculations.

The conceptually most simple method to solve properties despite a present wavefunction response is the finite perturbation, or numerical,

method. In it, the desired property value is calculated directly from finite differences

$$\left. \frac{\partial E}{\partial \lambda} \right|_{\lambda=0} \propto \frac{1}{\lambda} (E(\bar{\lambda}) - E(0)), \quad (2.7.6)$$

where $\bar{\lambda}$ is small. Additionally to numerical problems, which occur in all finite difference methods, the large number of calculations for vertical perturbations leads to errors.

Another approach constructs a Lagrange function \mathcal{L} . This variational Lagrangian still has the same energy as the wavefunction⁶⁴. For a CI wavefunction it is

$$\mathcal{L}_{\text{CI}} = E_{\text{CI}} + \kappa \frac{\partial E_{\text{HF}}}{\partial c}, \quad (2.7.7)$$

with κ being the Lagrange multiplier which is defined so that the energy is independent of the perturbation and stationary with respect to κ and the orbital and state coefficients. However, the wavefunction response is still necessary for higher order derivatives. One can also calculate the wavefunction response explicitly. This ansatz, which is called coupled-perturbed, is described by Almhöf and Taylor.

2.7.2 Gradient Calculations

The energy gradient is a $3N$ dimensional vector which contains the first derivative of the potential energy with respect to the nuclear coordinates. In MOLPRO, the so called Z-Vector formalism⁶⁴ is used in order to avoid the large number of calculations that would have to be carried out using the numerical, or the coupled-perturbed methods.

Looking at equation 2.7.6 for MCSCF wavefunctions, the one-electron atom-centered basis functions are dependent on the perturbation. Therefore, to calculate the gradients one needs the integrals over the derivatives of the basis functions. For the $3N$ displacement vectors, this requirement results in even more derivative integrals. To treat these derivative integrals in the same way as usual one- and two-electron integrals, one uses the characteristic that the derivative of a Gaussian basis function can be expressed as the sum of two other Gaussians.⁶¹

Further information on state-averaged MCSCF gradient calculations can be found in the literature^{65,66}.

2.7.3 Non-Adiabatic Couplings

Analytical Method

In multiconfigurational wavefunctions, one can consider two distinct contributions to calculate the analytical NAC component $T_{\beta\alpha,x}^1$ ^{67v}. Those are the CI contribution $T_{\beta\alpha,x}^{1,CI}$ and the CSF contribution $T_{\beta\alpha,x}^{1,CSF}$:

$$T_{\beta\alpha,x}^1 = \sum_i \sum_j \left\langle c_i^\beta \Psi_i \left| \frac{\partial}{\partial R_x} \right| c_j^\alpha \Psi_j \right\rangle = T_{\beta\alpha,x}^{1,CI} + T_{\beta\alpha,x}^{1,CSF}. \quad (2.7.8)$$

^v As an example, the NAC component in x direction is used in this example.

The CI contribution can be rewritten using the eigenvalue equation,

$$\mathbf{H} \cdot \mathbf{c}^\alpha = E^\alpha \mathbf{c}^\alpha, \quad (2.7.9)$$

with

$$H_{ij} = \langle \Psi | H | \Psi \rangle, \quad (2.7.10)$$

to obtain

$$T_{\beta\alpha,x}^{1,CI} = \left\langle \mathbf{c}^\beta \left| \frac{\partial}{\partial R_x} \mathbf{c}^\alpha \right. \right\rangle = \frac{1}{E^\alpha - E^\beta} \left\langle \mathbf{c}^\beta \left| \frac{\partial \mathbf{H}}{\partial R_x} \mathbf{c}^\alpha \right. \right\rangle. \quad (2.7.11)$$

The CSF contribution can be expressed as

$$T_{\beta\alpha,x}^{1,CSF} = \sum_i \sum_j (c_i^\beta)^* c_j^\alpha \left\langle \Psi_i \left| \frac{\partial}{\partial R_x} \Psi_j \right. \right\rangle, \quad (2.7.12)$$

and both terms can be solved similar to MRCI energy gradients.⁶⁷

Numerical Method

NACs can also be calculated using a numerical, or finite difference, method. Here, one can obtain the NAC vector, as well as the scalar product of the displacement vector of two slightly displaced geometries using a CI type wavefunction. Although one can calculate the full vectorial NAC by displacing the geometries in all $3N$ directions, one can also determine the nuclear velocity vector and the coupling vector needed to propagate the coefficients, see section 2.3.2. For the two geometries \mathbf{R}_0 and \mathbf{R}_1 , the two contributions are:⁶⁸

$$T_{\beta\alpha,x}^{1,CI} = \sum_i c_i^\beta(\mathbf{R}_0) \frac{c_i^\alpha(\mathbf{R}_1) - c_i^\alpha(\mathbf{R}_0)}{|\mathbf{R}_1 - \mathbf{R}_0|}, \quad (2.7.13)$$

$$T_{\beta\alpha,x}^{1,CSF} = \sum_i \sum_{i \neq j} M_{ij} \sum_\mu \sum_\nu C_{i\mu}(\mathbf{R}_0) C_{j\nu}(\mathbf{R}_1) \frac{\langle \xi_\mu(\mathbf{R}_0) | \xi_\nu(\mathbf{R}_1) \rangle}{|\mathbf{R}_1 - \mathbf{R}_0|}, \quad (2.7.14)$$

where $C_{i\mu}$ and $C_{j\nu}$ are MOs, while M_{ij} is the one-particle transition matrix and $\langle \xi | \xi \rangle$ are the overlap integrals between atomic basis functions.

2.7.4 Dipole Moments

In the presence of an external field ϵ the dipole moment can be described as

$$\boldsymbol{\mu} = - \left. \frac{\partial E}{\partial \mathbf{E}} \right|_{\mathbf{E}=0}. \quad (2.7.15)$$

This leads to certain problems, as the wavefunction response for non-variational wavefunctions is needed to calculate the energy derivative, although the basis functions are independent of the perturbation. However, when there is no external field present, i.e. when calculating the permanent dipole moment, one only needs to evaluate the expectation value of the dipole moment operator⁶¹

$$\boldsymbol{\mu}_0^{\text{el}} = e \langle \psi | \mathbf{r} | \psi \rangle. \quad (2.7.16)$$

To obtain the total dipole moment one needs to add the nuclear contribution (for electrons $e = -1$):

$$\boldsymbol{\mu}_0 = -\langle \psi | \mathbf{r} | \psi \rangle + \sum_A \mathbf{R}_A Z_A. \quad (2.7.17)$$

Evaluation of the electronic part can be done according to Almhöf and Taylor⁶².

Transition Dipole Moments

Transition dipole moments are important properties in non-adiabatic MD as they are necessary to determine the initial state populations. Another application of them is in determining the immediate action of a time-dependent electric field on the system. Transition dipole moments can generate off-diagonal elements in the electronic Hamiltonian inducing state transfers. Their calculation is similar to that of permanent dipole moments, as they are the inner-state expectation values of \mathbf{r} :

$$\boldsymbol{\mu}^{\beta\alpha} = e \langle \psi_\beta | \mathbf{r} | \psi_\alpha \rangle \quad (2.7.18)$$

In this case the transition dipole moment between states β and α can be calculated.

2.8 SPIN-ORBIT COUPLING

Each electron has a spin, which arises from the relativistic description, as in Dirac's theory.⁶⁹ This electronic spin is a non-classical property, which represents the intrinsic form of angular momentum. It has no counterpart in classical mechanics, and it is not connected to the motion of the electron around the nucleus. This angular momentum gives rise to a magnetic moment of the electron, even if there is no classical ring-current.

According to the Maxwell equations, the relative motion of the nucleus around the electrons induces a magnetic field. As in this case the electrons move around the nucleus, the magnetic moment depends on the angular momentum of the electrons.

The interaction of the magnetic moment of the electronic spin with the magnetic field arising from the electron's motion around the nucleus is defined as the SOCs. For states of different symmetry, this interaction introduces off-diagonal elements in the Hamiltonian. The calculation of these matrix elements is important for molecular dynamics and will be discussed in this section.

2.8.1 *The Spin-Orbit Operator*

As a fully Lorentz-invariant relativistic equation, the Dirac equation would provide the SOCs. However, it is a one-particle equation, and a relativistic many-body equation has yet to be derived.⁷⁰ Therefore, approximate operators have to be applied.

One way of doing so is using the Dirac-Coulomb-Breit operator, which replaces the non-relativistic Hamiltonian (Eqn 2.2.2) yielding

$$\hat{H}_e = \sum_{i=1}^n \hat{h}_D(i) + \sum_i \sum_{i \neq j} \left[\frac{1}{r_{ij}} - \hat{B}_{ij} \right], \quad (2.8.1)$$

where $\hat{h}_D(i)$ is the Dirac operator. The Breit operator \hat{B}_{ij} describes the decrease of Coulomb interaction between distant electrons arising from the influence of photons⁶¹, and from the fact that interactions are not immediate.

From the Hamiltonian in Eqn (2.8.1), Pauli derived the Breit-Pauli spin-orbit operator in 1927.⁷¹ Although he constructed it starting from the TDSE in an external field, it can also be derived from the Dirac-Coulomb-Breit operator within the Pauli approximation, i.e. for nuclei with nuclear masses $Z \ll 137$. The Breit-Pauli spin-orbit operator,⁷⁰

$$\hat{H}_{\text{BP}}^{\text{SO}} = \frac{1}{2c^2} \left[\sum_i^n \sum_A^N \frac{Z_A}{r_{iA}^3} (\hat{\mathbf{r}}_{iA} \times \hat{\mathbf{p}}_i) \cdot \hat{\mathbf{s}}_i - \sum_i^n \sum_{j \neq i}^n \frac{1}{r_{ij}^3} (\hat{\mathbf{r}}_{ij} \times \hat{\mathbf{p}}_i) \cdot (\hat{\mathbf{s}}_i + 2\hat{\mathbf{s}}_j) \right], \quad (2.8.2)$$

includes the displacement operators $\hat{\mathbf{r}}_{iA}$ and $\hat{\mathbf{r}}_{ij}$, the angular momentum operator $\hat{\mathbf{p}}_{iA}$, and the spin momentum operators $\hat{\mathbf{s}}_i$ and $\hat{\mathbf{s}}_j$. While the first sum in Eqn (2.8.2) describes the interaction of the electron's spin with the previously mentioned magnetic field, the second sum represents the electron-electron interaction. It is important to point out that the spin-orbit interaction is highly dependent on the inner-particle distances $\hat{\mathbf{r}}_{iA}$ and $\hat{\mathbf{r}}_{ij}$, and that it scales like Z_A^4 .

Although the Breit-Pauli operator is an improvement to the Dirac-Coulomb-Breit operator, it still has some major drawbacks. One of these drawbacks is the fact that it considers couplings between electronic and positronic states. For the latter, the energy is variationally unbounded, as they lie in a negative-energy continuum. Therefore, one calculates the SOCs as expectation values of $\hat{H}_{\text{BP}}^{\text{SO}}$, using a wavefunction obtained by standard electronic structure methods. This technique is correct to first-order in perturbation theory.

Another drawback of the Breit-Pauli operator is the computational demand of the two-electron integrals. As the operator acts on couples of states of different spin symmetry these integrals can be numerous. In 1996, Hess et al. proposed to treat the second sum in Eqn (2.8.2) in an averaged way (similar to the HF theory).⁷² Another approximation presented in the paper is neglecting all two-center two-electron spin-orbit integrals by replacing the molecular mean-field by a sum of orbital mean-fields. Thereby, only one-center two-electron integrals will be used. Both approximation speed up the spin-orbit calculation significantly, and they are implemented in the program AMFI⁷³ (atomic mean field integrals).

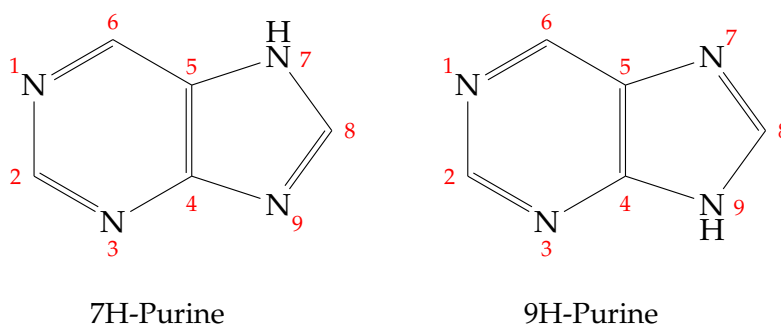
ABOUT PURINE

In this section, some general background on purine is given. First, we explain the concept of prototropic tautomerism (section 3.1) and its influence on the purine geometry. Then, the limited previous research, experimental and theoretical, is presented (section 3.2).

3.1 PROTOTROPIC TAUTOMERISM

Purine exhibits a prototropic tautomerism. This means that there is not one form of purine that dominates under all circumstances, but that the preferred form is rather dependent on the phase of matter (i.e. solid, liquid, gaseous), as well as on the solvent. The two predominant tautomers 7H- and 9H-purine are presented in figure 3.1.

Figure 3.1: Prototropic purine tautomers



In solid state, the 7H form is dominant⁷⁴, in gas phase the 9H tautomer prevails⁷⁵, and in liquid the preference depends on the polarity of the solvent⁷⁶. As our calculations are carried out for a single molecule in gas phase, we expect a higher probability of purine in the 9H form, rather than in the 7H one.

3.2 PREVIOUS RESEARCH

Although purine itself has not been found in nature yet, it is the skeletal structure of many essential and non-essential biomolecules. As mentioned in the introduction, the nucleobases A and G are purines, as are xanthine, coffeine and uric acid, among others. Despite its relevance, the scientific interest on purine itself has not been large over the last decades. Most research is focused on other purines, and mostly on the nucleobases, see e.g.⁷⁷⁻⁷⁹. To our knowledge, only very few studies have been done on the purine molecule itself. There have been several experimental papers on the electronic spectra⁸⁰⁻⁸⁴, but up to now there exist only two theoretical studies on purine. In 1999⁸⁵ Borin et al. investigated the excitation energies of several purines using CASPT2, while in 2008⁸⁶ Mburu et al. used MRMP2 to study several purines. No investigations on the deactivation mechanism of purine

after light irradiation, neither experimentally nor theoretically, have been carried out so far.

Therefore, the aim of this thesis is to get a novel understanding of the relaxation process of purine. Together with the quantum chemical calculations of Dr. Corral, our dynamical study is expected to provide a rationalization of the spectroscopic experiments of Prof. Crespo.

RESULTS FROM ELECTRONIC STRUCTURE

This chapter presents the electronic structure results obtained during this thesis. In section 4.1 the ground state purine geometries are presented and compared to the experiment, where available. Then, in section 4.2, the excited state calculations performed in this thesis are presented and discussed.

4.1 PURINE GEOMETRIES IN THE ELECTRONIC GROUND STATE

As explained in the previous section, purine exhibits a prototropic tautomerism, resulting in two separate molecules, 7H- and 9H-purine. We optimized both geometries using RI-MP2/def2-TZVP^{87,88} as implemented in TURBOMOLE⁸⁹. Both geometries are planar and exhibit C_s symmetry. The most relevant geometrical parameters for 7H- and 9H-Purine are shown in Figures 4.1 and 4.2, respectively.

Comparing the two geometries, we see several geometrical features. While the difference in the 6-member ring is minimal, the 5-member ring, on which nitrogens 7 and 9 are located, is different in both geometries. In 9H-purine, the N_7-C_8 bond (for nomenclature see Figure 3.1) is 1.316 Å long, while in 7H-purine it is 0.06 Å longer. This difference is in part caused by the fact, that in 9H-purine this bond has a large double bond character, which is shorter than the single bond it is in the 7H form. For the N_7-C_5 bond, this shortening cannot be observed to this extent, as it lacks the double bond character in both tautomers. The same characteristic occurs for the N_9-C_8 bond. All hydrogens, however have the same length for both geometries.

The ground state energies for both geometries were then refined with MOLPRO⁹⁰ using CCSD(T)⁹¹/cc-pVDZ. At this level of theory the energy difference is $E_{7H} - E_{9H} = 15.71 \text{ kJ mol}^{-1}$, which results in a probability of 544 : 1 for the molecule to be in the 9H-form in gas phase. Therefore, all further calculations were carried out using 9H-Purine.

Figure 4.1: Ground state structure of 7H-Purine optimized with RI-MP2/def2-TZVP.

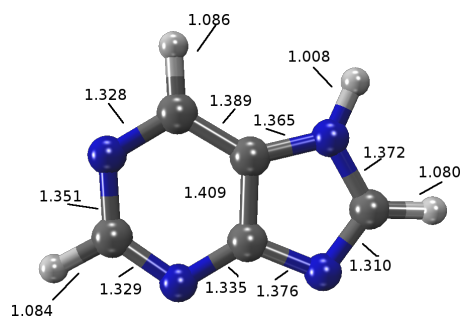


Figure 4.2: Ground state structure of 9H-Purine optimized with RI-MP2/def2-TZVP, CASSCF (in parenthesis), Experimental values in brackets.

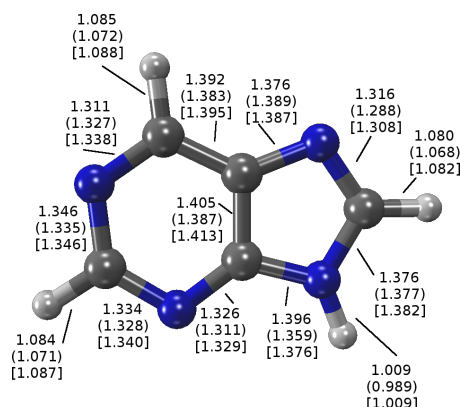


Table 4.1: Ground state energies for 9H- and 7H-Purine.

Method	Relative Energy	
	9H-Purine	7H-Purine
—		
RI-MP2/def2-TZVP	0	8.6 kJ mol ⁻¹
CCSD(T)/cc-pVDZ//RI-MP2/def2-TZVP	0	15.7 kJ mol ⁻¹

In Figure 4.2 the bond lengths for 9H-Purine also optimized at CASSCF/ANO-L^{92,93} (C,N[4s3p2d]/H[3s2p]) level of theory, as well as the experimental bond lengths are depicted. The CASSCF geometry was optimized by L. Martínez and Dr. I. Corral using MOLCAS⁹⁴. As the two calculated geometries are similar and in good agreement with the experimental one, all further calculations were carried out using the CASSCF/ANO-L geometry.

4.2 EXCITED STATE CALCULATIONS

In this section, different levels of theory will be applied to calculate the excitation energies for purine. First, in subsection 4.2.1 all used methods will be presented along with the employed quantum chemical program. Then, in section 4.2.2 the used active spaces will be presented, and in 4.2.3 the excitation energies will be discussed and compared to the experimental values⁸¹.

4.2.1 Nomenclature of the employed methods

Here, the different protocols for the methods used in the following section are collected. The nomenclature of SA-7S+7T means a state averaging over 7 singlets and 7 triplets, while SA-7S means a state averaging over only 7 singlets. All calculations were carried out without symmetry and for CASPT2 a level-shift parameter of 0.3 was used to prevent the appearance of intruder states. The contraction scheme used for ANO-S⁹⁵ was (10s6p3d)→[4s3p1d] for C,N and (7s3p)→[2s] for H, while for ANO-L^{92,93} the contraction scheme employed was (14s9p4d3f)→[4s3p2d] for C,N and (8s4p3d)→[3s2p] for H.

Table 4.2: Quantum chemistry methods used throughout this section, as well as the programs employed.

Method	Program
SA-7S+7T-CASSCF ^{96,97} (16,12)/6-31G*//CASSCF/ANO-L	MOLPRO ⁹⁰
SA-7S+7T-CASSCF(14,10)/6-31G*//CASSCF/ANO-L	MOLPRO
SA-7S+7T-CASSCF(12,9)/6-31G*//CASSCF/ANO-L	MOLPRO
SA-7S-CASSCF(16,12)/6-31G*//CASSCF/ANO-L	MOLCAS ⁹⁴
MS-CASPT ₂ ^{98,99} (16,12)/SA-7S-CASSCF(16,12)/ 6-31G*//CASSCF/ANO-S	MOLCAS
MS-CASPT ₂ (16,12)/SA-7S-CASSCF(16,12)/ ANO-S//CASSCF/ANO-S	MOLCAS
MS-CASPT ₂ (16,12)/SA-7S-CASSCF(16,12)/ ANO-L//CASSCF/ANO-S'	MOLCAS
MRCI(14,10)/6-31G*//CASSCF/ANO-L	ORCA ¹⁰⁰
EOM-CCSD ¹⁰¹ /cc-pvtz ¹⁰² /CASSCF/ANO-L	MOLPRO
TD-B ₃ LYP/cc-pvtz//CASSCF/ANO-L	GAUSSIAN ¹⁰³

4.2.2 Choice of the Active Space

For the calculation of excited states we use methods which require an active space, as explained in the theory chapter. Since we need to describe several excited states, we need an active space that ideally includes all orbitals associated with the relevant corresponding excitations. Vertical excitation of purine consists of $\pi\pi^*$ and $n\pi^*$ transitions. The active space therefore would need to include the whole π system and all nitrogen lone pairs.

Purine has a total of 9π orbitals, which can be classified into 5 bonding and 4 anti-bonding orbitalsⁱ. Together with the 3 lone pairs from the nitrogens 1, 3, and 7 (Figure 3.1) a complete active space would consist of 12 orbitals containing 16 electrons, i.e. (16,12), see Figure 4.3. Besides this active space, we also used two subsets, namely (14,10) and (12,9) for the calculations. In the (14,10) active space the two orbitals with the highest and lowest occupation numbers (named π and π^*) will be omitted. Their occupation numbers (see Table 4.3) are 1.98 and 0.07 respectively. In the (12,9) active space, the n₇ orbital is also left out, as it does not play a crucial role in the relevant excitations, as will be shown later on.

ⁱ Dividing the orbitals into pure bonding, anti-bonding, and non-bonding is often not a trivial task as delocalization makes a clear distinction between them difficult. For the purpose of calculating excited states this is not that important as we only need to include all of them in our active space, regardless of their bonding, non-bonding or anti-bonding character.

Figure 4.3: (16,12) active space of purine as obtained by a SA-7S+7T-CASSCF(16,12)/6-31G*//CASSCF/ANO-L, as obtained by CASSCF(16,12), containing the whole π system, as well as the 3 n orbitals of the 13 atoms. In the (14,12) active space the orbitals labeled as π and π^* are excluded, and in the (12,9) active space the π , π^* , and n_7 orbitals are excluded.

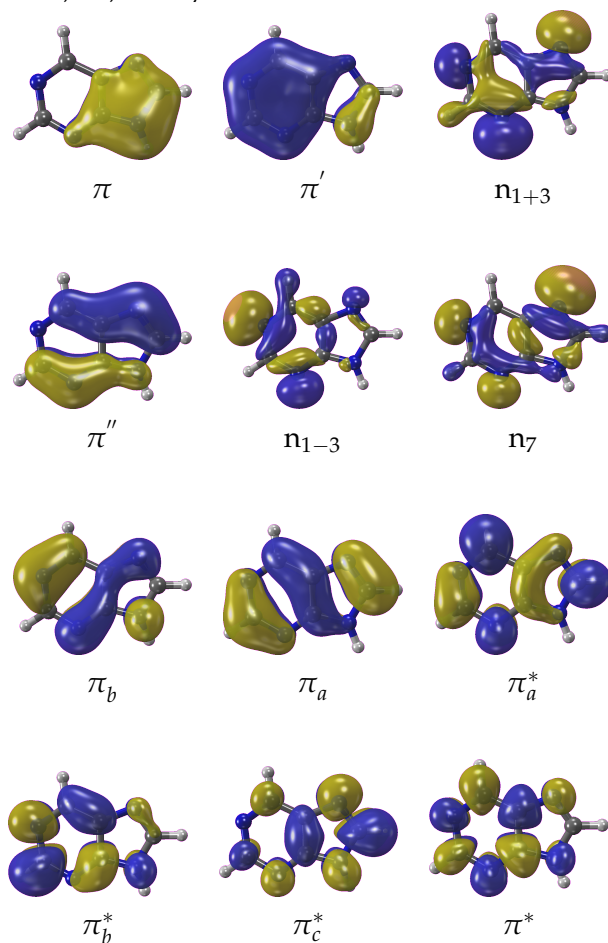


Table 4.3: Occupation numbers obtained at SA-7S+7T-CASSCF(16,12)/6-31G*//CASSCF/ANO-L level of theory.

π	π'	n_{1+3}	π''	n_7	π_b
1.98	1.94	1.92	1.89	1.85	1.77
n_{1-3}	π_a	π_a^*	π_b^*	π_c^*	π^*
1.72	1.70	0.61	0.35	0.20	0.07

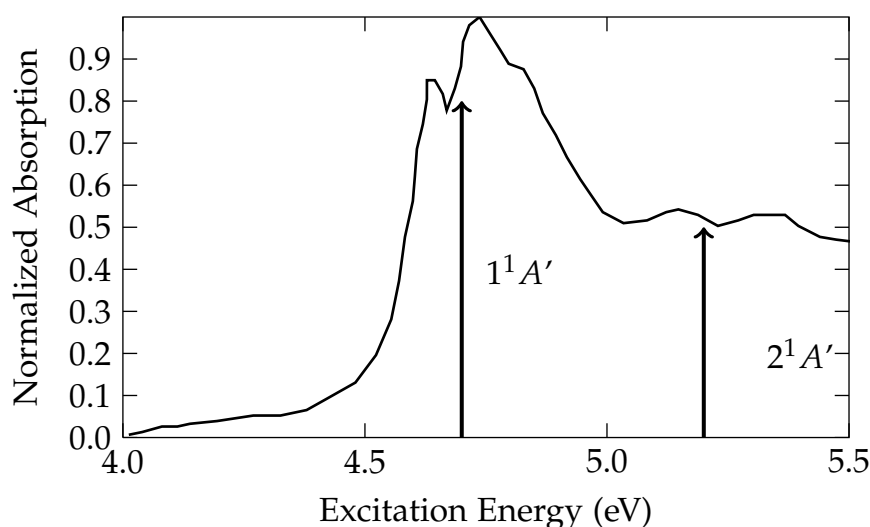
4.2.3 Performance of the quantum chemical methods on the vertical excitation energies

In this section, different quantum chemical methods described in the theory chapter will be applied to obtain the excitation energies of 9H-purine. In order to find a balance between accuracy and computational cost, several effects will be investigated, namely active space size, basis set size, and electronic correlation. Analyzing these effects and comparing the results to the available experimental data will allow us

better evaluating the overall error of our methods. These preliminary calculations are also essential to calibrate the accuracy of the CASSCF method that will be finally used in the MD calculations.

Figure 4.4 shows the experimental spectrum of purine in cyclohexane⁸¹. The locations of the two bright $\pi\pi^*$ states are marked in the plot by arrows and labelled with their IRREPs $1^1A'$ and $2^1A'$. Table 4.4 collects the excitation energies and wavelengths for both bright states. These values will serve as a reference for all further calculations carried out in this chapter. Additional information on the spectra of purine in several solvents will be given in section 5.1.

Figure 4.4: Experimental spectrum for 9H-purine in cyclohexane⁸¹. The two bright $\pi\pi^*$ states are marked as $1^1A'$ and $2^1A'$ according to their IRREP.



The locations of the two bright $\pi\pi^*$ states are marked in the plot by their IRREPs $1^1A'$ and $2^1A'$. Table 4.4 shows the excitation energies and wavelengths for both bright states. These values will serve as a reference for all further calculations carried out in this chapter. Additional information on the spectra of purine in several solvents will be given in section 5.1.

Table 4.4: Experimental excitation energies and wavelengths for the two first excited states of purine in cyclohexane⁸¹.

state	ΔE_{exp}	Exc. wavelength.
$1^1A'(\pi\pi^*)$	4.68 eV	265 nm
$2^1A'(\pi\pi^*)$	5.16 eV	240 nm

ACTIVE SPACE EFFECT Table 4.5 shows the CASSCF results for the largest active space (16,12) employed. Comparing the results to the experimental energies of Table 4.4 shows that the first $\pi\pi^*$ state (S_2) in our CASSCF(16,12) calculation is approx. 0.6 eV higher in energy. The second $\pi\pi^*$ state (S_5) is off by 2 eV. Since CASSCF does not include dynamical correlation large overestimations of the excitation energies are expected.

Table 4.5: Different active space for purine using SA-7S+7T-CASSCF/6-31G**/CASSCF/ANO-L. For a complete description of the methods see Table 4.2. The values for the corresponding triplet states are given in the appendix (Table A.1)

state	CASSCF(16-12)				CASSCF(14-10)				
	$\Delta E(\text{eV})$	f	character	w	$\Delta E(\text{eV})$	f	character	w	
S ₀			g.s.	0.85			g.s.	0.89	
S ₁	5.27	0.001	$n_{1-3}\pi_a^*$	0.70	5.52	0.006	$n_{1-3}\pi_a^*$	0.75	
S ₂	5.29	0.133	$\pi_a\pi_a^*$	0.24	6.00	0.151	$\pi_a\pi_a^*$	0.41	
			$\pi_b\pi_a^*$	0.24			$\pi_b\pi_a^*$	0.18	
S ₃	6.16	0.010	$n_{1-3}\pi_b^*$	0.68	6.54	0.010	$n_{1-3}\pi_b^*$	0.63	
S ₄	6.72	0.004	$n_7\pi_a^*$	0.55	6.84	0.004	$n_7\pi_a^*$	0.48	
S ₅	7.12	0.029	$\pi_b\pi_a^*$	0.29	7.61	0.028	$n_{1+3}\pi_a^*$	0.45	
			$\pi_a\pi_a^*$	0.20			—		
S ₆	7.3	0.126	$n_{1+3}\pi_a^*$	0.45	7.64	0.131	$\pi_b\pi_a^*$	0.28	
			$n_7\pi_a^*$	0.21			$\pi_a\pi_a^*$	0.25	
			CASSCF(12-9)						
S ₀			g.s.	0.89					
S ₁	5.61	0.010	$n_{1-3}\pi_a^*$	0.77					
S ₂	6.02	0.141	$\pi_b\pi_a^*$	0.35					
			$\pi_a\pi_a^*$	0.24					
S ₃	6.57	0.007	$n_{1-3}\pi_b^*$	0.76					
S ₄	7.46	0.007	$n_{1-3}\pi_a^*$	0.66					
S ₅	7.66	0.131	$\pi_a\pi_a^*$	0.44					
			$\pi_b\pi_a^*$	0.13					
S ₆	8.58	0.061	$\pi_a\pi_c^*$	0.28					
			$\pi''\pi_a^*$	0.20					

Taking the (16,12) values as reference, the effect of smaller active spaces has been analyzed. Table 4.5 also shows the results for the two smaller active spaces, (14,10) and (12,9). For (14,10) the state ordering is similar to (16,12), but the $2^1A'$ state changed from S₅ to S₆. The CASSCF(14,10) energies for $1^1A'$ and $2^1A'$ are 0.6 eV. - 0.7 eV higher in energy, compared to CASSCF(16,12). The $n\pi^*$ states are also higher in energy using the (14,10) active space. The (12,9) active space produces similar energies as the (14,10) one for the two $\pi\pi^*$ states. There is some deviation in the characters concerning the $n\pi^*$ states, as the n_7 orbital is left out of the (12,9) active space.

The best active space used is the (16,12) and accordingly its excitation energies are the lowest. A further decrease is expected upon inclusion of correlation energy. The (14,10) and (12,9) active spaces provide very similar results up to the S₄ state, as the character of this state, using (14,12), contains excitation out of the n_7 orbital, which is left out of the (12,9) active space.

ELECTRON CORRELATION EFFECT Our dynamics calculations have to be carried out at CASSCF level of theory for two reasons: First, we need a method that can calculate all quantum mechanical properties we need for the dynamics (gradients, non-adiabatic couplings, spin-orbit couplings) and this is currently only possible at CASSCF level of theory. And second, the on-the-fly electronic structure calculations should be performed in a reasonable amount of time, as we need to

calculate approx. 100 trajectories with 2000 timesteps each (i.e. 20000 single point calculations).

Despite the fact that our MD calculations are currently limited to CASSCF, some higher level of theory including electronic correlation was also employed to put the CASSCF results into perspective and to see its limitations as compared to the experiment⁸¹. The methods used were CASPT2, MRCI, EOM-CCSD, and TD-B3LYP (for a complete description of the methods see Table 4.2).

Table 4.6: Effect of correlation on the excited states of purine. Excitation energy, oscillator strength (f), character (ch.) and weight (w.) for different electron correlation methods used, as well as CASSCF(16,12) values. The exact nomenclature of the methods is given in Table 4.2. The CASPT2 values were calculated using the 6-31G* basis set. The triplet states at the CASPT2, and MRCI level of theory are given in the appendix (Table A.2).

state	CASSCF(16,12)				CASPT2			
	$\Delta E(\text{eV})$	f	ch.	w.	$\Delta E(\text{eV})$	f	ch.	w.
S ₀			g.s.	0.85			g.s.	0.85
S ₁	5.24	0.005	$n_{1-3}\pi_a^*$	0.70	4.52	0.005	$n_{1-3}\pi_a^*$	0.74
S ₂	5.29	0.127	$\pi_b\pi_a^*$	0.43	5.35	0.038	$\pi_a\pi_b^*$	0.41
			$\pi_a\pi_b^*$	0.18			$\pi_b\pi_a^*$	0.17
S ₃	6.16	0.002	$n_{1-3}\pi_b^*$	0.67	5.59	0.006	$n_{1-3}\pi_b^*$	0.74
S ₄	6.66	0.003	$n_7\pi_a^*$	0.56	5.80	0.002	$n_7\pi_a^*$	0.61
S ₅	6.98	0.400	$\pi_a\pi_a^*$	0.53	5.93	0.076	$\pi_b\pi_a^*$	0.51
S ₆	7.28	0.002	$n_{1+3}\pi_a^*$	0.45	6.69	0.017	$n_{1+3}\pi_a^*$	0.45
			$n_7\pi_c^*$	0.19			$n_7\pi_c^*$	0.18
state	MRCI				EOM-CCSD			
	$\Delta E(\text{eV})$	f	ch.	w.	$\Delta E(\text{eV})$	f		
S ₀			g.s.	0.80				
S ₁	4.90	0.002	$n_{1-3}\pi_a^*$	0.78	4.79	0.002		
S ₂	5.36	0.450	$\pi_a\pi_a^*$	0.78	5.38	0.082		
			—	—				
S ₃	5.51	0.110	$\pi_b\pi_a^*$	0.70	5.76	0.002		
S ₄	5.88	0.003	$n_{1-3}\pi_b^*$	0.79	6.05	0.072		
			—	—				
S ₅	5.89	0.000	$n_7\pi_a^*$	0.75	6.08	0.000		
S ₆	6.90	0.000	$n_{1+3}\pi_a^*$	0.74	6.90	0.009		
			—	—				
state	TD-B3LYP							
	$\Delta E(\text{eV})$	f	ch.	w.				
S ₀			g.s.					
S ₁	4.25	0.001	$n_{1-3}\pi_a^*$	0.70				
S ₂	5.25	0.001	$n_{1-3}\pi_b^*$	0.68				
			—	—				
S ₃	5.33	0.141	$\pi_a\pi_a^*$	0.65				
S ₄	5.34	0.000	$n_7\pi_a^*$	0.67				
			—	—				
S ₅	5.52	0.001	$\pi_b\pi_a^*$	0.61				
S ₆	6.32	0.005	$n_{1+3}\pi_a^*$	0.63				
	6.42	0.003	$n_{1-3}\pi_b^*$	0.67				

Table 4.6 shows all these correlated results, including CASSCF(16,12) for reference. Looking at the first bright $\pi\pi^*$ state we can see that all used correlation methods predict a similar energy of about 5.4 eV, which is still approx. 0.7 eV higher than the experimental value. For the second bright $\pi\pi^*$ state, the energy ranges from 5.5 eV - 6 eV, compared to the experimental value of 5.2 eV. The state ordering concerning this second bright state is not consistent for all the methods, as is the state ordering for all but the first $n\pi^*$ state. Since our dynamical calculations shall focus on the lowest energy band of the spectrum assigned to the $1^1A'$ state, the location of the second bright excited state is not that relevant. It is interesting to notice, that for TD-B3LYP the oscillator strength of the second $\pi\pi^*$ state (S_5) is only 0.001, predicting it darker than several $n\pi^*$ states. This fact, however, has not been observed for any of the multi-configurational methods used in this work. In Table 4.7 the energies for the first two $\pi\pi^*$ states are summarized and compared to the experimental values. Here, we can clearly see the general agreement of the electron correlation methods used for the $1^1A'$ state, and yet lying 0.7 eV higher in energy than the experimental value. The $2^1A'$ does not show this overall agreement of the methods used, and the difference to the experimental value of 5.2 eV is 0.3 - 0.8 eV.

Table 4.7: Excitation energies (in eV) for the first two $\pi\pi^*$ states of purine using different correlation methods, compared to the experimental value.

	CASPT2	MRCI	EOM-CCSD	TD-B3LYP	Exp
$1^1A'$	5.35	5.36	5.38	5.33	4.7
$2^1A'$	5.93	5.51	6.05	5.52	5.5

The comparison of the CASPT2 results shown in Table 4.6 with the corresponding CASSCF, also given in Table 4.6, illustrates the actual effect of electron correlation. While the S_1 state changes from 5.24 eV to 4.52 eV when introducing correlation, the S_2 state goes from 5.29 eV to 5.35 eV. The same trend can be observed in all other correlation methods used. Therefore, one can conclude that there is no significant effect of correlation on the S_2 state. Also the MRCI and EOM-CCSD methods predict an excited energy of ca. 5.3 eV - 5.4 eV for the S_2 . However, and none of the used methods are able to match the experimental value of 4.7 eV.

BASIS SET EFFECT In order to see if the difference between the obtained result and the experimental value is due to the limited basis set, the CASPT2 calculation was carried out using different basis sets. Table 4.8 shows these results for the previously shown 6-31G*, the ANO-S, and the ANO-L basis sets (for a detailed description see Table 4.2). Although the excitation energies decrease with larger basis sets, e.g. the S_2 state changes from 5.35 eV \rightarrow 5.24 eV \rightarrow 5.21 eV when increasing the number of basis functions, the effect is small and does not compensate for the high energy difference to the experimental value of 4.7 eV. This trend of slowly lowering of the excitation energies

when enhancing the basis set can be seen for all excited states. The basis set however, has no observed effect on the state ordering.

Table 4.8: Effect of different basis sets on the CASPT2 results. Excitation energy, oscillator strength (f), character (ch.) and weight (w.) for different basis set sizes. For a complete nomenclature of the methods see Table 4.2. The values for the corresponding triplet states are given in the appendix (Table A.3).

state	CASPT2(16,12)/6-31G*				CASPT2(16,12)/ANO-S			
	$\Delta E(\text{eV})$	f	character	weight	$\Delta E(\text{eV})$	f	character	weight
S ₀			g.s.	0.85			g.s.	0.85
S ₁	4.52	0.005	$n_{1-3}\pi_a^*$	0.74	4.51	0.005	$n_{1-3}\pi_a^*$	0.74
S ₂	5.35	0.038	$\pi_a\pi_b^*$	0.41	5.24	0.042	$\pi_b\pi_a^*$	0.39
			$\pi_b\pi_a^*$	0.17			$\pi_a\pi_b^*$	0.16
S ₃	5.59	0.006	$n_{1-3}\pi_b^*$	0.74	5.56	0.006	$n_{1-3}\pi_b^*$	0.74
S ₄	5.80	0.002	$n_7\pi_a^*$	0.61	5.75	0.002	$n_7\pi_a^*$	0.63
S ₅	5.93	0.078	$\pi_b\pi_a^*$	0.51	5.78	0.069	$\pi_a\pi_a^*$	0.49
S ₆	6.69	0.017	$n_{1+3}\pi_a^*$	0.45	6.63	0.017	$n_{1+3}\pi_a^*$	0.46
			$n_7\pi_c^*$	0.18			$n_7\pi_c^*$	0.17
			CASPT2(16,12)/ANO-L					
			243 basis functions					
state	$\Delta E(\text{eV})$	f	character	weight				
S ₀			g.s.	0.85				
S ₁	4.46	0.005	$n_{1-3}\pi_a^*$	0.74				
S ₂	5.21	0.044	$\pi_b\pi_a^*$	0.38				
			$\pi_a\pi_b^*$	0.16				
S ₃	5.51	0.006	$n_{1-3}\pi_b^*$	0.74				
S ₄	5.69	0.002	$n_7\pi_a^*$	0.63				
S ₅	5.73	0.069	$\pi_a\pi_a^*$	0.48				
S ₆	6.57	0.017	$n_{1+3}\pi_a^*$	0.46				
			$n_7\pi_c^*$	0.18				

4.2.4 Comparison to previous theoretical work

As stated in Chapter 3, there has not been much theoretical work done on the purine molecule. The two published studies are explained below, and the obtained $\pi\pi^*$ excitation energies are collected in Table 4.9. Both mentioned studies were carried out using C_s symmetry.

Table 4.9: Excitation energies (in eV) and oscillator strengths for purine. Only the first two $\pi\pi^*$ states are shown. The ΔE_{1999} values are by Borin et al.⁸⁵, and the ΔE_{2008} values are by Mburu and Matsika⁸⁶.

state	ΔE_{1999} (eV)	f	ΔE_{2008} (eV)	f	ΔE_{exp}
1 $^1A'$	4.66	0.034	4.80	0.031	4.68
2 $^1A'$	5.09	0.063	5.27	0.070	5.16

In 1999, Borin et al.⁸⁵ used CASPT2(16,12)/CASSCF(16,12)/ANO-S//MP2/6-31G* with a contraction scheme of C,N[4s3p1d]/H[2s] to calculate the excitation energies of 9H and 7H purine. Their excitation energies of 4.66 eV and 5.09 eV for the first two $\pi\pi^*$ states seem to be in good agreement with the experimental values of 4.7 eV and 5.2 eV, respectively (see Table 4.9). The disagreement of these values with those obtained in this work comes from the fact that in 1999 they used an older version of MOLCAS (MOLCAS 3) while we used the newest version (MOLCAS 7.8). This current version has been corrected and improved as resources and theory enhanced over time. Therefore, Borin et al. might have obtained the right result for a wrong reason.

In 2008, Mburu and Matsika⁸⁶ calculated the excited states of purine and some purine derivatives using MRMP2(16,12)/cc-pVDZ//MP2/cc-pVDZ. Interestingly, their results of 4.80 eV and 5.27 eV for the two $\pi\pi^*$ states (Table 4.9) indicate a better characterization of the system using MRMP2 than it is possible with any of our methods (see Table 4.6). Although it is not clear why MRMP2 should perform better than CASPT2 or EOM-CCSD, the calculation of the molecular properties required in AIMD is not possible in MRMP2; therefore, we cannot carry out the dynamics using MRMP2.

4.2.5 Method used in Dynamics

As stated above, the dynamics has to be carried out at a CASSCF level of theory. Therefore, looking at Table 4.5, the CASSCF(16,12) method would be the best choice. Unfortunately, using this active space, one single point calculation takes approx. 10 hours, making it not feasible for dynamics. Unfortunately, when using the (14,10) active space, the single point calculations only take about 1 hour, but the dynamics tend to crash, as the active space is not stable enough and easily switches orbitals during the run. Therefore, the (12,9) active space (30 minutes per single point) was used in the simulation. The excitation energies obtained with this method are repeated in Table 4.10, also including the triplet states. The corresponding orbital occupation numbers are in Table 4.11.

As stated before, our dynamics will focus on the lowest energy band of the spectrum, i.e. on the $1^1A'$ (S_2) state. Only looking at the Frank-Condon geometry energies in Table 4.10, the first 5 triplet states lie energetically below S_2 , the first 6 if we also want to consider the S_3 state in the dynamics. The triplet states consist, like the singlets, mostly of excitations from the π_a , π_b and n_{1-3} orbitals into the π_a^* and π_b^* orbitals. There is also one excitation occurring into the π_c^* orbital playing a vital role in T_4 . In section 5.1 we will analyze the triplet

state energies for all generated initial conditions, so that we can better determine how many triplet states are needed in the dynamics.

In Table 4.11 we can see the occupation numbers of all orbitals using SA-7S+7T-CASSCF(12,9)/6-31G**//CASSCF/ANO-S. One can see that the most important occupied orbitals are n_{1-3} , π_a , and π_b , while the most important virtual orbitals are π_a^* and π_b^* . This correlates to the characters presented in Table 4.10.

Table 4.10: Vertical excitation energies, oscillation frequencies, and character SA-7S+7TCASSCF(12,9)/6-31G**//CASSCF/ANO-S. Bright states are marked in grey.

state	ΔE (eV)	f	character	weight
S ₀			g.s.	0.89
S ₁	5.61	0.0098	$n_{1-3}\pi_a^*$	0.77
S ₂	6.02	0.1411	$\pi_b\pi_a^*$	0.35
			$\pi_a\pi_a^*$	0.24
S ₃	6.57	0.0065	$n_{1-3}\pi_b^*$	0.76
S ₄	7.46	0.0073	$n_7\pi_a^*$	0.66
S ₅	7.66	0.1313	$\pi_a\pi_a^*$	0.44
			$\pi_b\pi_a^*$	0.13
S ₆	8.85	0.0606	$\pi_a\pi_c^*$	0.28
			$\pi''\pi_a^*$	0.20
T ₁	4.39	—	$\pi_a\pi_a^*$	0.71
T ₂	5.40	—	$n_{1-3}\pi_a^*$	0.66
T ₃	5.62	—	$\pi_b\pi_a^*$	0.56
T ₄	5.88	—	$\pi_a\pi_c^*$	0.24
			$\pi_a\pi_b^*$	0.21
T ₅	5.95	—	$n_{1-3}\pi_b^*$	0.67
T ₆	6.26	—	$\pi_b\pi_b^*$	0.33
			$\pi_a\pi_b^*$	0.25
T ₇	7.25	—	$\pi_b\pi_b^*$	0.28
			$\pi_a\pi_b^*$	0.22
			$\pi_a\pi_b^*$	0.21

Table 4.11: Occupation numbers for active space of SA-7S+7T-CASSCF(12,9)/6-31G**//CASSCF

π'	n_{1+3}	π''	π_b	n_{1-3}	π_a	π_a^*	π_b^*	π_c^*
1.95	1.91	1.88	1.75	1.73	1.63	0.61	0.39	0.16

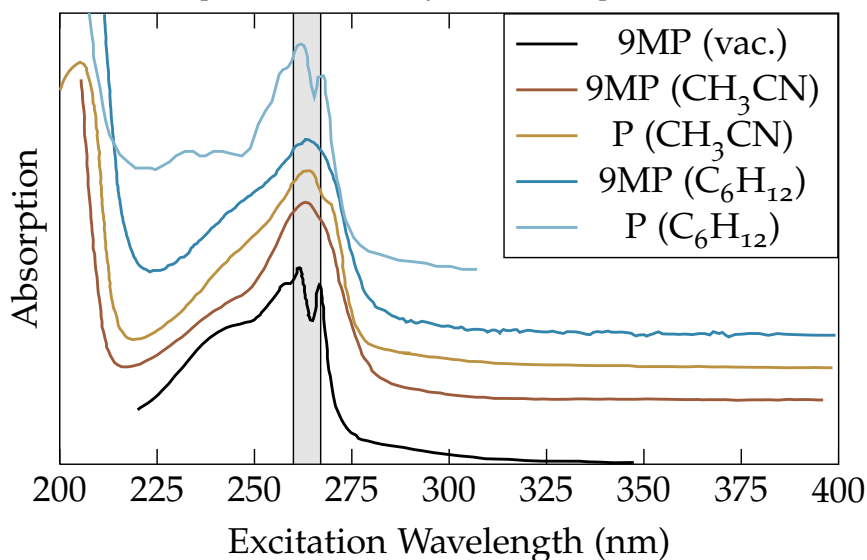
Before we can run the MD simulations we need to generate an absorption spectrum. Therefore, in section 5.1 the experimental and theoretical absorption spectra of purine are presented and discussed. Using the initial conditions obtained by the absorption spectrum, the AIMD simulation can be started, and the results will be presented in section 5.2.

5.1 ABSORPTION SPECTRA

In this subsection, the experimental absorption spectra will be presented and compared to the theoretical one. Using the calculated spectrum the initial conditions for the dynamics can be generated, and we can determine which states will be excited in each trajectory. The spectrum also tells us, over how many singlet and triplet states the simulation needs to be averaged.

5.1.1 Experimental Absorption Spectra

Figure 5.1: Absorption spectra for purine and 9-Methylpurine (9MP) for different solvents and gas phase. The gray area marks the first excitation band. All spectra except 9MP (vac.)⁸⁰ and P (C₆H₁₂)⁸¹ are unpublished results by Prof. C. Crespo.



There has been little experimental work done to characterize the absorption spectra of purine. To our knowledge, no gas phase spectrum has been published so far. The closest to gas phase we could find is a cyclohexane spectrum by Clark et al.⁸¹ from 1965. In 2006, J. Catalán⁸⁰ published a gas phase spectrum of 9-Methylpurine (9MP), claiming that due to the same behavior of purine and 9MP, one can assume that

the spectrum also holds for purine. This assumption seems plausible, as when looking at the different absorption spectra from all published sources^{80,81}, and at the spectra recorded in the group of Prof. C. Crespo Hernández (Figure 5.1), all peak at the same wavelength. In these spectra the first absorption band at approximately 265 nm (4.7 eV) stays the same for all solvents in both purine and gMP.

5.1.2 Theoretical Absorption Spectra

In order to evaluate which states are needed for the dynamics, an excitation spectrum around the Frank–Condon region was calculated. Therefore, 1000 geometries were selected from a classical Wigner distribution¹⁰⁴, as described in Refs.^{105,106}. These initial conditions were used to run 1000 single point calculations, from which an absorption spectrum was obtained. To be able to use the same initial conditions in the subsequent dynamics run, one has to check, whether a bright singlet state is excited. By using a Monte-Carlo type of algorithm, according to Ref.¹⁰⁷, one can get the excitations for each initial condition. The single point calculations were carried out using SA-5S+10T-CASSCF(12,9)/def2-svp//CASSCF/ANO-L.

Figure 5.2: Simulated and experimental absorption spectra for purine. The simulated spectrum was shifted by 1 eV. The gray region marks the excitation range of ± 0.25 eV around the experimental excitation energy of 4.7 eV, from which the initial conditions were chosen.

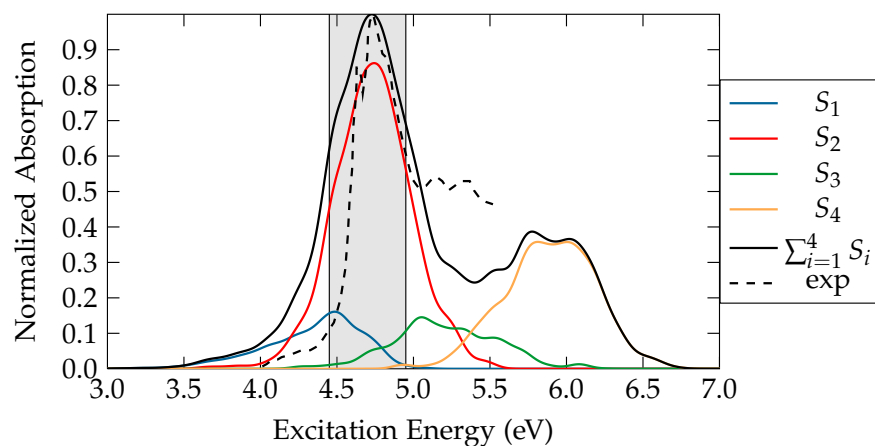


Figure 5.2 shows a bright (S_2) state flanked by the two less intense states (S_1 and S_3). This bright state aligning with the band of the spectrum is the S_2 and corresponds to a $\pi\pi^*$ transition. This state lies between two $n\pi^*$ states, the S_1 and S_3 .

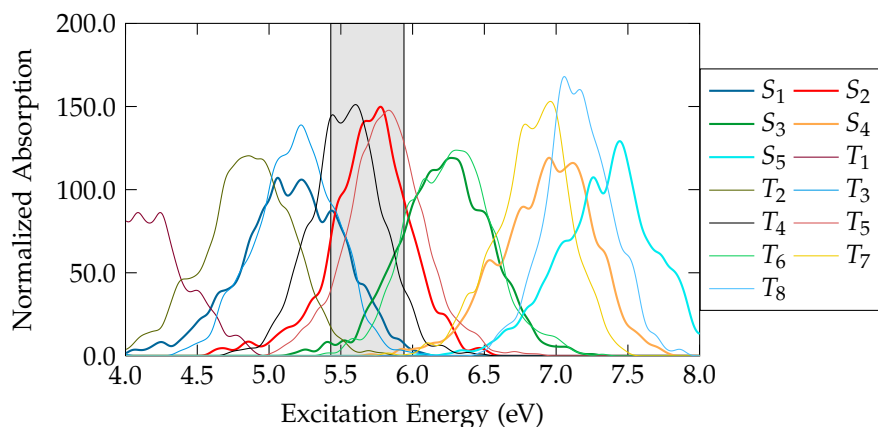
Looking at the excitation range (gray area), which is defined as ± 0.25 eV around the experimental excitation energy of 4.7 eV, we can see that a total of 4 singlet states – including S_0 – need to be considered in the dynamics. The S_4 content in the excitation range is negligible.

As was expected from the results in Table 4.5, the excitation energies needed to be shifted by 1 eV. This shift will not be implemented in the dynamics and is only used here to align the spectra in order to compare them. The fact that our results seem to be 1 eV higher than

the experimental value is expected not to be of big consequence for the dynamics, as the state ordering agrees with higher correlated methods (Table 4.6).

In Figure 5.2, only the singlet states are shown, as there are no allowed excitations into the triplets from the electronic ground state S_0 . Therefore, estimate how many triplet states we need to consider in the dynamics, the energies of all states – singlet and triplet – are plotted as a Gaussian distribution with a FWHM of 0.091. Figure 5.3 shows this distribution for the SA-5S+10T-CASSCF(12,9)/def2-svp//CASSCF/ANO-L level of theory.

Figure 5.3: Energy distribution of the absorption spectrum of purine, including singlet and triplet states using SA-5S+10T-CASSCF(12,9)/def2-svp//CASSCF/ANO-L. The gray area marks the excitation range from which the initial conditions were chosen.



Focusing on the excitation range of ± 0.25 eV around the experimental excitation energy of 4.7 nm (gray area in Figure 5.3), we need to include 4 singlet and 6 triplet states in the dynamics, meaning that the on-the-fly calculations will be performed at the SA-4S+6T-CASSCF(12,9)/def2-svp//CASSCF/ANO-L level of theory. The resulting energies are collected in Table 4.10, which shows that for the single point calculation at the Frank–Condon geometry the first 6 triplet states lie energetically lower than the S_3 state.

Using SA-4S+6T-CASSCF(12,9)/def2-svp//CASSCF/ANO-L, we can recalculate Table 4.5 using the current state averaging, in order to justify using the (12,9) active space. Table 5.1 shows the excitation energies for both the (16,12) and the (12,9) active spaces using the 4S+6T state averaging. Looking the singlet energies and characters, one can see that they are similar to the larger state averaging results reported in Table 4.5. When comparing the two active spaces, one can also look at the occupation numbers for the (16,12) calculation (Table 5.2). Comparing these values to the 7S+7T state averaging used for Table 4.3 in the previous chapter, one sees that the occupation number for the n_7 orbital goes from 1.85 for 7S+7T to 2.00 for 4S+6T. The π and π^* values do not change significantly (1.98 \rightarrow 1.99 and 0.07 \rightarrow 0.07, respectively). Therefore, these three orbitals are the best

choice to leave out of our (12,9) active space, when doing a 4S+6T state averaging.

Table 5.1: Excitation energies, oscillator strengths (f), state characters (ch), and corresponding weights (w) for SA-4S+6T-CASSCF/def2-svp//CASSCF/ANO-L using different active spaces.

state	(16-12)				(12-9)			
	$\Delta E(\text{eV})$	f	ch.	w.	$\Delta E(\text{eV})$	f	ch.	w.
S_0			g.s.	0.85			g.s.	0.85
S_1	5.16	0.008	$n_{1-3}\pi_a^*$	0.76	5.41	0.007	$n_{1-3}\pi_a^*$	0.81
S_2	5.29	0.028	$\pi_a\pi_a^*$	0.42	6.04	0.142	$\pi_a\pi_a^*$	0.58
			$\pi_b\pi_b^*$	0.23			—	
S_3	6.01	0.004	$n_{1-3}\pi_b^*$	0.74	6.42	0.005	$n_{1-3}\pi_b^*$	0.76
T_1	4.06		$\pi_b\pi_a^*$	0.32	4.50		$\pi_b\pi_a^*$	0.44
			$\pi_a\pi_a^*$	0.25			$\pi_a\pi_a^*$	0.25
T_2	4.84		$n_{1-3}\pi_a^*$	0.73	5.18		$n_{1-3}\pi_a^*$	0.78
T_3	5.28		$\pi_a\pi_a^*$	0.34	5.55		$\pi_a\pi_a^*$	0.42
			$\pi_b\pi_a^*$	0.29			$\pi_b\pi_a^*$	0.28
T_4	5.42		$\pi_a\pi_b^*$	0.49	5.80		$n_{1-3}\pi_b^*$	0.74
T_5	5.55		$n_{1-3}\pi_b^*$	0.68	6.00		$\pi_a\pi_b^*$	0.28
			—	—			$\pi''\pi_c^*$	0.13
			—	—			$\pi_a\pi_c^*$	0,13
T_6	5.98		$\pi_a\pi_c^*$	0.22	6.30		$\pi_a\pi_b^*$	0.45
			$\pi''\pi_a^*$	0.19			$\pi_b\pi_b^*$	0.10
			$\pi''\pi_c^*$	0.16			—	—

Table 5.2: Occupation numbers for active space of SA-4S+6T-CASSCF(16,12)/def2-svp//CASSCF/ANO-L

n_7	π_{CC}	n_{1+3}	π'_{CC}	π''_{CC}	π_{CCb}
2.00	1.99	1.95	1.94	1.88	1.74
π_{CCa}	n_{1-3}	π_{CCa}^*	π_{CCb}^*	π_{CCc}^*	π_{CC}^*
1.67	1.65	0.55	0.42	0.15	0.07

5.2 AB INITIO MOLECULAR DYNAMICS

The dynamics simulations were carried out using the SHARC¹⁵ program. The quantum mechanical part was done using SA-4S+6T-CASSCF

(12,9)/def2-svp//CASSCF/ANO-L, as implemented in MOLPRO⁹⁰. The computational reasons for using this method were discussed in the previous section. Due to convergence problems, the NACs were calculated by the finite difference method presented in section 2.7.3. A total of 94 trajectories were collected, with 12 starting in S_1 , 75 in S_2 , and 7 in S_3 . This distribution results from the Monte Carlo algorithm mentioned in the previous section.

As mentioned in the theory chapter, surface hopping AIMD uses an ensemble of trajectories to describe the dynamical process. To validate

this approach, the time-dependent populations of the electronic states, given by the squares of the coefficients c_α (see section 2.3.2) were analyzed for each of the whole set of 94 trajectories, as well as for half of it. Figure 5.4 shows the comparison of the two sets of trajectories for the singlet states. Although there is a slight deviation after 700 fs concerning the S_0 curve, the overall agreement is very good, validating the statistical approach.

Figure 5.4: State coefficients for whole set of trajectories, as well as for half of it – denoted by the superscript h .

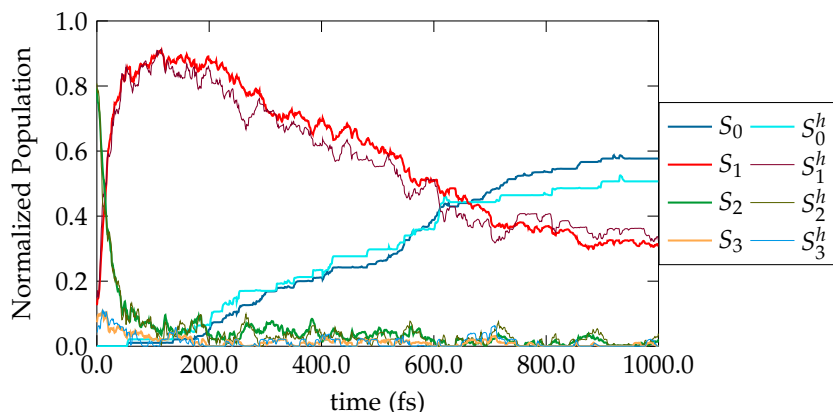
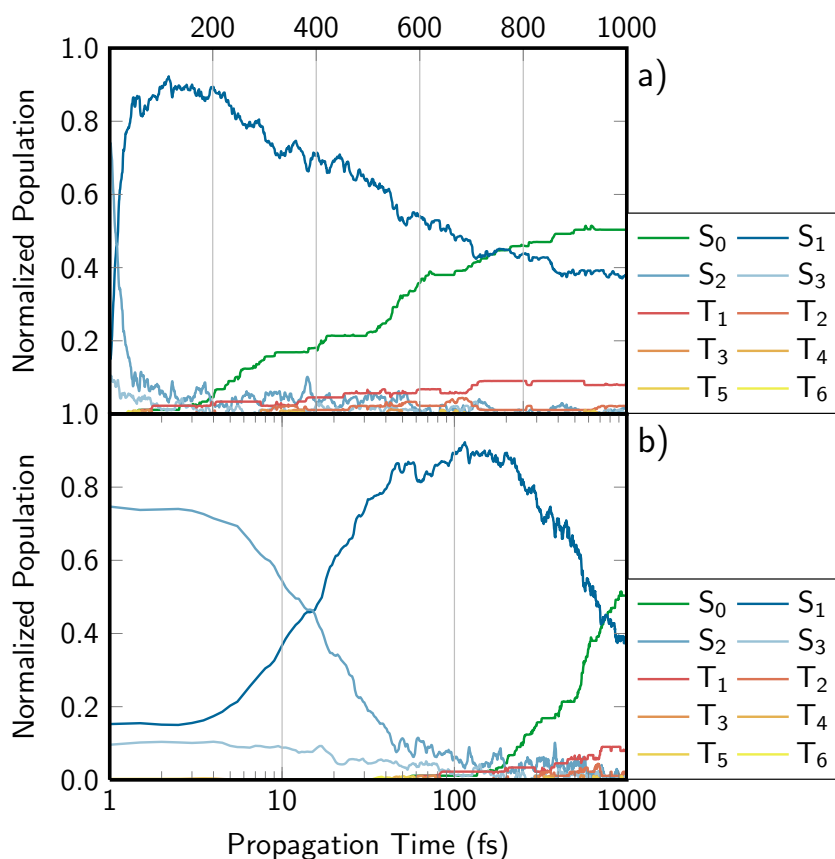


Figure 5.5 shows the time-dependent populations for all trajectories in a linear and a semi-logarithmic plot.

Figure 5.5: Time evolution of the state coefficients for purine. Figure *a* shows a normal time axis, while Figure *b* shows a logarithmic time axis.



Upon excitation, most of the population, starting in the S_2 state, will go to the S_1 via a S_2/S_1 conical intersection (CoIn). At this CoIn the S_2 state is mixed with the S_3 state and shows a $\pi\pi^*/n\pi^*$ character, while the S_1 state still has a predominant $n\pi^*$ character. After approx. 100 fs, almost all of the population is located in the S_1 state. This fast ($S_2 \rightarrow S_1$) switch has a time constant of 12 fs.

After 200 fs, relaxation to the ground state starts to occur via a S_1/S_0 CoIn. At the end of the simulation – after 1 ps – approx. 50 % of the population is in the ground state. The time constant for this process is 1200 - 1500 fs. At the S_1/S_0 CoIn, the S_1 state is mixed with S_2 and has a $\pi\pi^*/n\pi^*$ character, while the ground state has 60 % closed shell configuration.

There is also ISC involved, with 10 % of the population in the triplet state after 1 ps. The triplet population is mediated by a S_1/T_2 crossing, at which the S_1 state always has a $n\pi^*$ character while the T_2 state can be both $n\pi^*$ and $\pi\pi^*$, leading to two different CoIns. Then, the trajectory moves to the T_1 state via a T_2/T_1 CoIn. Due to convergence reasons, there were not enough optimized crossing geometries available to determine the characters of the relevant states at the T_2/T_1 CoIn. Both for the S_1/T_2 and the T_2/T_1 crossings no time constants could be determined, due to the limited data available. All higher triplet states, i.e. T_3 to T_6 do not play any significant role in the dynamics of purine. Similarly, the S_3 state also plays a negligible role in all calculations.

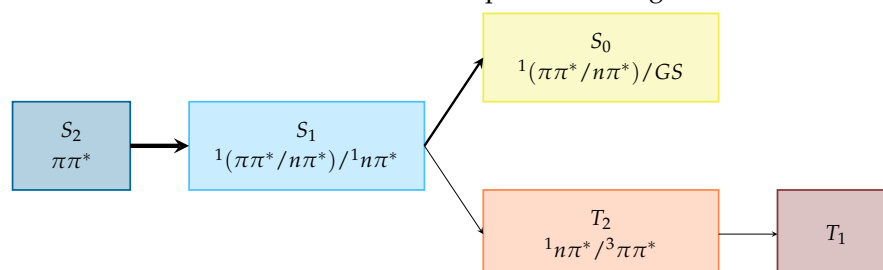
The characters of the states involved in all above mentioned crossings are given in Table 5.3.

Table 5.3: Main character of the states involved in the relevant stationary points of purine.

	FC	S_2/S_1	S_1/S_0	S_1/T_2
S_0	g.s.	—	60 % g.s.	—
S_1	$n\pi^*$	$n\pi^*$	$\pi\pi^*/n\pi^*$	$n\pi^*$
S_2	$\pi\pi^*$	$\pi\pi^*/n\pi^*$	—	—
T_2	$\pi\pi^*$	—	—	$\pi\pi^*$

Figure 5.6 summarizes the above explained processes. After relaxation to S_1 , the population either goes to S_0 or T_2 (and then to T_1). Almost half of the population is in the ground state after 1 ps, while 10 % is transformed to the triplet states. Our calculations then provide a rationale for an ultrafast relaxation mechanism for purine after UV excitation.

Figure 5.6: Summary and primary characters of IC and ISC processes involved in the deactivation of purine after light irradiation.



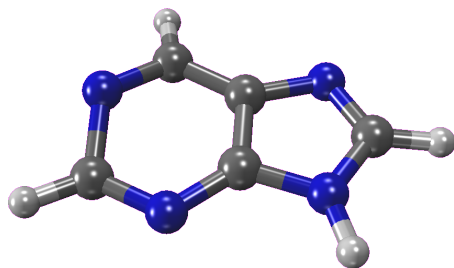
5.3 CONICAL INTERSECTION GEOMETRIES

At the time where jumps occurred in the dynamics, the involved geometries were extracted and optimized. Using all these jumping geometries, we can see how many distinct CoIns are important in the dynamics. We can also try to find any important geometric features which are relevant for the respective crossing. The results of this analysis will be presented in this section.

$(S_2 \rightarrow S_1)$

100 fs after irradiation almost all of the population starting in S_2 changes to the S_1 state, i.e. $(S_2 \rightarrow S_1)$. Figure 5.7 shows the optimized geometry of the essential CoIn involved in this process. This geometry is similar to the Frank–Condon geometry, which could explain the fast IC process seen in the dynamics, which has a time constant of ~ 12 fs.

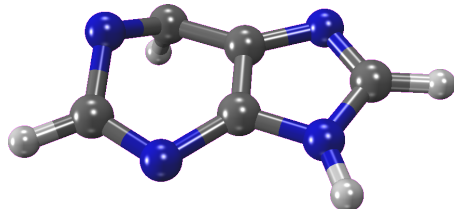
Figure 5.7: Optimized S_2/S_1 CoIn structure for purine.



$(S_1 \rightarrow S_0)$

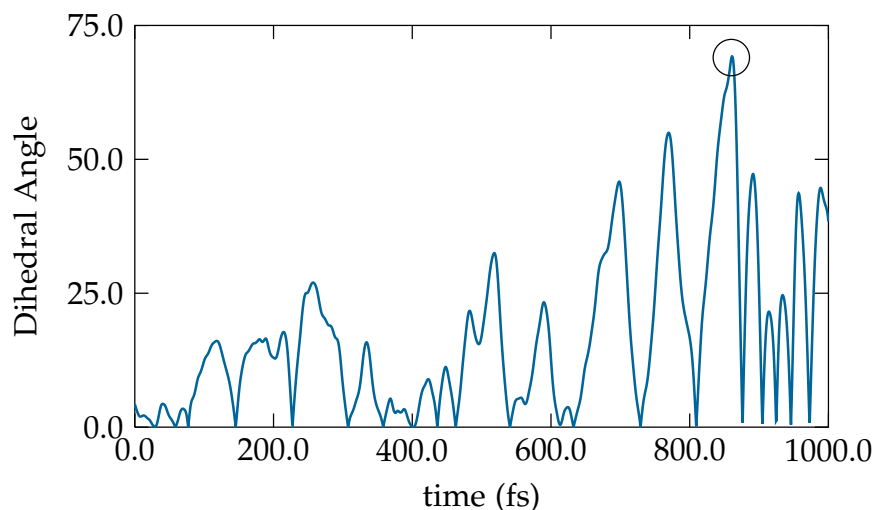
After 200 fs, the population of the S_0 state starts to increase as a result of deactivation via a S_1/S_0 CoIn. After 1 ps approximately 50% of population relaxed to the ground state via this CoIn, which is depicted in Figure 5.8.

Figure 5.8: Optimized S_1/S_0 CoIn structure for purine.



The primary geometric feature of this CoIn is the $C_2-N_1-C_6-C_5$ dihedral angle (see the nomenclature introduced in Figure 3.1. When the trajectory jumps to the S_0 state, this dihedral angle reaches a maximal value as can be seen in Figure 5.9, which shows the scan over this angle for one exemplary trajectory. We can see that the point it reaches the CoIn is in this case approx. 860 fs.

Figure 5.9: $C_2-N_1-C_6-C_5$ dihedral angle scan over one exemplary trajectory. The circle marks the CoIn crossing point.



This geometric hindrance of requiring a large dihedral angle could explain the slower timescale for the ($S_1 \rightarrow S_0$) process, which takes place in about 1200 - 1500 fs. In contrast, the CoIn relevant for the ($S_2 \rightarrow S_1$) process does not show any prominent geometric feature constraint and it has a time constant of only 12 fs.

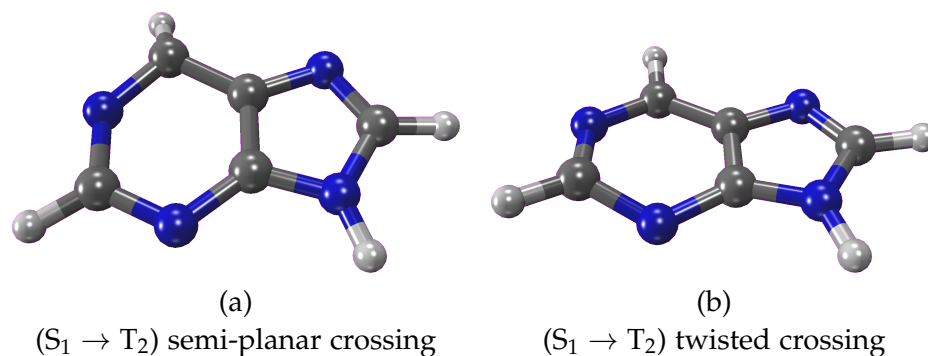
($S_1 \rightarrow T_2$)

As stated above, there is little ISC involved in the relaxation process. Optimizing all S_1/T_2 hopping geometries, two distinct crossing points have been found. While Figure 5.10 (a) shows a semi-planar configuration, 5.10 (b) is not semi-planar, but rather shows a twist in the 6-membered ring. Another distinct feature is that, while the semi-planar crossing geometry has a ${}^1n\pi^*/{}^3n\pi^*$ character, the twisted one has ${}^1n\pi^*/{}^3\pi\pi^*$. Of the 6 optimized geometries, 5 resulted in the twisted ${}^1n\pi^*/{}^3\pi\pi^*$ crossing, while only one resulted in the semi-planar one. Since little data is available no time-constant has been calculated for this process.

($T_2 \rightarrow T_1$)

The ($T_2 \rightarrow T_1$) transition has been observed but no CoIns could be optimized. There was also no conclusive information to specify the characters of the states involved, as there was a limited amount of crossing geometries available.

Figure 5.10: ISC geometries of purine.



5.4 COMPARISON WITH QUANTUM CHEMICAL AND EXPERIMENTAL RESULTS

As stated in the Introduction, this work has been performed in collaboration with an experimental and another theoretical group. In this section our results are put into the perspective of the data obtained from the other groups. First, the experimental results by Prof. C. Crespo are presented, and then, the theoretical results by L. Martínez and Dr. I. Corral are commented to explain the experiment.

The transient absorption experiments carried out by the group of Professor C. Crespo employed 267 nm and several solvents. Their results shows three solvent independent relaxation constants for purine in the range of 100s fs, 10s ps, and 100s ps. This data can be interpreted so that after an excitation to the S_2 state, which is of $\pi\pi^*$ character, an internal conversion to the $S_1(n\pi^*)$ state, occurring in 100s fs, takes place. The S_1 state relaxes probably by vibrational cooling (in 10s of ps), followed by ISC to $T_1(\pi\pi^*)$ in 100s of ps. In acetonitrile they see a triplet yield of 50% or more. Although this percentage has not been confirmed for other solvents, Prof. Crespo does not think that it will differ significantly.

These results can only be confirmed partially by our dynamical simulations. While they also see a fast $S_2 \rightarrow S_1$ transition, they measured no relaxation to the ground state. The ISC observed in our dynamics seems to be in agreement with the experimental data, although our simulations predict a faster timescale than the experiment would support for this process.

The theoretical work of L. Martínez and Dr. I. Corral is complementary to our results and very important to understand the experimental data presented above. By calculating minimum energy pathways (MEPs) and running single point calculations a relaxation pathway at CASPT2 level of theory can be put forward. Their proposed MEP is shown in Figure 5.11.

Figure 5.11 shows a S_2/S_1 CoIn of $(^1\pi\pi^*/^1n\pi^*)$ character close to the Frank–Condon geometry. From S_1 the system can either relax to the ground state via a $(^1n\pi^*/GS)$ CoIn, or it could go to the triplet state via a $(^1n\pi^*/^3\pi\pi^*)$ crossing. There also exists an accessible S_0/T_1 crossing point of $(^3\pi\pi^*/GS)$ character.

Table 5.4 shows the characters of optimized states obtained by L. Martínez and Dr. I. Corral using MEPs, and by our AIMD simulations.

Figure 5.11: Relaxation pathway of purine using minimum energy pathways. This Figure was generously provided by L. Martínez and Dr. I. Corral.

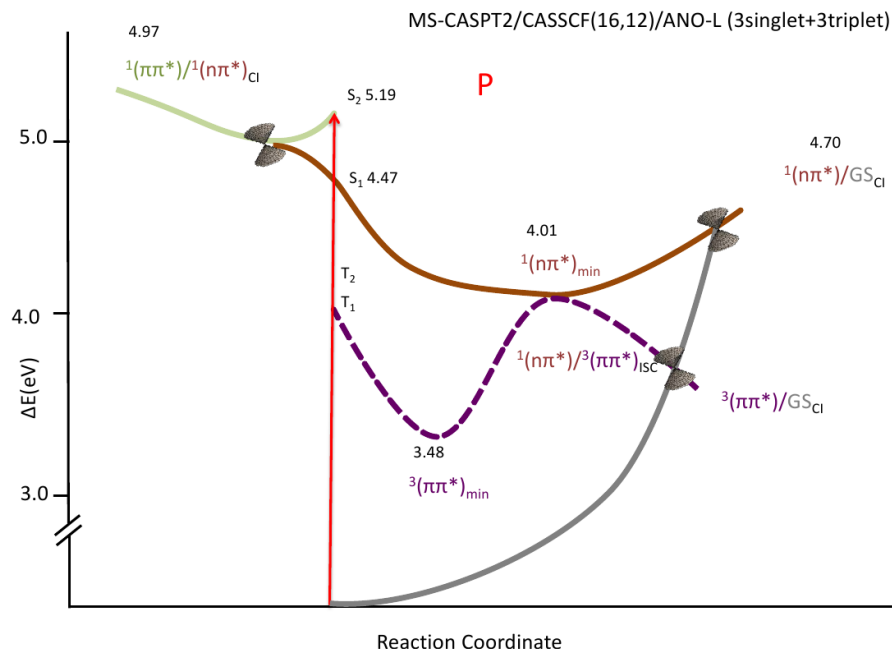


Table 5.4: Dominant characters of the optimized crossing points for purine obtained by minimum energy pathways (MEP) and ab initio molecular dynamics (AIMD)

CoIN	MEP	AIMD
S_2/S_1	$1\pi\pi^*/1n\pi^*$	$1(\pi\pi^*/n\pi^*)/1n\pi^*$
S_1/S_0	$1n\pi^*/GS$	$1(\pi\pi^*/n\pi^*)/GS$
S_1/T_1	$1n\pi^*/3\pi\pi^*$	—
S_1/T_2	—	$1n\pi^*/3\pi\pi^*$

In our dynamics results, the S_2 state at the S_2/S_1 CoIN is mixed with the S_3 state resulting in a $\pi\pi^*/n\pi^*$ character. This has not been observed using MEPs, where S_2 shows a predominant $\pi\pi^*$ character. However, the S_3 state has not been included in the state averaging used for the MEP calculations. The S_1 character at the S_2/S_1 crossing has $n\pi^*$ character using both theoretical approaches. At the S_1/S_0 CoIN, the S_1 state has a mixed $\pi\pi^*/n\pi^*$ character in our simulation, while it has a predominant $\pi\pi^*$ character at the MEP crossing.

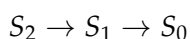
Concerning ISC, the MEP predicts an S_1/T_1 crossing, which we do not observe to play a role in our dynamics. The crossing seen in our simulations is S_1/T_2 . Additionally, we found a second S_1/T_2 crossing point, which is also not observed using MEPs.

When optimizing the S_1/S_0 CoIN, L. Martínez and Dr. I. Corral found a barrier of 0.7 eV at the CASPT2 level of theory, which does not exist on the CASSCF level of theory. This barrier inhibits state transfer to the ground state, which could account for the low S_0 yield proposed

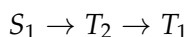
in the experiment. Therefore, we can see that the limit of our results is that the CASSCF PES is very different from the CASPT2 one. These results cannot be improved by using a better active space or analytical NACs as it is an inherent CASSCF problem. To improve our dynamics, we would need a method that includes electronic correlation beyond CASSCF.

SUMMARY

The goal of this work was to get an understanding of the relaxation dynamics of purine after UV light irradiation. Using the AIMD program SHARC, we obtained the state probabilities, as well as the geometries of the relevant crossing points. After excitation to the S_2 , the trajectories go to the S_1 state via a $^1(\pi\pi^*/n\pi^*)/^1n\pi^*$ CoIn – whose geometry is close to the Frank–Condon one – with a timescale of 12 fs. After 200 fs, relaxation to the ground state S_0 begins and after 1 ps approx. 50% of the population relaxed to S_0 . This leads to a time constant of 1200 - 1500 fs. The primary geometric feature of the S_1/S_0 CoIn is the $C_2-N_1-C_6-C_5$ dihedral angle. The singlet-state dynamics can be summarized as follows:



There is also ISC involved, with 10% of population in the T_1 state after 1 ps. Here, two distinct singlet-triplet crossings are accessed, one is semi-planar while the other one is twisted. There was not sufficient data available to analyze the timescales of the both the ($S_1 \rightarrow T_2$) and ($T_2 \rightarrow T_1$) transitions. For this process no timescales could be measured with the little data available. The dynamics involving triplets can be summarized as:



Although included in the dynamical simulations, no other triplet states showed any population, apart from statistical deviations.

Analyzing the data obtained by our collaborators, we can reinterpret our results as follows. The experimental measurements of Prof. C. Crespo show no relaxation to the ground state, but rather to the T_1 state, with a population of 50% after 100s of ps. The mismatch is explained by the results of L. Martínez and Dr. I. Corral, who detected that CASSCF – the level of electronic structure theory for our dynamics – on-the-fly is not able to describe a barrier present to access the S_1/S_0 CoIn. A higher level of theory, including more electronic correlation is needed to describe this barrier in the dynamics. However, at the moment this is technically not feasible.

As a prerequisite for the dynamics, the quantum chemistry of purine was also investigated in this thesis. Compared to the limited amount of published data available, none of our results managed to match the experimental excitation energies within less than 0.5 eV accuracy. By comparing the results obtained at different levels of theory, we estimated the errors in the excitation energies. The fact that none of the employed methods could quantitatively reproduce the absorption spectrum of purine is a fascinating aspect, which should be investigated beyond this thesis.

In summary, we obtained novel information on the relaxation dynamics of purine. We could measure the role of ISC, both qualitatively and quantitatively. This information will be very useful for any further investigations on the role of ISC in the dynamics of purine nucleobases.

OUTLOOK

As mentioned in section 5.4, one limitation of our calculations is the presence of an energetic barrier, which cannot be seen at CASSCF level of theory. Therefore, two distinct methods can be conceived to overcome this problem so that the barrier is included in the dynamics.

1. MRCI: Using the program COLUMBUS^{108–111}, it is possible to run dynamics calculations at MRCI level of theory. The necessary SHARC/COLUMBUS interface is currently being developed in our group. As MRCI is computationally very demanding, we would have to use a very simple reference space. Quantum mechanical calculations need to be performed to test whether this energetic barrier is described using a computationally affordable MRCI.
2. CASPT2: It is not possible to run the dynamics using CASPT2, since the relevant couplings can not be calculated at this level of theory. However, we could do an energy CASPT2 calculation every 5 to 10 timesteps and scale our energies accordingly. This ansatz has the disadvantage that we cannot guarantee, that the state ordering of the states will not change. Therefore, we might scale the states with the wrong factors. To avoid this, we would need to run the dynamics simulations for as few states as possible, ideally two singlets and two triplets. We are currently testing whether the implementation of this on-the-fly CASPT2 is feasible or not.

Using one of these approaches, we hope to describe better the PES for the purine molecule, as well as to generate a general efficient tool for other systems for which CASSCF cannot adequately describe the energy profile.

APPENDIX

A.1 TRIPLET STATES

Table A.1: Triplet energies of purine at SA-7S+7T-CASSCF/6-31G**/CASSCF/ANO-L level of theory. Excitation energies, characters (ch) and weights (w) are included.

state	CASSCF(16-12)			CASSCF(14-10)			CASSCF(12-9)		
	$\Delta E(\text{eV})$	ch.	w.	$\Delta E(\text{eV})$	ch.	w.	$\Delta E(\text{eV})$	ch.	w.
T ₁	4.04	$\pi_a\pi_a^*$	0.50	4.39	$\pi_a\pi_a^*$	0.56	4.39	$\pi_a\pi_a^*$	0.71
T ₂	4.96	$n_{1-3}\pi_a^*$	0.64	5.31	$n_1\pi_a^*$	0.69	5.40	$n_1\pi_a^*$	0.66
T ₃	5.26	$\pi_b\pi_a^*$	0.31	5.57	$\pi_b\pi_a^*$	0.40	5.62	$\pi_b\pi_a^*$	0.56
		$\pi_a\pi_a^*$	0.19		$\pi_a\pi_a^*$	0.19		—	
T ₄	5.40	$\pi_a\pi_b^*$	0.40	5.84	$\pi_a\pi_b^*$	0.25	5.88	$\pi_a\pi_c^*$	0.24
		$\pi_b\pi_a^*$	0.22		$\pi_a\pi_c^*$	0.19		$\pi_a\pi_b^*$	0.21
T ₅	5.67	$\pi_a\pi_a^*$	0.34	5.90	$n_1\pi_b^*$	0.66	5.95	$n_1\pi_b^*$	0.67
T ₆	5.89	$\pi''\pi_a^*$	0.25	6.25	$\pi_a\pi_b^*$	0.35	6.26	$\pi_b\pi_b^*$	0.33
		$n_7\pi_c^*$	0.43		$\pi_b\pi_b^*$	0.24		$\pi_a\pi_b^*$	0.25
T ₇	6.44	$\pi_b\pi^*$	0.17	6.44	$n_7\pi_a^*$	0.39	7.25	$\pi_b\pi_b^*$	0.28
		—	—		$n_7\pi_c^*$	0.25		$\pi\pi_a^*$	0.22
		—	—		—	—		$\pi_a\pi_b^*$	0.21

Table A.2: Triplet energies of purine. Excitation energies, characters (ch) and weights (w) for CASPT2 and MRCI.

state	CASPT2(16,12)/6-31G*			MRCI(14,10)/6-31G*		
	$\Delta E(\text{eV})$	ch.	weight	$\Delta E(\text{eV})$	ch.	weight
T ₁	4.26	$\pi_a\pi_a^*$	0.51	3.66	$\pi_a\pi_a^*$	0.77
T ₂	4.35	$n_{1-3}\pi_a^*$	0.67	4.40	$n_{1-3}\pi_a^*$	0.76
T ₃	5.19	$n_{1-3}\pi_b^*$	0.67	4.43	$\pi_b\pi_a^*$	0.75
T ₄	5.26	$\pi_b\pi_a^*$	0.55	4.49	$\pi_a\pi_b^*$	0.76
T ₅	5.45	$\pi_a\pi_a^*$	0.48	4.89	$n_{1-3}\pi_b^*$	0.78
T ₆	5.91	$n_7\pi_b^*$	0.48	5.08	$\pi_b\pi_a^*$	0.59
T ₇	5.99	$\pi_b\pi_a^*$	0.30	5.10	$n_7\pi_a^*$	0.75
		$\pi''\pi_a^*$	0.29		—	—

Table A.3: Triplet energies of purine at MS-CASPT2(16,12)//CASSCF/ANO-L level of theory using different basis set sizes. Excitation energies, characters (ch) and weights (w) are included.

state	CASPT2/6-31G*			CASPT2/ANO-S			CASPT2/ANO-L		
	146 basis functions			179 basis functions			243 basis functions		
	$\Delta E(\text{eV})$	ch.	w.	$\Delta E(\text{eV})$	ch.	w.	$\Delta E(\text{eV})$	ch.	w.
T ₁	4.26	$\pi_a \pi_a^*$	0.51	4.19	$\pi_a \pi_a^*$	0.54	4.17	$\pi_a \pi_a^*$	0.55
T ₂	4.35	$n_{1-3} \pi_a^*$	0.67	4.36	$n_{1-3} \pi_a^*$	0.67	4.33	$n_{1-3} \pi_a^*$	0.67
T ₃	5.19	$n_{1-3} \pi_b^*$	0.67	5.19	$\pi_b \pi_a^*$	0.56	5.15	$n_{1-3} \pi_b^*$	0.66
T ₄	5.26	$\pi_b \pi_a^*$	0.55	5.19	$n_{1-3} \pi_b^*$	0.66	5.16	$\pi_b \pi_a^*$	0.57
T ₅	5.45	$\pi_a \pi_a^*$	0.48	5.34	$\pi_a \pi_b^*$	0.51	5.31	$\pi_a \pi_b^*$	0.51
T ₆	5.91	$n_7 \pi_b^*$	0.48	5.86	$\pi_a \pi_c^*$	0.32	5.82	$\pi_a \pi_c^*$	0.33
		—	—		$\pi'' \pi_a^*$	0.29		$\pi'' \pi_a^*$	0.29
T ₇	5.99	$\pi_a \pi_c^*$	0.30	5.89	$n_7 \pi_a^*$	0.48	5.84	$n_7 \pi_a^*$	0.47
		$\pi'' \pi_a^*$	0.29		$n_7 \pi_c^*$	0.21		$n_7 \pi_c^*$	0.21

A.2 CONICAL INTERSECTION GEOMETRIES

Figure A.1: S₂/S₁ CoIn geometry optimized at SA-4S+6T-CASSCF(12,9)/def2-svp/CASSCF//ANO-L level of theory.

N	3.4646189570	2.5306977610	-1.9912387661
C	2.3248512915	2.3489488800	-2.5635039498
H	1.4198075917	2.1002028468	-2.0488373742
C	3.6364439600	2.8157194013	-4.2684276364
C	4.3251930632	2.8580549071	-3.0265521283
N	6.0404503130	3.5234187300	-4.3442488070
N	4.1453520236	2.8850552043	-5.4679535093
C	5.4930047382	3.0133051572	-5.5334420286
H	5.9693250652	3.2557686730	-6.4574609341
C	5.6793991147	3.1042023699	-3.0847280307
H	6.3914103326	3.0407411935	-2.2882647177
N	2.3442509133	2.5192560307	-3.9268072490
H	1.5983930591	2.3528847502	-4.5610863818

Figure A.2: S_1/S_0 CoIn geometry optimized at SA-4S+6T-CASSCF(12,9)/def2-svp/CASSCF//ANO-L level of theory.

N	3.4591527167	2.3833244944	-2.0087938767
C	2.3254138903	2.1662386342	-2.6069038751
H	1.4184885383	1.8680560434	-2.1254474862
C	3.6881350536	2.6912571450	-4.2145511155
C	4.3292223146	2.6962489054	-3.0266862628
N	6.1756226695	2.7868915472	-4.3249157939
N	4.2052321373	3.0632507371	-5.4659865308
C	5.4942737185	3.2161959086	-5.4591342681
H	6.0264904977	3.4198532540	-6.3665341686
C	5.6889072937	3.2698938593	-3.1044464063
H	5.7913496458	4.3336800558	-2.9176594484
N	2.4005266699	2.3504962332	-3.9604510812
H	1.6714926612	2.2423560892	-4.6267385102

Figure A.3: S_1/T_2 crossing geometry optimized at SA-4S+6T-CASSCF(12,9)/def2-svp/CASSCF//ANO-L level of theory

N	3.4385168112	2.3825645069	-2.0430781392
C	2.2696025874	2.2991146525	-2.6020987152
H	1.3455160637	2.0668667611	-2.0980869703
C	3.6196606137	2.7949964669	-4.2379587724
C	4.3010173963	2.6961692671	-3.0642441423
N	6.1424628147	3.1318506465	-4.3942456661
N	4.1448214920	3.0771720286	-5.4810513250
C	5.4619276088	3.2142089683	-5.5199795233
H	5.9751543249	3.4011061431	-6.4498465082
C	5.7363209079	2.9624281971	-3.0744512495
H	6.4469129798	2.5361085309	-2.3834731880
N	2.3198904772	2.5459521350	-3.9508747570
H	1.5618809053	2.5326751650	-4.5991059174

Figure A.4: T_2/T_1 crossing geometry optimized at SA-4S+6T-CASSCF(12,9)/def2-svp/CASSCF//ANO-L level of theory

N	3.3531055609	2.5872661611	-2.0168449356
C	2.2049438186	2.4584199021	-2.5759446876
H	1.2511377324	2.4772612183	-2.0829666782
C	3.6048336527	2.6393356297	-4.2175841488
C	4.2759564667	2.7196318747	-3.0369787217
N	6.2805577358	3.2528044400	-4.2647469921
N	4.3687753324	2.6904549483	-5.3550382887
C	5.6491150865	3.2641897827	-5.3944635936
H	6.1032926581	3.5578701446	-6.3224412225
C	5.6878415932	3.0129171573	-3.0610600243
H	6.2556465923	3.2101398544	-2.1771506679
N	2.2998232266	2.5411227068	-3.9748975410
H	1.5747438017	2.3557987219	-4.6321973540

BIBLIOGRAPHY

- [1] E. C. Friedberg: DNA damage and repair. *Nature*, **421**, 436–440 (2003).
- [2] J. Cadet, P. Vigny: The photochemistry of nucleic acids. In H. Morrison (editor), *Bioorganic Photochemistry*, volume 1, 1–272 (1990).
- [3] M. Barbatti, A. J. Aquino, J. J. Szymczak, D. Nachtigallová, P. Hobza, H. Lischka: Relaxation mechanisms of UV-photoexcited DNA and RNA nucleobases. *Proc. Natl. Acad. Sci.*, **107**(50), 21453–21458 (2010).
- [4] L. Serrano-Andrés, M. Merchán: Are the five natural DNA/RNA base monomers a good choice from natural selection?: A photochemical perspective. *J. Photochem. Photobiol. C*, **10**(1), 21–32 (2009).
- [5] P. Krause, S. Matsika, M. Kotur, T. Weinacht: The influence of excited state topology on wavepacket delocalization in the relaxation of photoexcited polyatomic molecules. *J. Chem. Phys.*, **137**, 22A537 (2012).
- [6] E. Goulielmakis, Z. Loh, A. Wirth, R. Santra, N. Rohringer, V. S. Yakovlev, S. Zherebtsov, T. Pfeifer, A. M. Azzeer, M. F. Kling, S. R. Leone, F. Krausz: Real-time observation of valence electron motion. *Nature*, **466**(7307), 739–743 (2010).
- [7] L. Nugent-Glandorf, M. Scheer, D. A. Samuels, A. M. Mulhisen, E. R. Grant, X. Yang, V. M. Bierbaum, S. R. Leone: Ultrafast Time-Resolved soft X-Ray photoelectron spectroscopy of dissociating Br₂. *Phys. Rev. Lett.*, **87**(19), 193002 (2001).
- [8] W. Li, X. Zhou, R. Lock, S. Patchkovskii, A. Stolow, H. C. Kapteyn, M. M. Murnane: Time-Resolved dynamics in N₂O₄ probed using high harmonic generation. *Science*, **322**(5905), 1207–1211 (2008).
- [9] H. J. Wörner, J. B. Bertrand, D. V. Kartashov, P. B. Corkum, D. M. Villeneuve: Following a chemical reaction using high-harmonic interferometry. *Nature*, **466**(7306), 604–607 (2010).
- [10] H. J. Wörner, J. B. Bertrand, P. B. Corkum, D. M. Villeneuve: High-Harmonic homodyne detection of the ultrafast dissociation of Br₂ molecules. *Phys. Rev. Lett.*, **105**(10), 103002 (2010).
- [11] M. Meckel, D. Comtois, D. Zeidler, A. Staudte, D. Pavičić, H. C. Bandulet, H. Pépin, J. C. Kieffer, R. Dörner, D. M. Villeneuve, P. B. Corkum: Laser-Induced electron tunneling and diffraction. *Science*, **320**(5882), 1478–1482 (2008).

- [12] C. Z. Bisgaard, O. J. Clarkin, G. Wu, A. M. D. Lee, O. Geßner, C. C. Hayden, A. Stolow: Time-Resolved molecular frame dynamics of Fixed-in-Space CS₂ molecules. *Science*, **323**(5920), 1464–1468 (2009).
- [13] M. Beck, A. Jäckle, G. Worth, H.-D. Myer: The multiconfiguration time-dependent hartree (MCTDH) method: a highly efficient algorithm for propagating wavepackets. *Phys. Rep.*, **324**, 1–105 (2000).
- [14] M. Ben-Nun, J. Quenneville, T. J. Martínez: Ab initio multiple spawning: Photochemistry from first principles quantum molecular dynamics. *J. Phys. Chem. A*, **104**(22), 5161–5175 (2000).
- [15] M. Richter, P. Marquetand, J. González-Vázquez, I. Sola, L. González: SHARC: ab initio molecular dynamics with surface hopping in the adiabatic representation including arbitrary couplings. *J. Chem. Theory Comput.*, **7**(5), 1253–1258 (2011).
- [16] M. Kasha: Characterization of electronic transitions in complex molecules. *Discuss. Faraday Soc.*, **9**, 14 (1950).
- [17] D. Golomb, K. Watanabe, F. F. Marmo: Absorption coefficients of sulfur dioxide in the vacuum ultraviolet. *J. Chem. Phys.*, **36**(4), 958–960 (1962).
- [18] M. A. El-Sayed: Triplet state. its radiative and nonradiative properties. *Acc. Chem. Res.*, **1**(1), 8–16 (1968).
- [19] M. A. El-Sayed: Spin-Orbit coupling and the radiationless processes in nitrogen heterocyclics. *J. Chem. Phys.*, **38**(12), 2834–2838 (1963).
- [20] R. Englman, J. Jortner: The energy gap law for radiationless transitions in large molecules. *Mol. Phys.*, **18**(2), 145–164 (1970).
- [21] T. Chu, X. Zhang, K. Han: A quantum wave-packet study of intersystem crossing effects in the O+H₂ reaction. *J. Chem. Phys.*, **122**(21), 214301–214301–6 (2005).
- [22] S. Cogan, Y. Haas, S. Zilberg: Intersystem crossing at singlet conical intersections. *J. Photoch. Photobio. A*, **190**(2–3), 200–206 (2007).
- [23] H. Ando, S. Iuchi, H. Sato: Theoretical study on ultrafast intersystem crossing of Chromium(III) acetylacetonate. *Chem. Phys. Lett.*, **535**(0), 177–181 (2012).
- [24] J. J. Cavaleri, K. Prater, R. M. Bowman: An investigation of the solvent dependence on the ultrafast intersystem crossing kinetics of xanthone. *Chem. Phys. Lett.*, **259**(5–6), 495–502 (1996).
- [25] H. Satzger, B. Schmidt, C. Root, W. Zinth, B. Fierz, F. Krieger, T. Kiefhaber, P. Gilch: Ultrafast quenching of the xanthone triplet by energy transfer: New insight into the intersystem crossing kinetics. *J. Phys. Chem. A*, **108**(46), 10072–10079 (2004).

- [26] M. Takezaki, N. Hirota, M. Terazima: Relaxation of nitrobenzene from the excited singlet state. *J. Chem. Phys.*, **108**(11), 4685–4686 (1998).
- [27] J. S. Zugazagoitia, C. X. Almora-Díaz, J. Peon: Ultrafast inter-system crossing in 1-nitronaphthalene. an experimental and computational study. *J. Phys. Chem. A*, **112**(3), 358–365 (2008).
- [28] C. Reichardt, R. A. Vogt, C. E. Crespo-Hernández: On the origin of ultrafast nonradiative transitions in nitro-polycyclic aromatic hydrocarbons: Excited-state dynamics in 1-nitronaphthalene. *J. Chem. Phys.*, **131**(22), 224518–224518–15 (2009).
- [29] R. S. Minns, D. S. N. Parker, T. J. Penfold, G. A. Worth, H. H. Fielding: Competing ultrafast intersystem crossing and internal conversion in the “channel 3” region of benzene. *Phys. Chem. Chem. Phys.*, **12**(48), 15607–15615 (2010).
- [30] M. Barbatti: Nonadiabatic dynamics with trajectory surface hopping method. *WIREs Comput. Mol. Sci.*, **1**(4), 620–633 (2011).
- [31] J. C. Tully: Molecular dynamics with electronic transitions. *J. Chem. Phys.*, **93**(2), 1061–1071 (1990).
- [32] E. Schrödinger: An undulatory theory of the mechanics of atoms and molecules. *Phys. Rev.*, **28**(6), 1049–1070 (1926).
- [33] M. Born, R. Oppenheimer: Zur quantentheorie der molekeln. *Ann. Phys.*, **84**(20), 457 (1927).
- [34] A. Adebí, N. Maitra, E. Gross: Exact factorization of the time-dependent electron-nuclear wave function. *Phys. Rev. Lett.*, **105**, 123002 (2010).
- [35] G. Hunter: Conditional probability amplitudes in wave mechanics. *Int. J. Q. Chem.*, **9**, 237–242 (1975).
- [36] M. Born, V. Fock: Beweis des adiabatensatzes. *Z. Phys.*, **51**(3-4), 165–180 (1928).
- [37] I. Newton: *Philosophiae Naturalis Principia Mathematica* (1687).
- [38] L. Verlet: Computer "Experiments" on classical fluids. I. thermodynamical properties of Lennard-Jones molecules. *Phys. Rev.*, **159**(1), 98–103 (1967).
- [39] V. E. Lamberti, L. D. Fosdick, E. R. Jessup, C. J. C. Schauble: A Hands-On introduction to molecular dynamics. *J. Chem. Educ.*, **79**(5), 601 (2002).
- [40] J. C. Tully, R. K. Preston: Trajectory surface hopping approach to nonadiabatic molecular collisions: The reaction of H⁺ with D₂. *J. Chem. Phys.*, **55**(2), 562–572 (1971).
- [41] J. Subotnik: Augmented ehrenfest dynamics yields a rate for surface hopping. *J. Chem. Phys.*, **132**, 134112 (2010).

- [42] G. Granucci, M. Persico, G. Spighi: Surface hopping trajectory simulations with spin-orbit and dynamical couplings. *J. Chem. Phys.*, **137**, 22A501 (2012).
- [43] G. Granucci, M. Persico, A. Toniolo: Direct semiclassical simulation of photochemical processes with semiempirical wave functions. *J. Chem. Phys.*, **114**(24), 10608–10615 (2001).
- [44] F. Plasser, G. Granucci, J. Pittner, M. Barbatti, M. Persico, H. Lischka: Surface hopping dynamics using a locally diabatic formalism: Charge transfer in the ethylene dimer cation and excited state dynamics in the 2-pyridone dimer. *J. Chem. Phys.*, **137**, 22A514 (2012).
- [45] A. Szabo, N. S. Ostlund: *Modern Quantum Chemistry: Introduction to Advanced Electronic Structure Theory*. Dover, Mineola, New York (1996).
- [46] J. A. Pople, R. K. Nesbet: Self Consistent orbitals for radicals. *J. Chem. Phys.*, **22**(3), 571–572 (1954).
- [47] C. C. J. Roothaan: New developments in molecular orbital theory. *Rev. Mod. Phys.*, **23**(2), 69 (1951).
- [48] P. Löwdin: Correlation problem in Many-Electron quantum mechanics I. Review of different approaches and discussion of some current ideas. *Adv. Chem. Phys.*, **2**, 207–322 (1959).
- [49] J. W. Hollett, P. M. W. Gill: The two faces of static correlation. *J. Chem. Phys.*, **134**(11), 114111–114111–5 (2011).
- [50] J. Olsen, P. Jørgensen, J. Simons: Passing the one-billion limit in full configuration-interaction (FCI) calculations. *Chem. Phys. Lett.*, **169**(6), 463–472 (1990).
- [51] S. R. Langhoff, E. R. Davidson: Configuration interaction calculations on the nitrogen molecule. *Int. J. Quantum Chem.*, **8**(1), 61–72 (1974).
- [52] C. Møller, M. S. Plesset: Note on an approximation treatment for Many-Electron systems. *Phys. Rev.*, **46**(7), 618 (1934).
- [53] L. Piela: *Ideas of Quantum Chemistry*. Elsevier, Amsterdam (2007).
- [54] W. Kutzelnigg: Almost variational coupled cluster theory. *Mol. Phys.*, **94**(1), 65–71 (1998).
- [55] B. O. Roos: *Lecture Notes in Quantum Chemistry: European Summer School in Quantum Chemistry*, volume 1. Springer, Berlin, Heidelberg (1992).
- [56] J. Paldus: Group theoretical approach to the configuration interaction and perturbation theory calculations for atomic and molecular systems. *J. Chem. Phys.*, **61**(12), 5321–5330 (1974).
- [57] K. Andersson, P. A. Malmqvist, B. O. Roos, A. J. Sadlej, K. Wolinski: CASPT2: second-order perturbation theory with a CASSCF reference function. *J. Phys. Chem.*, **94**(14), 5483–5488 (1990).

- [58] B. O. Roos, K. Andersson: Multiconfigurational perturbation theory with level shift – the Cr₂ potential revisited. *Chem. Phys. Lett.*, **245**(2-3), 215–223 (1995).
- [59] J. Finley, P. A. Malmqvist, B. O. Roos, L. Serrano-Andrés: The multi-state CASPT2 method. *Chem. Phys. Lett.*, **288**(2-4), 299–306 (1998).
- [60] B. O. Roos: Multiconfigurational quantum chemistry for ground and excited states. In M. K. Shukla, J. Leszczynski (editors), *Radiation Induced Molecular Phenomena in Nucleic Acids*, volume 5, 125–156, Springer Netherlands, Dordrecht (2008).
- [61] F. Jensen: *Introduction to Computational Chemistry*. John Wiley & Sons, Ltd, 2 edition (2007).
- [62] J. Almlöf, P. R. Taylor: Molecular properties from perturbation theory: A unified treatment of energy derivatives. *Int. J. Quantum Chem.*, **27**(6), 743–768 (1985).
- [63] R. P. Feynman: Forces in molecules. *Phys. Rev.*, **56**(4), 340–343 (1939).
- [64] N. C. Handy, H. F. Schaefer: On the evaluation of analytic energy derivatives for correlated wave functions. *J. Chem. Phys.*, **81**(11), 5031–5033 (1984).
- [65] J. Stålring, A. Bernhardsson, R. Lindh: Analytical gradients of a state average MCSCF state and a state average diagnostic. *Mol. Phys.*, **99**(2), 103–114 (2001).
- [66] T. Busch, A. D. Esposti, H. Werner: Analytical energy gradients for multiconfiguration self-consistent field wave functions with frozen core orbitals. *J. Chem. Phys.*, **94**(10), 6708 (1991).
- [67] H. Lischka, M. Dallos, P. G. Szalay, D. R. Yarkony, R. Shepard: Analytic evaluation of nonadiabatic coupling terms at the MR-CI level. i. formalism. *J. Chem. Phys.*, **120**(16), 7322 (2004).
- [68] G. Hirsch, P. J. Bruna, R. J. Buenker, S. D. Peyerimhoff: Non-adiabatic coupling matrix elements $\langle \Psi^\alpha | \partial / \partial Q | \Psi^\beta \rangle$ for large CI wavefunctions. *Chem. Phys.*, **45**(3), 335–347 (1980).
- [69] P. a. M. Dirac: The quantum theory of the electron. *Proc. R. Soc. A*, **117**(778), 610–624 (1928).
- [70] C. M. Marian: Spin-Orbit coupling in molecules. In K. B. Lipkowitz, D. B. Boyd (editors), *Reviews in Computational Chemistry*, 99–204, John Wiley & Sons, Inc. (2001).
- [71] W. Pauli: Zur Quantenmechanik des magnetischen Elektrons. *Z. Phys. - Hadon Nucl*, **43**(9), 601–623 (1927).
- [72] B. A. Heß, C. M. Marian, U. Wahlgren, O. Gropen: A mean-field spin-orbit method applicable to correlated wavefunctions. *Chem. Phys. Lett.*, **251**(5-6), 365–371 (1996).
- [73] B. Schimmelpfennig: Atomic spin-orbit mean-field integral program AMFI (1996).

- [74] D. G. Watson, R. M. Sweet, R. E. Marsh: The crystal and molecular structure of purine. *Acta Cryst.*, **19**(4), 573–580 (1965).
- [75] A. Broo, A. Holmén: Ab initio MP2 and DFT calculations of geometry and solution tautomerism of purine and some purine derivatives. *Theo. Chem. Acc.*, **97**(1), 331–340 (1997).
- [76] M. Majoube, P. Millie, L. Chinsky, P. Y. Turpin, G. Vergoten: Resonance raman spectra for purine. *J. Mol. Struct.*, **355**(2), 147–158 (1995).
- [77] S. Ullrich, T. Schultz, M. Z. Zgierski, A. Stolow: Direct observation of electronic relaxation dynamics in adenine via time-resolved photoelectron spectroscopy. *J. Am. Chem. Soc.*, **126**(8), 2262–2263 (2004).
- [78] L. Serrano-Andrés, M. Merchán, A. C. Borin: Adenine and 2-aminopurine: Paradigms of modern theoretical photochemistry. *Proc. Natl. Acad. Sci.*, **103**(23), 8691–8696 (2006).
- [79] M. Barbatti, J. J. Szymczak, A. J. Aquino, D. Nachtigallová, H. Lischka: The decay mechanism of photoexcited guanine- a nonadiabatic dynamics study. *J. Chem. Phys.*, **134**, 014304 (2011).
- [80] J. Catalan: On the absorption and emission spectra for the purine chromophore in weakly perturbative environments. *Chem. Phys.*, **303**, 205–218 (2004).
- [81] L. Clark, I. Tinoco: Correlations in the ultraviolet spectra of the purine and pyrimidine bases. *J. Am. Chem. Soc.*, **87**(23), 5487–5490 (1965).
- [82] B. J. Cohen, L. Goodman: Luminescence of purines. *J. Am. Chem. Soc.*, **87**(23), 5487–5490 (1965).
- [83] E. Quinones, R. Arce: Photochemistry and photophysics of purine free base and 6-methylpurine. *J. Am. Chem. Soc.*, **111**(21), 8218–8223 (1989).
- [84] H. Börresen: On the luminescence properties of some purine and pyrimidines. *Act. Chem. Scand.*, **17**, 921–929 (1963).
- [85] A. C. Borin, L. Serrano-Andrés, M. P. Fülcher, B. O. Roos: A theoretical study of the electronic spectra of n₉ and n₇ purine tautomers. *J. Phys. Chem. A*, **103**(12), 1838–1845 (1999).
- [86] E. Mburu, S. Matsika: An ab initio study of substituent effects on the excited states of purine derivatives. *J. Phys. Chem. A*, **112**(48), 12485–12491 (2008).
- [87] Weigend, F., Häser, M.: RI-MP2: first derivatives and global consistency. *Theo. Chem. Acc.*, **97**, 311–340 (1997).
- [88] F. Weigend, M. Häser, H. Patzelt, R. Ahlrichs: RI-MP2: optimized auxiliary basis sets and demonstration of efficiency. *Chem. Phys. Lett.*, **294**(1), 143–152 (1998).
- [89] TURBOMOLE v5.1, a development of university of karlsruhe and forschungszentrum karlsruhe GmbH (1989).

- [90] H.-J. Werner, P. J. Knowles, G. Knizia, F. R. Manby, M. Schütz, P. Celani, T. Korona, R. Lindh, A. Mitrushenkov, G. Rauhut, K. R. Shamasundar, T. B. Adler, R. D. Amos, A. Bernhardsson, A. Berning, D. L. Cooper, M. J. O. Deegan, A. J. Dobbyn, F. Eckert, E. Goll, C. Hampel, A. Hesselmann, G. Hetzer, T. Hrenar, G. Jansen, C. Köppl, Y. Liu, A. W. Lloyd, R. A. Mata, A. J. May, S. J. McNicholas, W. Meyer, M. E. Mura, A. Nicklass, D. P. O'Neill, P. Palmieri, K. Pflüger, R. Pitzer, M. Reiher, T. Shiozaki, H. Stoll, A. J. Stone, R. Tarroni, T. Thorsteinsson, M. Wang, A. Wolf: Molpro, version 2010.1, a package of ab initio programs (2010), see.
- [91] G. Knizia, T. B. Adler, H.-J. Werner: Simplified CCSD(T)-F12 methods: Theory and benchmarks. *J. Chem. Phys.*, **130**(5), 054104 (2009).
- [92] P.-O. Widmark, P. Malmqvist, B. O. Roos: Density matrix averaged atomic natural orbital (ANO) basis sets for correlated molecular wave functions. i. first row atoms. *Theor. Chim. Acta*, **77**(5), 291–306 (1990).
- [93] P.-O. Widmark, B. J. Persson, B. O. Roos: Density matrix averaged atomic natural orbital (ANO) basis sets for correlated molecular wave functions. ii. second row atoms. *Theor. Chim. Acta*, **79**(6), 419–432 (1991).
- [94] F. Aquilante, L. De Vico, N. Ferré, G. Ghigo, P. Malmqvist, P. Neogrády, T. B. Pedersen, M. Pitoňák, M. Reiher, B. O. Roos, L. Serrano-Andrés, M. Urban, V. Veryazov, R. Lindh: MOLCAS 7: The next generation. *J. Comput. Chem.*, **31**(1), 224–247 (2010).
- [95] K. Pierloot, B. Dumez, P.-O. Widmark, B. O. Roos: Density matrix averaged atomic natural orbital (ANO) basis sets for correlated molecular wave functions. *Theor. Chim. Acta*, **90**(2-3), 87–114 (1995).
- [96] H.-J. Werner, P. J. Knowles: A second order MCSCF method with optimum convergence. *J. Chem. Phys.*, **82**, 5053 (1985).
- [97] P. J. Knowles, H.-J. Werner: An efficient second order MCSCF method for long configuration expansions. *Chem. Phys. Letters*, **115**, 259–267 (1985).
- [98] K. Andersson, P. A. Malmqvist, B. O. Roos, A. J. Sadlej, K. Wolinski: Second-order perturbation theory with a CASSCF reference function. *J. Phys. Chem.*, **94**(14), 5483–5488 (1990).
- [99] K. Andersson, P.-\ Malmqvist, B. O. Roos: Second-order perturbation theory with a complete active space self-consistent field reference function. *J. Chem. Phys.*, **96**, 1218 (1992).
- [100] F. Neese: The ORCA program system. *WIREs Comput. Mol. Sci.*, **2**(1), 73–78 (2012).
- [101] T. Korona, H.-J. Werner: Local treatment of electron excitations in the EOM-CCSD method. *J. Chem. Phys.*, **118**, 3006 (2003).

- [102] T. H. Dunning: Gaussian basis sets for use in correlated molecular calculations. i. the atoms boron through neon and hydrogen. *J. Chem. Phys.*, **90**(2), 1007 (1989).
- [103] M. J. Frisch, G. W. Trucks, H. B. Schlegel, G. E. Scuseria, M. A. Robb, J. R. Cheeseman, G. Scalmani, V. Barone, B. Mennucci, G. A. Petersson, H. Nakatsuji, M. Caricato, X. Li, H. P. Hratchian, A. F. Izmaylov, J. Bloino, G. Zheng, J. L. Sonnenberg, M. Hada, M. Ehara, K. Toyota, R. Fukuda, J. Hasegawa, M. Ishida, T. Nakajima, Y. Honda, O. Kitao, H. Nakai, T. Vreven, J. A. Montgomery, Jr., J. E. Peralta, F. Ogliaro, M. Bearpark, J. J. Heyd, E. Brothers, K. N. Kudin, V. N. Staroverov, R. Kobayashi, J. Normand, K. Raghavachari, A. Rendell, J. C. Burant, S. S. Iyengar, J. Tomasi, M. Cossi, N. Rega, J. M. Millam, M. Klene, J. E. Knox, J. B. Cross, V. Bakken, C. Adamo, J. Jaramillo, R. Gomperts, R. E. Stratmann, O. Yazyev, A. J. Austin, R. Cammi, C. Pomelli, J. W. Ochterski, R. L. Martin, K. Morokuma, V. G. Zakrzewski, G. A. Voth, P. Salvador, J. J. Dannenberg, S. Dapprich, A. D. Daniels, Ö. Farkas, J. B. Foresman, J. V. Ortiz, J. Cioslowski, D. J. Fox: Gaussian 09. Gaussian Inc. Wallingford CT 2009.
- [104] E. Wigner: On the quantum correction for thermodynamic equilibrium. *Phys. Rev.*, **40**, 749–750 (1932).
- [105] J. González-Vázquez, L. González: A Time-Dependent picture of the ultrafast deactivation of keto-Cytosine including Three-State conical intersections. *ChemPhysChem*, **11**(17), 3617–3624 (2010).
- [106] M. Barbatti, A. J. A. Aquino, J. J. Szymczak, D. Nachtigallová, H. Lischka: Photodynamical simulations of cytosine: Characterization of the ultrafast bi-exponential uv deactivation. *Phys. Chem. Chem. Phys.*, **13**, 6145–6155 (2011).
- [107] M. Barbatti, A. J. A. Aquino, H. Lischka: The UV absorption of nucleobases: semi-classical ab initio spectra simulations. *Phys. Chem. Chem. Phys.*, **12**, 4959–4967 (2010).
- [108] H. Lischka, R. Shepard, I. Shavitt, R. M. Pitzer, M. Dallos, T. Müller, P. G. Szalay, F. B. Brown, R. Ahlrichs, H. J. Böhm, A. Chang, D. C. Comeau, R. Gdanitz, H. Dachsel, C. Ehrhardt, M. Ernzerhof, P. Höchtl, S. Irle, G. Kedziora, T. Kovar, V. Parasuk, M. J. M. Pepper, P. Scharf, H. Schiffer, M. Schindler, M. Schüler, M. Seth, E. A. Stahlberg, J.-G. Zhao, S. Yabushita, Z. Zhang, M. Barbatti, S. Matsika, M. Schuurmann, D. R. Yarkony, S. R. Brozell, E. V. Beck, J.-P. Blaudeau: Columbus, an ab initio electronic structure program, release 5.9.1 (2006).
- [109] H. Lischka, R. Shepard, F. B. Brown, I. Shavitt: New implementation of the graphical unitary group approach for multireference direct configuration interaction calculations. *Int. J. Quantum Chem.*, **20**(S15), 91–100 (1981).
- [110] R. Shepard, I. Shavitt, R. M. Pitzer, D. C. Comeau, M. Pepper, H. Lischka, P. G. Szalay, R. Ahlrichs, F. B. Brown, J. Zhao: A progress report on the status of the COLUMBUS MRCI program system. *Int. J. Quantum Chem.*, **34**(S22), 149–165 (1988).

- [111] H. Lischka, R. Shepard, R. M. Pitzer, I. Shavitt, M. Dallos, T. Müller, P. G. Szalay, M. Seth, G. S. Kedziora, S. Yabushita, Z. Zhang: High-level multireference methods in the quantum-chemistry program system COLUMBUS: analytic MR-CISD and MR-AQCC gradients and MR-AQCC-LRT for excited states, GUGA spin-orbit CI and parallel CI density. *Phys. Chem. Chem. Phys.*, 3(5), 664–673 (2001).

ACKNOWLEDGEMENTS

The content of this diploma thesis was developed from October 2012 to May 2013 in the group of Prof. González at the Institut für Theoretische Chemie of the University of Vienna.

I would like to thank Prof. Leticia González for giving me the opportunity to work in her group, and for her guidance and support during this work.

I also want to thank Dr. Philipp Marquetand for supervising me during my thesis, and for helpful discussions and proofreading of my thesis.

Furthermore, I would like to thank Sebastian Mai for providing me with the SHARC program and for helping me with its usage

On the technical side, I want to thank Dr. Markus Opperl and Jackie Klaura for maintaining the computational resources of the González group.

I am very grateful to my office mates Leon Freitag and Michael Gastegger for numerous helpful discussions and the nice working atmosphere, along with Federico Latorre, Rana Obaid, Martin Richter, Christoph Bauer, Dr. Daniel Kinzel, Dr. Dirk Deubel, Marianna Assmann, and Kathrine Baumann.

Finally, I want to thank my family and my friends for their support and encouragement during this thesis.

Curriculum Vitae

Personal data

Last name: Rauer
First name: Clemens
Address: Institute of Theoretical Chemistry
Währinger Str. 17, 1090 Vienna, Austria
Birth date/place: May 4, 1989, Mödling
Nationality: Austrian

Academic career

10/2012 - 05/2013 Master thesis in the group of Prof. Dr. L. González
Title: Ab initio molecular dynamics study of the relaxation of purine after UV excitation considering singlet-triplet interactions
10/2011-06/2013 Master studies in Chemistry at the University of Vienna
06/2011 Bachelor thesis in the Group of Prof. Dr. S. Boresch
Title: Calculation of solvation free energies by molecular dynamics simulations
2008-2011 Bachelor studies in Chemistry at the University of Vienna
06/2007 Matura at the Bundesrealgymnasium Gröhrmühlgasse

Further qualifications

Language skills German (mother tongue)
English (fluent)
Teaching experience Mathematics Tutor, Wintersemester 2012/2013